Positioning with Combined GPS and GLONASS Observations

Pedro Filipe Faria Nogueira Ferrão

Thesis to obtain the Master of Science Degree in

Aerospace Engineering

Examination Committee

Chairperson: Prof. João Manuel Lage de Miranda Lemos
Supervisor: Prof. José Eduardo Charters Ribeiro da Cunha Sanguino
Co-Supervisor: Prof. António José Castelo Branco Rodrigues
Members of the Committee: Prof. Francisco António Bucho Cercas

May 2013

*"The cold war would become the great engine, the supreme catalyst
that sent rockets and their cargoes far above Earth and worlds away
If Tsiolkovsky, Oberth, Goddard, and others were the fathers of rocketry,
the competition between capitalism and communism was its midwife"*
William E. Burrows

Dedicated to my family and to all my friends

Abstract

The use of multiple Global Navigation Satellite System (GNSS) constellations in the determination of one's Position Velocity and Time (PVT) brings several advantages such as faster startup times and convergence times, higher accuracies, and improved Dilution of Precision (DOP) values. These advantages are especially noticeable for applications where the view of the sky is partially obscured.

Currently four GNSS' are being developed/operating, the United States GPS, the Russian GLONASS, the European GALILEO and Chinese COMPASS. However up until recently only the GPS was fully operational, and many previous works with the combination of GPS and GLONASS focused on that fact that GPS signals were affected by the selective availability. Since then the GPS selective availability was deactivated and in 2011 following the modernization plans in place since 1998, the GLONASS achieved its full operational status.

This thesis focuses on combining the two fully operational GNSS constellations, the GPS and the GLONASS in single receiver scenarios suitable for real-time applications, presenting and solving its main interoperability issues and their different implementations and finally the performance of both systems and the combined system are evaluated using both Standard Point Positioning (SPP) approach and Precise Point Positioning (PPP) approach.

Keywords: GPS, GLONASS, PVT, SPP, PPP.

Resumo

A utilização de várias constelações GNSS trazem várias vantagens para a determinação da posição, velocidade e tempo (PVT) do utilizador, tais como menores tempos de inicialização e menores tempos de convergência, precisões mais elevadas, e melhores valores de diluição de precisão. Estas vantagens são especialmente notáveis em aplicações onde a visibilidade do céu está parcialmente obscurecida.

Actualmente, quatro sistemas GNSS estão em desenvolvimento ou operacionais, o sistema Norte-americano GPS, o sistema Russo GLONASS, o sistema Europeu GALILEO e o sistema chinês COMPASS. No entanto, até recentemente apenas o sistema GPS estava totalmente operacional, e muitos trabalhos anteriores sobre a combinação dos sistemas GPS e GLONASS focavam-se no facto de os sinais GPS serem afectados pela disponibilidade seletiva. Desde então, a disponibilidade seletiva do GPS foi desativada e em 2011, seguindo os planos de modernização em vigor desde 1998, sistema GLONASS ficou completamente operacional.

Esta tese foca-se na combinação das duas constelações GNSS operacionais, o sistema GPS e o sistema GLONASS em cenários com um único receptor adequados para aplicações em tempo real. São apresentados os principais problemas de interoperabilidade e suas diferentes implementações e finalmente o desempenho de ambos os sistemas e o de sua combinação são avaliados utilizando as abordagens *Standard Point Positioning* (SPP) e *Precise Point Positioning* (PPP).

Palavras-Chave: GPS, GLONASS, PVT, SPP, PPP.

Contents

List of Figures

List of Tables

List of Acronyms

CDMA   Code Division Multiple Access

FDMA   Frequency Division Multiple Access

GNSS   Global Navigation Satellite System

GPS   Global Positioning System

GLONASS   Globalnaya Navigatsionnaya Sputnikovaya Sistema

PZ-90.02   Parameters of the Earth 1990

WGS-84   World Geodetic System 1984

RK4   Fourth-order Runge–Kutta

EKF   Extended Kalman Filter

LWLS   Linear Weighted Least Squares

ECI   Earth-Centered Inertial

IERS   International Earth Rotation and Reference Systems Service

ECEF   Earth-Centered, Earth-Fixed

BIH   Bureau International de l'Heure

UTC   Coordinated Universal Time

DOP   Dilution of Precision

SPP   Standard Point Positioning

PPP   Precise Point Positioning

IGS   International GNSS Service

PVT   Position, Velocity and Time

SNR   Signal to Noise Ratio

List of Variables and Subscripts

c – Speed of light in vacuum (299792458 m·s^{-1})

P – Pseudorange measurement

Φ – Carrier-Phase measurement

D – Doppler shift measurement

λ – Signal wavelength

N – Carrier-phase ambiguity

ρ – Geometric range

δt – Clock offset

G – Subscript for GPS related variable

R – Subscript for GLONASS related variable

$\oplus$ – Subscript for Earth related variable

$\odot$ – Subscript for Sun related variable

$\mathbb{C}$ – Subscript for Moon related variable

sat – Subscript for satellite related variable

rcv – Subscript for receiver related variable

IF – Subscript for ionosphere-free combination

Chapter 1

Introduction

1.1 Motivation

A Global Navigation Satellite System (GNSS) is a system comprising a constellation of satellites which is capable of providing autonomous geo-spatial positioning and timing at a global scale. Two GNSS systems are currently in operation: the United States' Global Positioning System (GPS) and the Russian Federation's Globalnaya Navigatsionnaya Sputnikovaya Sistema (GLONASS). Another two GNSS systems are currently in development stage: the European's GALILEO and the Chinese's COMPASS.

These GNSS systems are currently used in numerous applications ranging from commercial applications to scientific and military applications and many of those applications can potentially benefit from the combination of the different available GNSS constellations.

The combination of multiple GNSS can significantly improve many applications, as the increased number of satellites strengthens the orbit geometry, resulting in an increased precision/accuracy, reduction the initialization times and increases the overall availability.
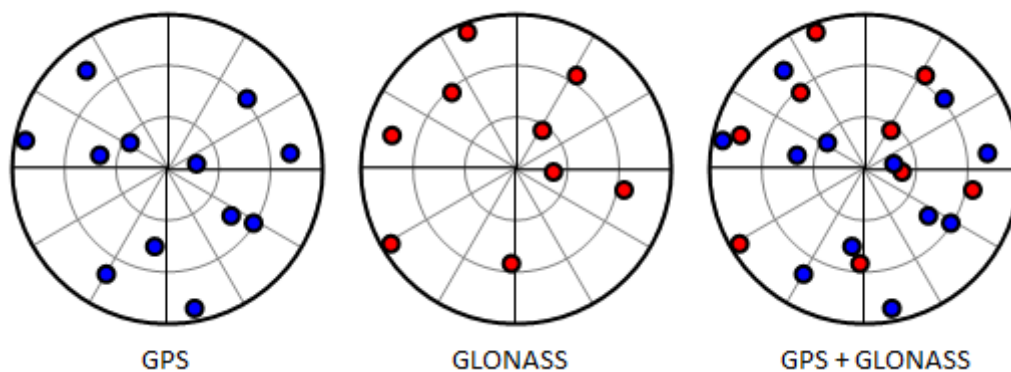
Figure 1.1: Sky-plots for the different GNSS combinations

These improvements are particularly important for kinematic applications, for applications at mid-latitude regions and for applications in difficult environments where the visibility of the sky is restricted such as in urban areas, under heavy tree foliage or in the vicinity of geographic formations such as mountains and canyons. Additionally scientific-grade applications benefit from the additional available signals and their frequencies, and the different orbital characteristics of each GNSS satellites.

1.2 State of the Art

Both GPS and GLONASS constellations were considered fully operational by 1995, and the first developed works to combine both systems focused mainly in how the GLONASS could be combined with GPS to improve its performance since GPS was affected by the selective availability (an intentional degradation of the its public radio-navigation signals).

However in 2000 the GPS selective availability was turned off and since the collapse of the Russian economy the GLONASS system was suspended and quickly losing satellites making the combination of both systems less and less attractive.

During the time in which the GLONASS constellation was undergoing through its modernization process, many positioning techniques were developed for the GPS only. Precise Point Positioning techniques along with the receiver technology evolved and reached a point where it is possible to achieve estimations within decimetre to centimetre using International GNSS Service (IGS) products.

Now twelve years later and following the GLONASS modernization program the GLONASS constellation is once again fully operational and the quest for more precise and robust positioning solutions led to the reconsideration of combining both systems again.

Currently state of the art GNSS receivers are capable of tracking multiple GNSS constellations and their respective dual-frequency signals. This thesis will focus on the combination of GPS with the modernized GLONASS solving their different implementations and using the latest Precise Point Positioning techniques applied to single-receiver real-time applications to obtain one's position, velocity and time.

1.3   Objectives and Structure

The main objective of this thesis is to assess the performance of the combination of the GPS system with the GLONASS system in the determination of one's position velocity and time. It's focused on techniques suitable for single receiver, real-time applications. This is accomplished by following the both standard point positioning and precise point positioning approaches mainly developed for the GPS system.

In chapter two, an overview of both GPS and GLONASS systems development, history and operational architecture is presented followed by a presentation of the fundamental concepts of a GNSS system.

In chapter three, the different implementations of GPS and GLONASS system are presented along a brief discussing on how they can be solved in order to combine both systems.

In chapter four, error analyses and modelling are discussed in depth along with the theory of GNSS positioning and the fundamentals of the standard point position approach and the precise point positioning approach. Additionally estimation methods for one's velocity and time are also presented.

In chapter five, the practical issues of the implementation of the theory and algorithms from chapter four are presented, along with a general description of the developed software. Finally the experimental setup used to test the developed work is presented.

In chapter six the experimental results obtained are presented, focusing on the improvements of a GPS+GLONASS solution when compared to a GPS-Only solution and a GLONASS-Only solution.

Chapter Seven summarizes the conclusions drawn from this work and provides recommendations for future works.

Chapter 2

Basic Concepts

2.1 Introduction

The first steps towards a GNSS came after the launch of the first man-made satellite Sputnik 1 by U.S.S.R. in 1957, when two American physicists, William Guier and George Weiffenbach realized that they could pinpoint the satellite position in its orbit by monitoring its radio transmissions' Doppler shift.

The first satellite navigation system, Transit, developed by U.S. Navy was successfully tested in 1960 with a constellation of five satellites it was able to provide a navigational fix once per hour and in 1967 the U.S. Navy launched the Timation satellite proving the ability to place accurate atomic clocks in space (a requirement of modern GNSS). Additional radio/satellite navigation systems were developed by U.S. Air Force and U.S. Army.

In 1967 the U.S.S.R. developed their own satellite navigation system, Tsiklon to provide an accurate positioning method for submarines, with a constellation of 31 satellites. It was highly accurate for quasi-stationary users but it required several hours of observations in order to get a navigational fix, rendering it almost useless in terms of the project requirements.

With the heat of the Cold War, the need to overcome past limitations of those previous systems and the need for a more universal and accurate navigation solution, lead to the creation of the GPS in 1973 by the U.S., and the creation of the GLONASS in 1976 by the U.S.S.R.

Figure 2.1: GPS and GLONASS emblems

2.1.1 Highlights of the GPS development

- On 1978, the U.S. military successfully launched the first Block-I GPS satellite.

- In September 1st, 1983, President Ronald Reagan issued a directive making GPS freely available for civilian users, after Korean Air Lines - flight 007 incident in U.S.S.R.'s prohibited airspace.

- By the end 1985, ten more Block-I GPS satellites were launched.

- On December 1993, GPS achieved its initial nominal constellation of 24 satellites fully providing Standard Positioning Service (SPS) and by 1995 the Air Force Space Command announced that Precise Positioning Service (PPS) was fully available for authorized users.

- On 1998, U.S. Vice President Al Gore announced plans to upgrade GPS with two new civilian signals to improve user accuracy and reliability.

- On May 2nd, 2000, GPS' Selective Availability (SA) was discontinued through executive order as a result of the Bill Clinton directive in 1996, allowing civilian users to receive a non-degraded signal globally.

- On 2005, the first modernized GPS satellite was launched providing a second civilian signal (L2C) to enhance user performance.

- As critical part of GPS modernization, the U.S. Air Force was awarded with the contract to develop the GPS Next Generation Operation Control System (OCX) in 2010.

- On July 16th, 2011 and October 4, 2012, the GPS IIF-2 satellite and GPS IIF-3 satellite were launched.

2.1.2 Highlights of the GLONASS development

- On October 12, 1982, the first GLONASS satellite was launched.

- From 1982 through April 1991, a total of 43 GLONASS and GLONASS related satellites were launched.

- In 1991, with the fall of U.S.S.R., the Russian Federation took over control of GLONASS project.

- In 1993 with 12 satellites, the GLONASS was declared operational over Russian territory.

- By December 1995, the GLONASS constellation achieved its nominal operation with 24 operational satellites, due to the low life span of the first generation GLONASS satellites, to keep the system operational at its nominal capacity, at least two launches per year were required.

- With the collapse of Russian economy, the space program's funding was cut by 80% and GLONASS project fell in disrepair, unable to afford the launch rate required to maintain the constellation fully operational.

- By 2001, GLONASS constellation got to its lowest point, with just six operational satellites.

- On August 2001, with the recovery of the Russian economy, the Federal Targeted Program "Global Navigation System" was launched aiming to restore the full GLONASS constellation by the end 2009.

- On May 18th, 2007 most of the signal restrictions were lifted, and the formerly military-only signal with a precision of 10 m was made available to civilian users free of charge and without limitations.

- On September 20th, 2007, all operational GLONASS satellites started transmitting his ephemeris information in PZ-90.02 coordinate system, facilitating the integration of GLONASS with the fully operational GPS.

- On October 2nd, 2011 the 24th satellite of the system was successfully launched, making the GLONASS constellation fully restored for the first time since 1996.

2.1.3 Other Systems

- **GALILEO**

  GALILEO is Europe's own global navigation satellite system, designed to provide a highly accurate and guaranteed global positioning service under civilian control [1].

  The first two GALILEO satellites were launched in 2005 and 2008 respectively, reserving radio frequencies and serving as test platforms for the GALILEO technologies.

  GALILEO services will come with quality and integrity guarantees to civilian users that in other systems are restricted to military and authorized users only, marking the key difference between GALILEO and others GNSS'.

  The fully developed GALILEO constellation will consist of 30 satellites (27 operational + 3 spares), orbiting in 3 circular Medium Earth Orbit planes with 23 222 Km of altitude above the Earth with a nominal inclination of 56 degrees relative to the equator.

- **COMPASS**

  COMPASS is China's second generation satellite navigation system and aimed to provide positioning, navigation and timing services to users on a continuous worldwide basis, similar to the GPS, GLONASS and GALILEO systems.

  The Chinese Government approved its development and deployment in 2004, and by December 2011 it became operational in China and surrounding regions, with a constellation of 10 satellites. It's expected to reach global coverage and its nominal constellation of 35 satellites by 2020.

Figure 2.2: GALILEO and COMPASS emblems

2.2 GNSS Architecture

2.2.1 Control Segment

The Control Segment sometimes referred as Ground Segment or Operational Control System, consists in a network of ground facilities that track the GNSS satellites, monitoring their transmissions, perform analyses and uploads new data to their respective constellation in order to maintaining the proper operation of the system.

			Description
GPS	2	–	Master Control Center (Main and Alternative)
	16	–	Monitor Stations
	8	–	Remote Tracking Stations
	4	–	Ground Antennas
GLONASS	2	–	System Control Center (1 fully operational)
	10	–	Monitor Stations (4 fully operational)
	3	–	Laser Ranging Stations
	3	–	Upload Stations
	1	–	Central Clock

Table 2.1: GPS [2] and GLONASS [3] Control Segment

2.2.2 Space Segment

The Space Segment is composed by a constellation of satellites orbiting the Earth, this constellation is designed to ensure a visibility of at least four satellites at all times. The main function of the Space Segment is to transmit the radio-navigation signals required by GNSS users to estimate their Position, Velocity and Time (PVT), these radio-navigation signals are controlled by highly stable on-board atomic clocks and contain ranging codes, navigation messages and corrections relayed by the Control Segment.
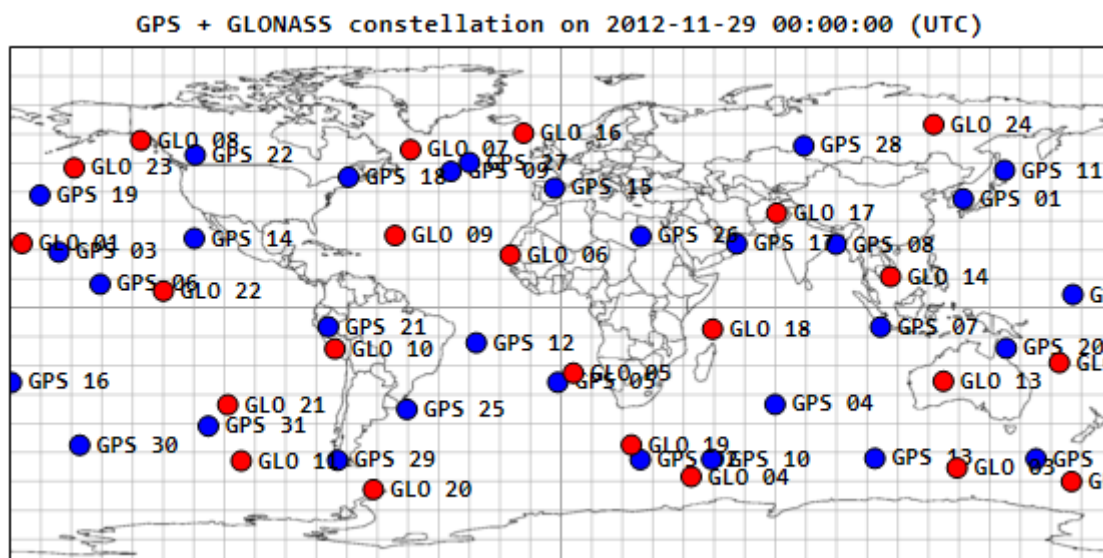
Figure 2.3: Snapshot of the GPS + GLONASS constellation

- **GPS Space Segment**

  The GPS nominal constellation consists of 24 satellites (although 32 are available), distributed over six orbital planes at an altitude of 20180 km and a nominal inclination of 55° in relation to the equator; with an orbital period of 11 hours and 58 minutes, the same satellite geometry repeats every sidereal day, with all satellites at the same spot in sky.

  Each satellite transmits a coarse acquisition code (C/A code) in L1 frequency (modernized satellites also transmit this code on L2 frequency), and encrypted code (P code, only available for authorized users) on both frequencies.

  Since every GPS satellite uses the same L1 and L2 frequencies, each satellite have its own Pseudo-Random Number (PRN) which does not correlate with any other satellite's PRN forming a Code Division Multiple Access (CDMA) allowing the receiver to recognize multiple satellites on the same frequencies.

- **GLONASS Space Segment**

  The GLONASS nominal constellation consists of 24 satellites distributed over three orbital planes at an altitude of 19140 km and a nominal inclination of 64.8° in relation to the equator; with an orbital period of 11 hours and 15 minutes, the same satellite geometry repeats about once every 8 days, but because each orbital plane contains eight satellites equally spaced, one will be at the same spot in the sky every sidereal day.

  Like the GPS satellites, GLONASS satellites also transmit a C/A code and encrypted P code (also only available to authorized users) on both L1 and L2 carrier frequencies, but unlike GPS satellites, each GLONASS satellite transmits the same PRN code but at slightly different carrier frequencies (14 frequency channels), forming a Frequency Division Multiple Access (FDMA), allowing the receiver to recognize multiple satellites with the same code.

  The 24 GLONASS satellites can operate with only 14 frequency channels by having antipodal satellites sharing the same frequency channel. Antipodal satellites are in the same orbital plane but separated by 180° in latitude, thus ensuring that the two satellites sharing the same frequencies are never visible at the same time.
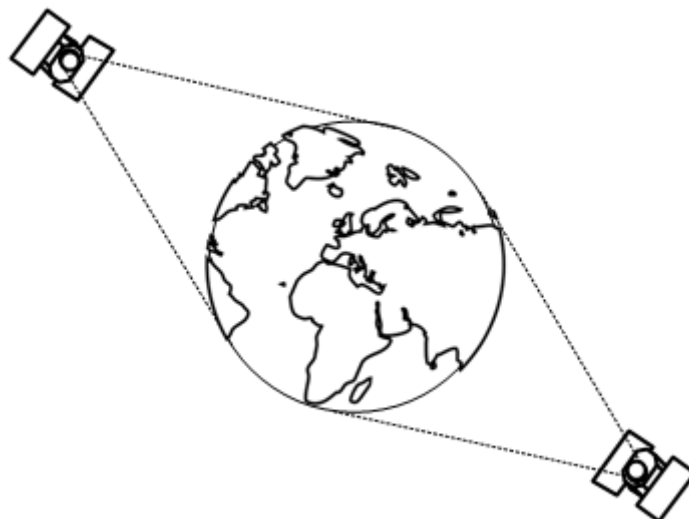
Figure 2.4: GLONASS antipodal satellites

The GPS and GLONASS satellite constellation properties and their radio-frequency signal properties are summarized in table 2.2.

		GPS	GLONASS
Satellites	**Available satellites**	32	24
	Orbital planes	6	3
	Orbital inclination	$55°$	$64.8°$
	Orbital altitude	20.180 km	19.140 km
	Period of revolution	11h 58m	11h 15m
Signal	**Separation technique**	CDMA	FDMA
	Fundamental Frequency	10.24 MHz	5.0 MHz
	Carrier frequencies L1	1575.42 MHz	1598.0625–1609.3125 MHz
	L2	1227.60 MHz	1242.9375–1251.6875 MHz
	Code clock rate C/A	1.023 MHz	0.511 MHz
	P	10.23 MHz	5.11 MHz
	Code length C/A	1023 Chip	511 Chip
	P	$6.187104 \cdot 10^{12}$ Chip	$5.11 \cdot 10^{6}$ Chip

Table 2.2: Resume of the GPS and GLONASS Space Segment

2.2.3 User Segment

The User Segment encompasses all private, commercial and military users equipped with L-band radio-frequency receivers, processors and antennas which are capable of receive, decode and process the GNSS' signals transmitted by the satellites in order to estimate their PVT.

Figure 2.5: Examples of User Segment equipment

A notable part of the user segment is the IGS, formerly known as International GPS Service, it's composed by a voluntary federation of more than 200 worldwide agencies that gather resources and permanent GPS & GLONASS station data to generate precise GPS & GLONASS products, providing the highest quality data and products as the standard for preciseGNSS; IGS is the highest-precision international civilian GNSS community [4].

2.3 GLONASS Present and Future Status

The GLONASS present and future status is presented here because over the last decade, GLONASS underwent major modernizations which improved its performance, putting it on par with GPS.

As of 2012, the GLONASS constellation is operating at its nominal capacity of 24 satellites and all of its first generation satellites have been replaced by either GLONASS–M or GLONASS–K satellites

(second and third generation respectively), table 2.3 contains the current (retrieved in 12/09/2012) GLONASS constellation configuration.

		Configuration							
Plane 1	Slot	1	2	3	4	5	6	7	8
	Channel	1	-4	5	6	1	-4	5	6
	Class	M	M	K1	K1	M	M	M	M
Plane 2	Slot	9	10	11	12	13	14	15	16
	Channel	-2	-7	0	-1	-2	-7	0	-1
	Class	M	M	M	M	M	M	M	M
Plane 3	Slot	17	18	19	20	21	22	23	24
	Channel	4	-3	3	2	4	-3	3	2
	Class	M	M	M	M	M	M	M	M

Table 2.3: GLONASS constellation configuration [5]

These new generations of satellites represent major advances for GLONASS constellation and its most notable features are, [6, 7]:

- Increased satellite life-span from three to seven years, reducing the system maintenance costs;
- Increased stability of the on-board clocks and improved satellite motion models resulting in an increase of the pseudoranges accuracy;
- Addition of the C/A code on L2 carrier frequency, allowing civilian users to correct the iono-spheric delay without the aid of ionospheric models;
- Additional navigation message parameters.

The new navigation message parameters were added to the previous navigation message (in its previously spare bits) ensuring retro-compatibility with older GLONASS equipment, from this new parameters is worth mentioning, [7]:

- Satellite slot number, which can be used to improve *cold-boot* times;
- Integrity checking, providing reports of problems within ten seconds of its detection;
- Information about forthcoming leap seconds corrections to Coordinated Universal Time (UTC);
- Hardware delay between the L1 and L2 carrier frequencies for single-frequency users;
- Increased resolution of the time offset between the GLONASS time scale and UTC;
- GLONASS-time to GPS-time offset improving the interoperability between the two systems;
- An estimate of the pseudorange accuracy allowing the receiver to weight the observations more efficiently;
- Absolute time representation (currently GPS data only allows time determination for about 20 years unambiguously).

And unlike GPS, in this new satellites its also guaranteed that no navigation message data will *cut in half*, when the Control Segment uploads the new data to the satellites, simplifying the signal acquisition hardware/software.

The currently orbiting class-K satellites are in test phase (being designed class-K1), the final class-K (designed class-KM) satellites will further improve its on-board clock stability, include two new civilian signals and will also implement CDMA to differentiate between its satellites along with the current FDMA scheme [3].

2.4 Satellite Navigation Problem

The Satellite Navigation Problem consists in the determination of one's PVT and its basis consists in solving a geometric problem known as trilateration. Trilateration is a geometric process used to determine the location of a point based in its distance to a set of other points which their locations are known, using the geometric properties of circles, spheres or triangles. In the Satellite Navigation Problem, the unknown point location corresponds to the receiver position, and the set of points with known locations corresponds to visible satellites positions, as depicted in figure 2.6.
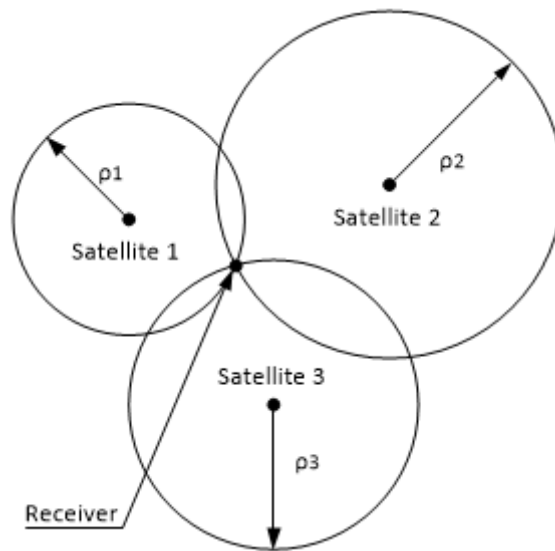
Figure 2.6: Concept of trilateration

Taking into account the fact that the measured distances between the receiver and the respective visible satellites contains errors and uncertainties, the resulting receiver position will also contain errors and uncertainties, meaning that this resulting position will be an estimate of the receiver true position. The receiver true position will be inside an uncertainty region, as depicted in figure 2.7.
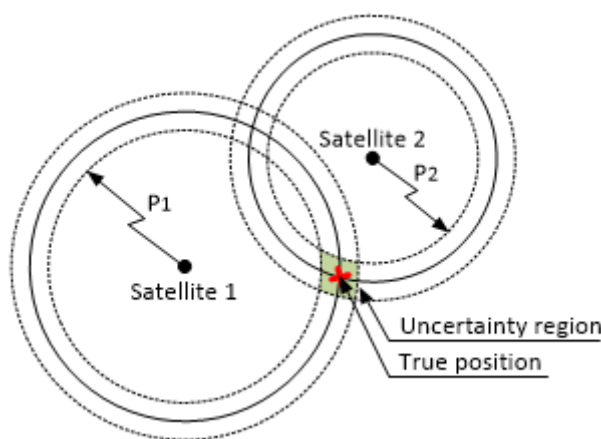
Figure 2.7: Concept of uncertainty region

The size of this uncertainty region represents the quality of the estimation process as well as the quality of the GNSS measurements. The quality of the GNSS measurements depends on equipment and survey site conditions, and the quality of the estimation process depends on how accurately one can model the errors and uncertainties that affect the measured distances, therefore it's mandatory to know main sources of errors that affect the GNSS measurements.

2.5 Main sources of errors

As mentioned in the previous section, its mandatory to know the main sources of errors that affect the measured distances between the receiver and the respective visible satellites. Generally the main sources of errors are ephemeris errors, satellite clocks offsets, ionospheric and tropospheric delays, multipath effects and hardware delays [8, 9]. A brief description of this errors and their properties will be provided in this section and in-depth models will be presented in chapter 4.

Figure 2.8: Error components of the distance
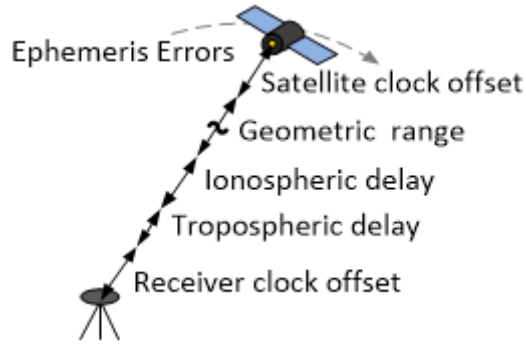
Source	Error (1σ)
Ephemeris Errors	0.8 m
Satellite Clock Offset	1.1 m
Ionospheric Delay	7.0 m
Tropospheric Delay	0.2 m
Receiver Clock Offset	1.1 m
Multipath and Hw. delays	0.2 m

Table 2.4: Measurement expected error budget [9]

2.5.1 Ephemeris Errors

The Control Segment generates the ephemeris parameters using a curve-fit interpolation over its best prediction of the satellite orbits. This operation results in a residual error between the satellite estimated position and its true position, with typical magnitudes in the range of 1 to 6 meters [9].

By design the satellite ephemeris parameters allows one to determine the satellite positions at transmission time in an Earth-Centered, Earth-Fixed (ECEF) coordinate system. During the signal travelling time, the ECEF coordinate can rotate more than a micro-radian, causing a Sagnac-like effect [10].

Furthermore when combining multiple GNSS constellations, special care must be taken as the reference coordinate system used on one system may not be the same used for other systems, as in the case of GPS and GLONASS [11, 7].

2.5.2 Satellite clock offset

The satellite time reference is obtained from on-board atomic clocks, which are highly stable and accurate, however this clocks have drifts leading to offsets from its GNSS time-scale which in turn lead to errors in the measured signal travelling time. For instance a drift of 1 ms in GPS satellite clock leads to an error of 300 km in the measured distance [9].

The Control Segment, determines and relays the clock corrections parameters to the satellites for their navigation messages. As in the case of the ephemeris parameters, the satellite clock corrections parameters are also generated using a curve-fit interpolation and again some residual error remains. This residual clock error results in ranging errors in the range of 0.3 to 4 meters [9].

2.5.3 Atmospheric delays

As the GNSS signals travel from the satellite to the Earth's surface, they leave free-space and enter the Earth's atmosphere, which is composed by several layers which are defined based on their altitude from the surface and their properties. The properties of each atmospheric layer delay the GNSS signals by changing their propagation speed and an atmospheric layer is considered a dispersive

medium to the signal if the signal's propagation speed is a function of it's frequency, and considered non-dispersive medium otherwise.
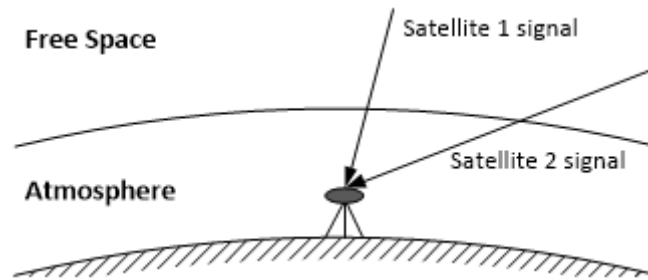
Figure 2.9: Atmosphere and GNSS signals

The delays caused by the Earth's atmosphere are also dependent of the satellite elevation angle relative to receiver as the signals from satellites at lower elevation angles must travel through *more* atmosphere than the signals from satellites at higher elevation angles [9], as depicted in figure 2.9.

The main atmosphere layers that affect the GNSS-signals are the ionosphere and the troposphere [8, 9], and their contribution to the observations error must be taken into account:

- **Ionospheric Delay**

  The ionosphere layer extends from about 60 Km until about 2000 Km and it is characterized by a partially ionized medium as a result of stellar winds and solar radiation. To GNSS signals the ionosphere acts as a dispersive medium, delaying the pseudorange measurements (group delay) and advancing the carrier-phase measurements (the ionospheric error in the pseudor-ange measurements is symmetric to the ionospheric error of carrier-phase measurements). If left uncompensated, the distance equivalent of the ionospheric delay can reach up to few tens of meters, depending on the satellite elevation and the ionospheric conditions [9].

- **Tropospheric Delay**

  The troposphere layer extends from the Earth's surface until about an altitude of 60 Km and for signals with frequencies up to 15 GHz, the troposphere is characterized as a non-dispersive medium. Both the pseudorange measurements and carrier-phase measurements are delayed in same way, and this delay depends only on the atmospheric conditions such as temperature, pressure and humidity. If left uncompensated, the distance equivalent of the tropospheric delay can vary from about 2.4 m for a satellite near the zenith to about 25 m for a satellite near the horizon [9].

2.5.4 Receiver clock offset

In the same way that satellite on-board clock drifts from its GNSS time-scale, the receiver internal clock also drifts from the GNSS time-scale, and unfortunately most of the commercial GNSS receivers are equipped with quartz-based clocks [9, 8], which are much more economical but less stable and accurate than the satellite on-board atomic clocks; and unlike the satellite clock offset, the only way to compensate for the receiver clock offset is to estimate it together with the receiver position.

Furthermore when combining multiple GNSS constellations, it's also necessary to take into account that each GNSS operates under its own time-scales, requiring that the offset with each one of the GNSS time-scales to be known.

2.5.5 Multipath and hardware delays

The interference caused by multipath occurs when multiple versions of the same signal reach the receiver's antenna. This interference is related mainly to the antenna closeness to reflecting surfaces, being specially important when the signals arrive from satellites at low elevation angles. The multipath effects can be mitigated by proper antenna design and placement (if possible), as well as in the in receiver signal processing [8, 9]
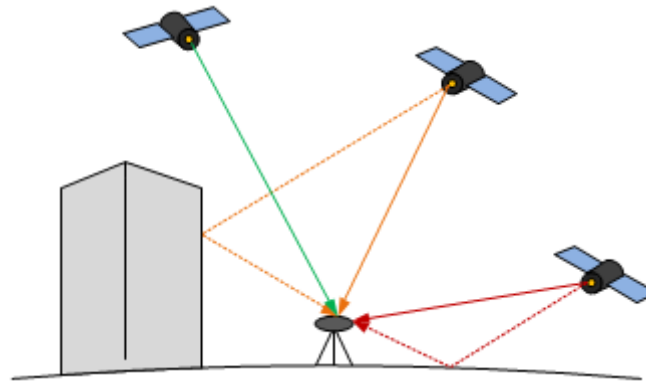
Figure 2.10: Examples of multipath

The hardware delays are introduced by the receiver in the signal acquisition process as result of internal thermal noise and interference between the GNSS signals and other signals in the same frequency bands. To compensate for these hardware delays the receivers usually include hard-coded corrections determined by calibration in its process of manufacture, and high-end receivers usually include some form of calibration processes in its start-up that allows the significant removal of this hardware delays [12].

In a combined GPS+GLONASS receiver further care must be taken in its design as GPS and GLONASS require different hardware to track their respective radio-navigation signals; furthermore because GLONASS uses FDMA to distinguish between each of its satellites, hardware delays between the GLONASS channels exists as well and it also have to be accounted for.

2.6 GNSS Observables

The GNSS observables are the measurements from the satellites that can be used to estimate one's PVT. The two basic GNSS observables are the pseudorange measurements and the carrier-phase measurements which represent the measured distance between the receiver and respective visible satellites. A third GNSS observable is also considered, the Doppler frequency shift measurements which is a by-product of the receiver signal processing.

2.6.1 Pseudorange

The pseudorange (sometimes referred as pseudodistance or code measurements), is the apparent distance between the receiver and the satellite. The receiver obtains this distance by determining the travelling time of the GNSS signal from the satellite to the receiver and scaling it to distance units by multiplying it by the signal propagation speed (speed of light).

As mentioned in section 2.2.2, each satellite transmits a ranging code that allows the receiver to compute the travelling time; by generating a replica of the satellite code and correlating it with the incoming GNSS signal, this replica is shifted in time until the maximum correlation is obtained, the amount of time shifted corresponds to the signal travelling time (ΔT), as depicted in figure 2.11.

This distance is designated as apparent because it doesn't match with the geometric distance between the receiver and satellite due to synchronism errors in receiver-satellite clocks, atmospheric delays, hardware bias and multipath effects mentioned previously.
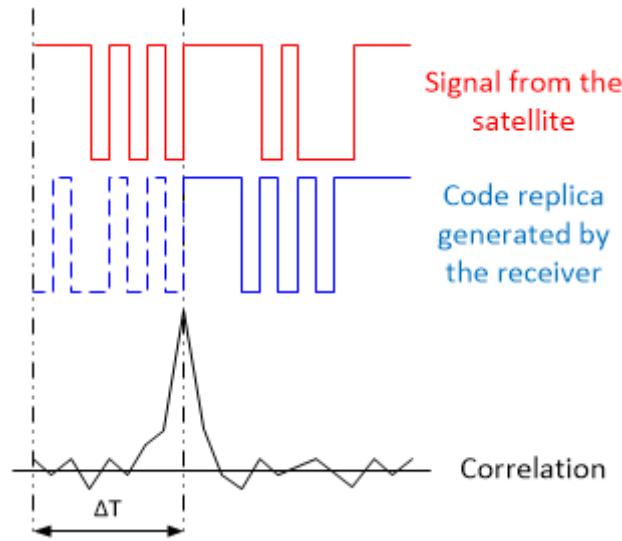
Figure 2.11: Example of ΔT determination

Taking into account the main sources of errors described in the previous section, the pseudorange measurement can be expressed as:

$$P = \rho + c \cdot (\delta t_{rcv} - \delta t_{sat}) + T_d + I_d + \epsilon_P \tag{2.1}$$

where:

- ρ represents the geometric range between the satellite position (X_s, Y_s, Z_s) at the time of signal transmission and the receiver position (x, y, z), and is defined as:

$$\rho = \sqrt{(X_s - x)^2 + (Y_s - y)^2 + (Z_s - z)^2} \tag{2.2}$$

- δt_{rcv} represents the receiver clock offset from the respective GNSS time-scale;

- δt_{sat} represents the satellite clock offset from the respective GNSS time-scale;

- T_d represents the tropospheric delay;

- I_d represents the ionospheric delay;

- ϵ_R represents the relevant measurement noise components including multipath.

2.6.2 Carrier-phase

The carrier-phase also represents the apparent distance between the receiver and the satellite, and is obtained by counting the number of carrier cycles during the signal travelling time and scaling it to distance units by multiplying it by the signal wavelength.

Since the carrier frequencies of the GNSS signals are over 1000 times higher than the frequency of ranging codes, this results in an apparent distance up to three orders of magnitude more precise than the pseudorange measurement, however since the carrier-phase is so uniform, the complete number of cycles cannot be determined resulting in an ambiguity of an integer number of carrier-phase cycles which remains constant as long as the signal is being tracked, as depicted in the figure 2.12.
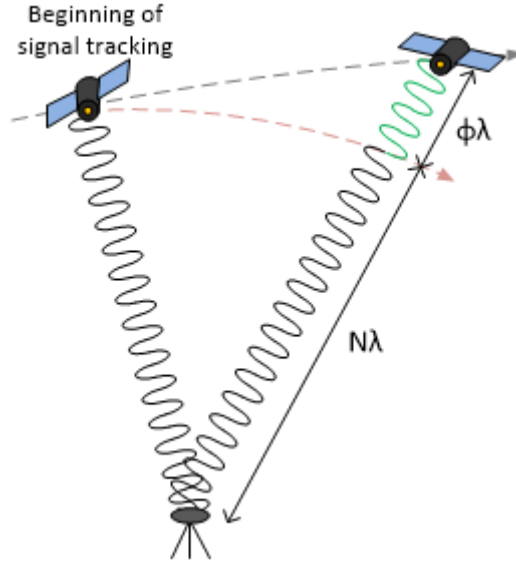
Figure 2.12: Carrier-phase ambiguity concept

- **Cycle-slips**

  Cycle-slips are arbitrary jumps of an integer number of cycles in the carrier-phase ambiguity resulting from a temporary loss-of-lock in the carrier tracking loop of a receiver. The causes for cycle-slips are listed below:

  - Obstructions of the satellite signal caused by environmental elements such as trees, mountains, buildings, etc...;
  - Low Signal to Noise Ratio (SNR), due to exceptional ionospheric conditions, multipath or high receiver dynamics;
  - Failures in the receiver signal processing hardware/software.

In order to use the carrier-phase measurements in the position estimation, the carrier-phase ambiguity must be correctly estimated and possible occurrences of cycle-slips must be detected and dealt with.

Similarly to the pseudorange, the carrier-phase measurement scaled to distance units can be expressed as:

$$\Phi = \lambda\phi = \rho + c \cdot (\delta t_{rcv} - \delta t_{sat}) + T_d - I_d + \lambda N + \epsilon_\Phi \tag{2.3}$$

where:

- ρ represents the geometric range between the satellite and receiver defined by 2.2;

- δt_{rcv} represents the receiver clock offset from the respective GNSS time-scale;

- δt_{sat} represents the satellite clock offset from the respective GNSS time-scale;

- λ represents the carrier signal wavelength;

- N represents the carrier-phase integer ambiguity;

- T_d represents the tropospheric delay;

- I_d represents the ionospheric delay;

- ϵ_Φ represents the relevant measurement noise components including multipath.

15

2.6.3   Doppler Frequency Shift

The Doppler frequency shift is the frequency difference between the received signal and the source signal due to Doppler effect which is caused by the relative motion between the receiver and the satellite and the signal propagation medium.

In a GNSS receiver the Doppler frequency shift measurements, are usually obtained by sampling the frequency setting of the numerically controlled oscillator that tracks the phase of the incoming signal.

The Doppler frequency shift measurements relates to the carrier-phase measurements as its first order derivative with respect to time and it can be expressed as (scaled to velocity units):

$$D = \lambda f_d = \lambda \dot{\phi} = \dot{\rho} + c \cdot \left(\delta \dot{t}_{rcv} - \delta \dot{t}_{sat} \right) + \dot{T}_d - \dot{I}_d + \dot{\epsilon}_\Phi \tag{2.4}$$

where:

- $\dot{\rho}$ represents the geometric range change-rate between the satellite and the receiver;

- $\delta \dot{t}_{rcv}$ represents the receiver clock drift from the respective GNSS time-scale;

- $\delta \dot{t}_{sat}$ represents the satellite clock drift from the respective GNSS time-scale;

- $\dot{T}_d$ represents the tropospheric delay change-rate;

- $\dot{I}_d$ represents the ionospheric delay change-rate;

- $\dot{\epsilon}_\Phi$ represents the relevant measurement noise components including multipath change-rate.

Compared to the carrier-phase measurements, its noticeable that Doppler frequency shift measurements are free of integer ambiguity problems, and in general this measurements are much *cleaner* than the carrier-phase measurements as its errors and uncertainties are derivatives in time.

The Doppler frequency shift measurements also relates to the receiver–satellite mutual motion, as mentioned earlier, and this relationship can be expressed as (scaled to velocity units), [13]:

$$D = \lambda f_d = \vec{n} \cdot \left(\vec{v}_{sat} - \vec{v}_{rcv} \right) + c \cdot \left(\delta \dot{t}_{rcv} - \delta \dot{t}_{sat} \right) + \dot{T}_d - \dot{I}_d + \dot{\epsilon}_\Phi \tag{2.5}$$

where:

- $\vec{n}$ represents the directional cosine vector pointing from the receiver (x, y, z) to the satellite (X_s, Y_s, Z_s), and is defined as:

$$\vec{n} = \left(\frac{x - X_s}{\rho}, \frac{y - Y_s}{\rho}, \frac{z - Z_s}{\rho} \right) \tag{2.6}$$

- $\delta \dot{t}_{rcv}$ represents the receiver clock drift from the respective GNSS time-scale;

- $\delta \dot{t}_{sat}$ represents the satellite clock drift from the respective GNSS time-scale;

- $\dot{T}_d$ represents the tropospheric delay change-rate;

- $\dot{I}_d$ represents the ionospheric delay change-rate;

- $\dot{\epsilon}_\Phi$ represents the relevant measurement noise components including multipath change-rate.

Due to its properties the Doppler frequency shift measurements are useful to estimate the receiver velocity and they can also be used to detected and repair cycle-slips in the carrier-phase measurements.

2.7 Dilution of Precision

The term Dilution of Precision (DOP) is used to specify the multiplicative effect of the visible GNSS constellation geometry on solution precision. Following the example on figure 2.7, the concept of DOP can be illustrated as:
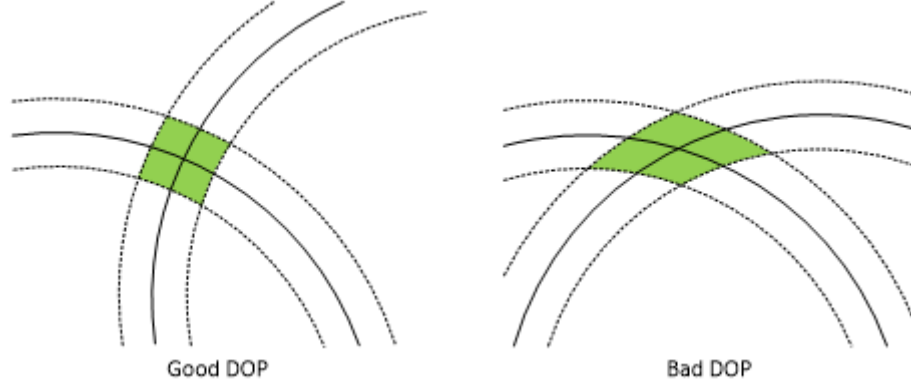
Figure 2.13: Effects of satellite geometry

When the visible GNSS satellites are close together in the sky, its geometry is designated as weak and the respective DOP value is high, and when the visible GNSS satellites are spread apart in the sky its geometry is designated as strong the respective DOP value is low.

The combination of multiple GNSS constellations, increases the number of visible satellites and consequently improves the solution DOP. This is especially important for applications where the view of the sky is partially obscured by surroundings.

Depending on the requirements of the application, some solutions may have to be discarded due to weak geometry of the visible satellites, the following table presents the DOP values range and their meaning:

DOP	Rating	Description
1	Ideal	Highest possible confidence level
$1-2$	Excellent	At this level of DOP, the most precise solutions are obtained
$2-5$	Good	Represents the bare minimum for sensitive applications
$5-10$	Moderate	Represents the requirements for most applications
$10-20$	Fair	Should be used only to provide rough position estimations
>20	Poor	At this level of DOP the solution should be discarded

Table 2.5: DOP meaning

DOP Determination

The DOP for n visible satellites can be determined by, [14]:

$$H = \begin{bmatrix} \dfrac{x - X_{s,1}}{\rho} & \dfrac{y - Y_{s,1}}{\rho} & \dfrac{z - Z_{s,1}}{\rho} & 1 \\ \dfrac{x - X_{s,2}}{\rho} & \dfrac{y - Y_{s,2}}{\rho} & \dfrac{z - Z_{s,2}}{\rho} & 1 \\ \vdots & \vdots & \vdots & \vdots \\ \dfrac{x - X_{s,n}}{\rho} & \dfrac{y - Y_{s,n}}{\rho} & \dfrac{z - Z_{s,n}}{\rho} & 1 \end{bmatrix} \qquad (2.7)$$

$$\mathbf{DOP} = \sqrt{\text{trace}\left[\left(H^T \cdot H\right)^{-1}\right]} \qquad (2.8)$$

where:

- $X_{s,i}$, $Y_{s,i}$, $Z_{s,i}$ are the satellite coordinates.

- x, y and z are the receiver coordinates.

2.8   Accuracy and Precision

Accuracy and precision are two important metrics to measure the quality of the estimation process, [15]:

- Accuracy refers to the degree of how close are the position estimations from the true position and it can be evaluated statistical by the mean or the root mean square of the obtained estimates relative to the true position.

- Precision refers to the degree of how close together are the position estimations and it can be evaluated statistical by standard deviation of the obtained estimates.
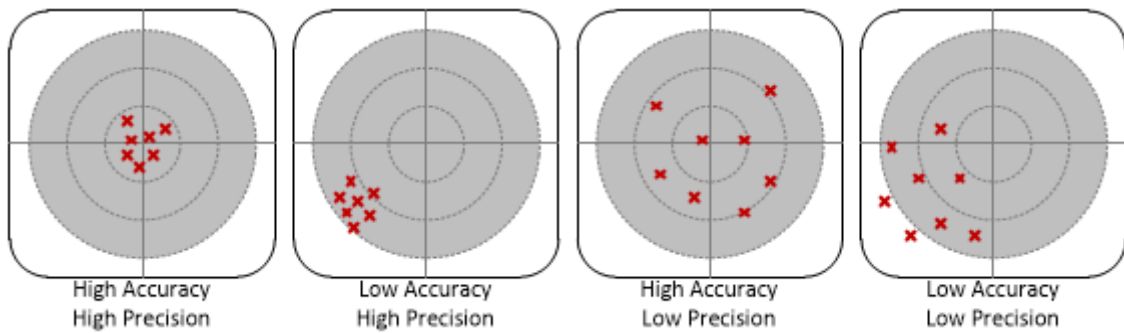
Figure 2.14: Accuracy and Precision

Chapter 3

Combining GPS and GLONASS

3.1 Introduction

As both GPS and GLONASS were designed for military only purposes, issues related to the combined use of GPS and GLONASS were not taken into account in their original design. However when both systems became available to civilian use, it became clear that a GPS+GLONASS receiver could outperform a GPS-only or GLONASS-only receiver, if the major interoperability issues were resolved. Since then many studies and investigations were conducted and with the modernization of both systems, these issues have been resolved at sufficient level for practical use of a GPS+GLONASS receiver.

In this chapter, the different reference frames (coordinate system, geodetic datums and time-scale) employed by GPS and GLONASS will be discussed along with methods to combine them; finally the different algorithms to determine the satellite orbital positions and velocities are presented.

3.2 Coordinate Systems

In order to formulate and solve the satellite navigation problem, it is necessary to choose a coordinate system in which both the states of the satellites positions/velocities and the receiver position/velocity can be represented.

Both GPS and GLONASS use its own coordinate system to define its satellite orbits and its own geodetic datum that maps the coordinates into the Earth's surface; GPS uses the World Geodetic System 1984 (WGS-84) and GLONASS uses the Parameters of the Earth 1990 (PZ-90.02) which are defined in a very similar way.
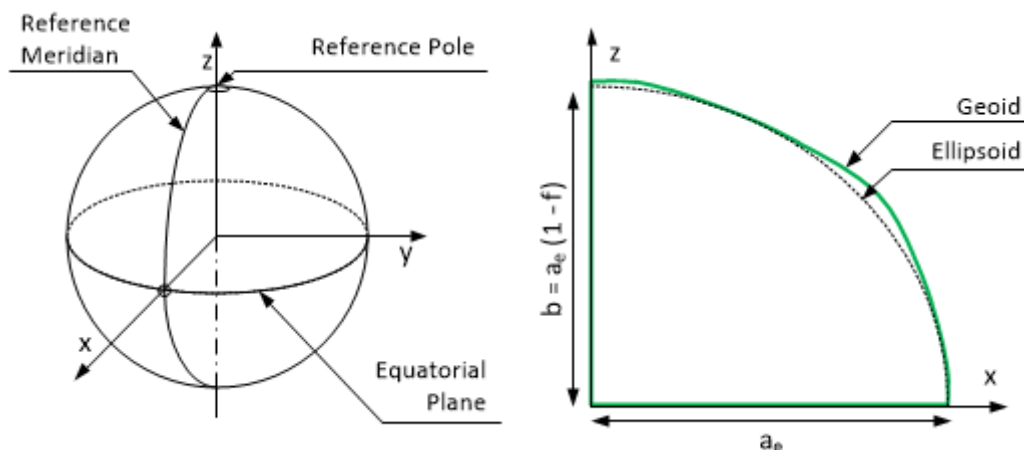
Figure 3.1: Coordinate system and ellipsoid

3.2.1 GPS – WGS-84

The WGS-84 is an ECEF coordinate system and geodetic datum used by GPS and it is a refined realization of World Geodetic System 1972 (WGS-72) inherited from the GPS predecessor, the U.S. Navy Transit.

The WGS-84 ECEF coordinate system is defined as, [11]:

- Origin in the Earth's center of mass;

- Z-axis in the direction of the International Earth Rotation and Reference Systems Service (IERS) reference pole;

- X-axis is the intersection of the IERS reference meridian and the plane passing by origin and normal to the Z-axis;

- Y-axis completes a right-handed orthogonal coordinate system;

and its geodetic parameters are presented in table 3.1.

Parameter	Value
Earth's rotation rate ($\omega_\oplus$)	$7.2921151467 \cdot 10^{-5}$
Earth's gravitational constant[1] ($\mu_\oplus$)	$3.986005 \cdot 10^{14}$
Semi-major axis ($a_\oplus$)	6378137
Flattening ($f_\oplus$)	1 / 298.256223563
2nd zonal harmonic (C_{20})	$-484.16685 \cdot 10^{-6}$

Table 3.1: Geodetic parameters of WGS-84 datum

3.2.2 GLONASS – PZ-90.02

The PZ-90.02 is an ECEF coordinate system and geodetic datum used by GLONASS. GLONASS originally used the Soviet Geodetic System 1985 (SGS-85) inherited from its predecessor the Tsiklon which its realization was later refined into the SGS-90. After the collapse of the U.S.S.R., the SGS-90 was renamed to Parameters of the Earth 1990 (PZ-90) maintaining its definitions and realization.

In 2007 as part of the GLONASS interoperability and modernization plan, PZ-90 definitions and realization were altered to match the International Terrestrial Reference Frame (ITRF) definitions [16], resulting in the PZ-90.02.

Currently the PZ-90.02 ECEF coordinate system is defined as, [7]:

- Origin in the Earth's center of mass;

- Z-axis in the direction of the IERS reference pole;

- X-axis in the direction of the point of intersection of the Earth's equatorial plane and the zero meridian established by Bureau International de l'Heure (BIH);

- Y-axis completes a right-handed orthogonal coordinate system;

---

[1]The actual value for WGS-84 Earth's gravitational constant is $3.986004418 \cdot 10^{14}$, but the GPS Control Segment still uses the old value of $3.986005 \cdot 10^{14}$ for orbit propagation, to maintain compatibility with older equipments

and its geodetic parameters are presented in table 3.2.

Parameter	Value
Earth's rotation rate ($\omega_\oplus$)	$7.292115 \cdot 10^{-5}$
Earth's gravitational constant ($\mu_\oplus$)	$3.986004 \cdot 10^{14}$
Semi-major axis ($a_\oplus$)	6378136
Flattening ($f_\oplus$)	1 / 298.25784
2nd zonal harmonic (C_{20})	$1082625.75 \cdot 10^{-9}$

Table 3.2: Geodetic parameters of PZ-90.02 datum

3.2.3 Combining the coordinate systems

Although their definitions are very similar, each coordinate system employs a different set of reference stations in its realization and, therefore the WGS-84 coordinates of an arbitrary location may not correspond to its PZ-90.02 coordinates.

When solving the satellite navigation problem, the resulting receiver position will be expressed in the same coordinate system as the satellites used, meaning if only GPS satellites were used the result will be expressed in WGS-84 coordinates and likewise if only GLONASS satellites were used the result will be expressed in PZ-90.02 coordinates.

If GPS satellites and GLONASS satellites are used without taking into account the differences its coordinate systems realizations, the result will be less accurate and will be expressed in an undefined coordinate system. To combine both systems one of the following options must be applied:

1. All WGS-84 GPS satellites positions are transformed into PZ-90.02;

2. All PZ-90.02 GLONASS satellites positions are transformed into WGS-84.

Usually the second option is the most common as the WGS-84 coordinate system is more widely adopted than the PZ-90.02.

Prior to September 20th, 2007 the combination of both coordinate systems wasn't officially defined and the lack of official publications by the Russian Military Space Forces on PZ-90, made very difficult the combination of both systems. Many groups of scientists tried independently to determinate a set of transformation parameters, but usually these would differ as much their methodologies to obtain them [17].

- **Helmert transformation**

The Helmert transformation (also known as 7-parameter transformation) is a similarity transformation method used in geodesy to convert from a datum to another:

$$\begin{bmatrix} x \\ y \\ z \end{bmatrix}_{\text{Datum 1}} = \begin{bmatrix} \Delta x \\ \Delta y \\ \Delta z \end{bmatrix} + (1 + \delta s) \begin{bmatrix} 1 & \delta\omega & -\delta\psi \\ -\delta\omega & 1 & \delta\epsilon \\ \delta\psi & -\delta\epsilon & 1 \end{bmatrix} \begin{bmatrix} x \\ y \\ z \end{bmatrix}_{\text{Datum 2}} \tag{3.1}$$

where:

- $\Delta x, \Delta y, \Delta z$ are the origin shift between the coordinate systems;
- $\delta\epsilon, \delta\psi, \delta\omega$ are the rotations which establish parallelism between the coordinate systems;
- δs is the scale factor between the coordinate systems.

	Δx	Δx	Δy	$\delta\epsilon$	$\delta\psi$	$\delta\omega$	δs
Boykov et al., 1993	0	0	1.5	0	0	-0.076	0
Mitrikas et al., 1998	-0.47	-0.51	-2	-0.002	-0.001	-0.356	$22 \cdot 10^{-9}$
Bazlov et al., 1999	-1.1	-0.3	-0.9	0	0	-0.169	$-12 \cdot 10^{-8}$
Misra & Abbot, 1994	0	0	4	0	0	-0.6	0
Misra et al., 1996	0	2.5	0	0	0	0.4	0
Cook, 1997	0	0	0	0	0	-0.33	0
Roßbach et al., 1996	0	0	0	0	0	-0.33	0

Table 3.3: Previous transformations between PZ-90 and WGS-84 [17]

However, after September 20th, 2007 all operational GLONASS satellites switched to PZ-90.02 which its transformation to WGS-84 is officially defined as, [16, 3]:

$$
\begin{bmatrix} x \\ y \\ z \end{bmatrix}_{WGS-84} = \begin{bmatrix} x \\ y \\ z \end{bmatrix}_{PZ-90.02} + \begin{bmatrix} -0.36 \\ 0.08 \\ 0.18 \end{bmatrix}
\tag{3.2}
$$

This switch represents an huge improvement in terms of interoperability between GPS and GLONASS [3] as depicted in figure 3.2.
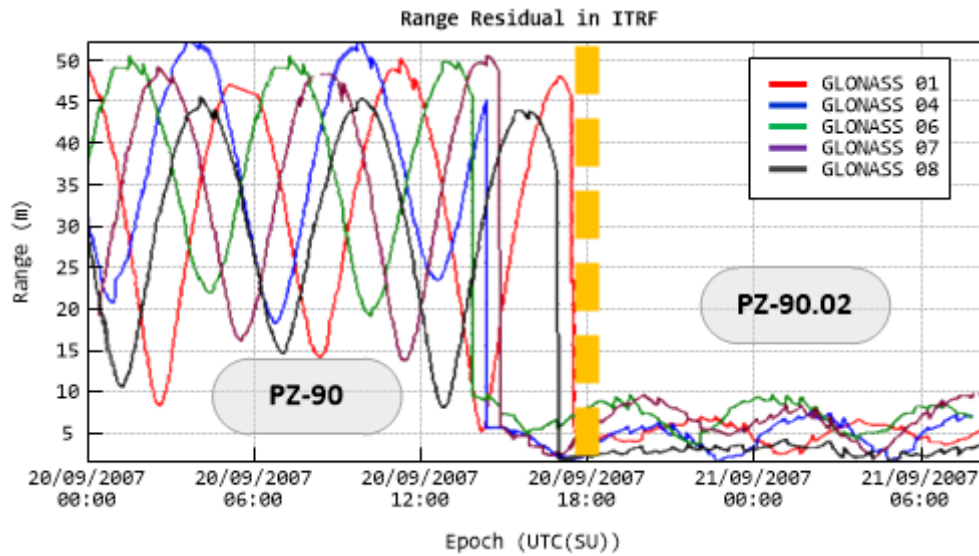
Figure 3.2: PZ-90 to PZ-90.02 update impact

3.3 Time-Scales

In the same way that a common coordinate system is required to solve the satellite navigation problem, it's also necessary a common time-scale or time reference to determine the signal travelling time.

Both GPS and GLONASS defines its own time-scale which is closely tied to the UTC time-scale, and in order to accurately estimate the user position, the receiver must be able to synchronize its internal clock with the current GNSS time-scale.

When combining multiple GNSS's systems, the receiver must be able to synchronize each GNSS measurement with its respective time scale and, therefore it's necessary to know or estimate the offsets between the receiver internal clock and the GNSS's time-scales.

The following figure depicts the current differences between the UTC time-scale, GPS time-scale, GLONASS time-scale and International Atomic Time (TAI) time-scale:
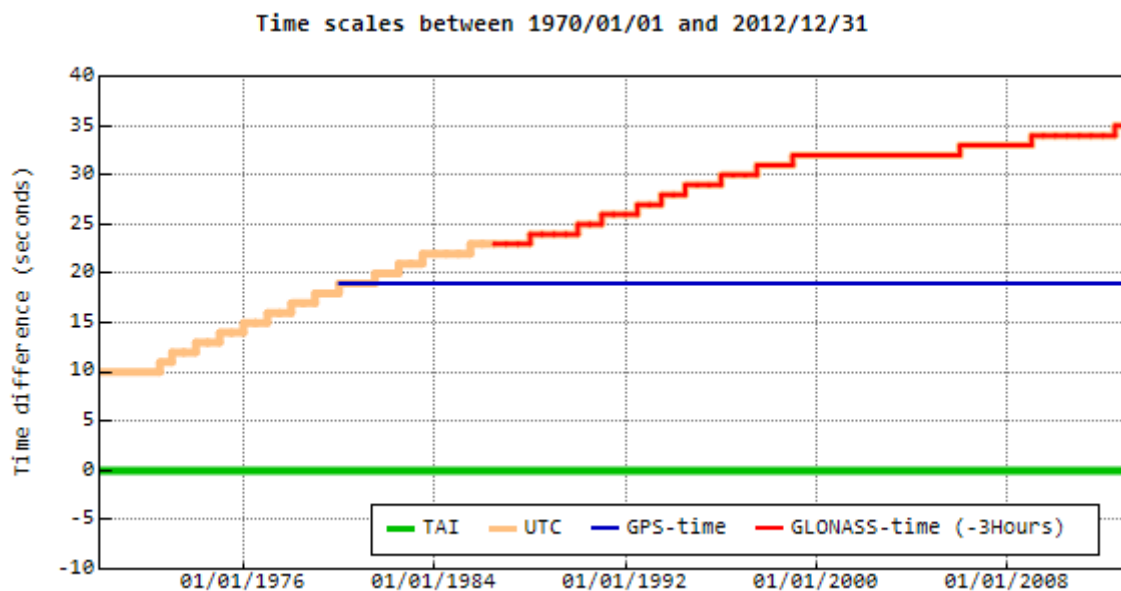
Figure 3.3: Time scales differences

3.3.1 GPS Time-scale

The GPS time-scale is maintained by the GPS Master Control Center, it started coincident with the UTC(USNO) time-scale maintained by U.S. Naval Observatory at 6th January, 1980 (00:00 hours), but was kept as continuous time scale so it doesn't account for leap seconds later introduced to the UTC time-scale (as of August 2012, 16 leap seconds were added).

Additional offsets between the GPS time-scale and the UTC(USNO) time-scale are kept in the order of a few nanoseconds by the GPS Control Segment [11].

The GPS time-scale is represented in its navigation message by:

- GPS Week Number – Number of weeks since January 6, 1980 (WN)[2];

- GPS Time of Week – Number of seconds within the GPS Week (TOW).

---

[2]Most instances of the WN in the GPS navigation message, may not reflect the current full GPS Week Number [11]

3.3.2 GLONASS Time-scale

The GLONASS time-scale maintained by GLONASS Central Clock, being coincident with Moscow Time UTC(SU) (UTC+03:00 hours)[3]and unlike GPS time-scale, the GLONASS time-scale isn't continuous and accounts for the leap seconds introduced to the UTC time-scale by the IERS.

Again additional offsets between the GLONASS time-scale and the UTC time-scale are kept in the order of a few nanoseconds by the GLONASS Control Segment [7].

The GLONASS time-scale is represented in its navigation message by:

- GLONASS Day Number – Number of days since last leap year (N_T);

- GLONASS Time of Day – Number of seconds within the GLONASS day (t).

Since the GLONASS time-scale isn't continuous, it is necessary that the receiver has knowledge of forthcoming additions of leap seconds to the time-scale in order to guarantee that no interruption will occur during the estimation of one's PVT.

GLONASS provides information about forthcoming additions of leap seconds up to eight weeks prior to correction in its navigation message (word KP) [7]:

KP value	Description
00	No leap seconds corrections will occur in the end of the current quarter
01	A positive leap second will be added in the end of the current quarter
11	A negative leap second will be added in the end of the current quarter
10	No information is currently available

Table 3.4: GLONASS Forthcoming leap seconds information

GPS time-scale to GLONASS time-scale offset

As mentioned in section 2.3, the GLONASS navigation message also provides the fractional part of the offset between the GLONASS time-scale and GPS time-scale, allowing the users to combining both system more effectively, [7]:

$$t_G - t_R = \Delta T + \tau_{GPS} \tag{3.3}$$

where:

- t_G is the time described in the GPS time scale;

- t_R is the time described in the GLONASS time scale;

- ΔT is the integer part of the offset between the two time-scales, and is defined by:

$$\Delta T = 3^h\,00^m\,00^s + \Delta T_{LS,GPS} \tag{3.4}$$

and $\Delta T_{LS,GPS}$ is the current leap seconds offset between the GPS time-scale and the UTC time-scale determined from parameters provided in the GPS navigation message;

- τ_{GPS} is the fractional part of the offset between the two time-scales provided in the GLONASS navigation message.

---

[3]In 27th March, 2011 the Moscow time was defined to UTC+04:00 hours, but GLONASS still employs the older definition of UTC+03:00 for compatibility reasons

3.3.3 Combining the Time-Scales

As mentioned in section 2.5.4, the receiver clock offset must be estimated together with the receiver position, therefore a straight forward approach to combine the GPS time-scale with the GLONASS time-scale is to estimate the clock offsets with two time-scales separately, however as drawback of this approach is that an additional visible satellite is required to solve the satellite navigation problem.

Another approach is to estimate the clock offset with either the GPS time-scale or the GLONASS time-scale, and use the relationship defined in equation 3.3, to get the other clock offset [17]. The drawback of this approach is that when the parameters of one of the GNSS constellations are updated (namely satellite clock offset corrections) by the Control Segment, it may cause small discontinuities in the time-scale [18] as depicted in the following figures:
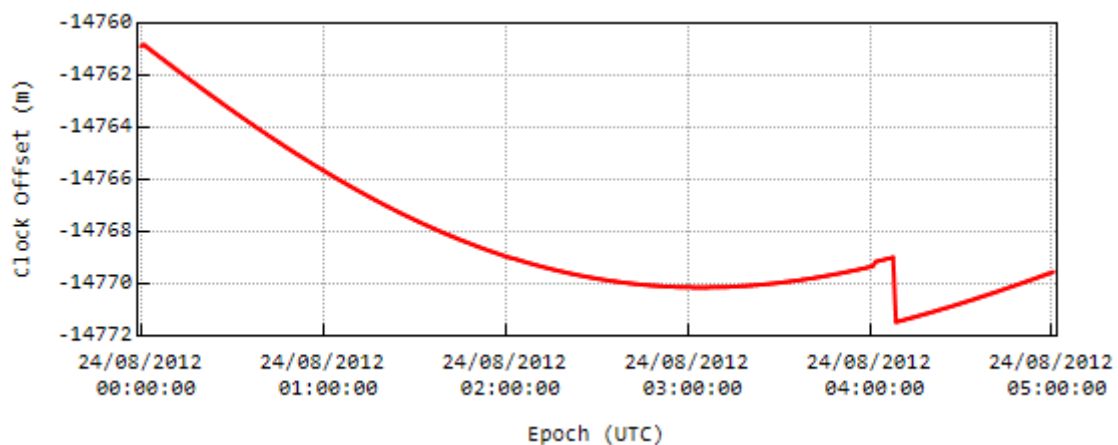
Figure 3.4: Satellite clock offset (GPS 10)
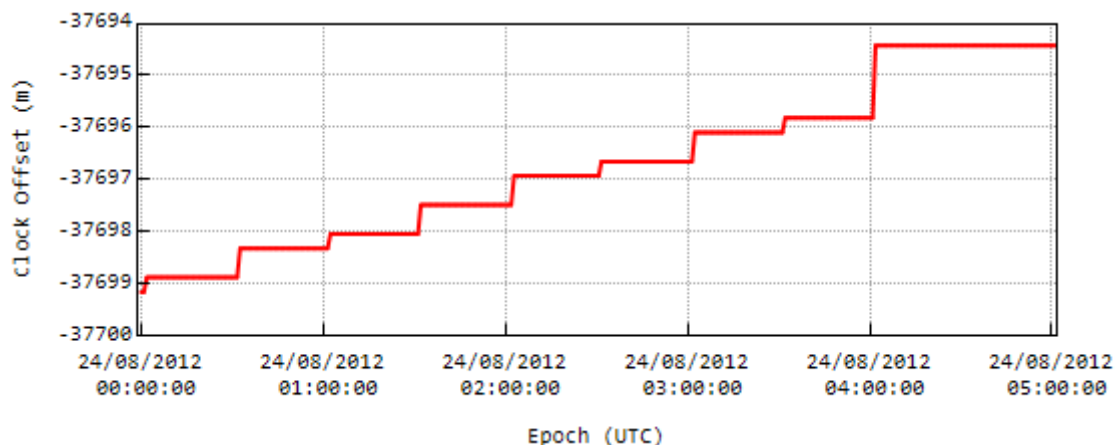
Figure 3.5: Satellite clock offset (GLONASS 03)

These discontinuities are usually absorbed into the estimate of the receiver clock offset along with un-calibrated hardware delays. By using only one receiver clock offset, the discontinuities affecting only one of the constellations will be propagated to the other constellation thus degrading the overall quality of the solution.

The first approach is preferred to the second at least for autonomous real-time applications, as its drawback has far less impact in the final solution because the combination of GPS and GLONASS constellations practically doubles the number of visible satellites.

25

3.4 Satellite orbit determination

Finally to solve the satellite navigation problem, it's necessary to know the satellite orbits (namely their positions and in some cases their velocities). These can be determined using the information provided by the satellite navigation message.

Each satellite transmits in its navigation message two sets of parameters:

- Ephemeris parameters which allows the users to determine the satellite position, velocity and clock offset for short intervals of time around their reference time (in order of minutes/hours); they are used to solve the satellite navigation problem.

- Almanac parameters which allows the users to determine the satellite position, velocity and clock offset with decreased accuracy but valid for longer intervals (in order of days/months); they are used to select witch satellites should be tracked and to plan satellite observations.

Examples of the application of the algorithms described in this section are presented in appendix C.

3.4.1 GPS – Orbit determination

From the Ephemeris parameters

The GPS ephemeris parameters consists in a set of Keplerian orbital elements and their perturbation factors that describes the satellite osculating orbit at a reference time (t_{oe}). These ephemeris parameters are usually updated every 2 to 4 hours intervals (depending on the GPS Control Segment).

Parameter	Description
t_{oe}	Reference time in seconds of GPS Week
$\sqrt{A}$	Square root of semi-major axis
e	Eccentricity
M_0	Mean anomaly at reference time
ω	Argument of perigee
i_0	Inclination at reference time
Ω_0	Longitude of ascending node at reference time
δn	Mean motion difference
$\dot{i}$	Rate of inclination
$\dot{\Omega}$	Rate of node's right ascension
c_{uc}, c_{us}	Latitude argument correction
c_{rc}, c_{rs}	Orbital radius correction
c_{ic}, c_{is}	Orbital inclination correction

Table 3.5: GPS Ephemeris parameters

The GPS satellite position coordinates at an instant t (seconds within the ephemeris GPS Week), are determined according to the following algorithm, [11]:

- Time from transmission to ephemeris reference time:

$$t_k = \begin{cases} t - t_{oe} - 604800 & \text{if} \quad t - t_{oe} > 302400 \\ t - t_{oe} + 604800 & \text{if} \quad t - t_{oe} < -302400 \\ t - t_{oe} & \text{otherwise} \end{cases} \tag{3.5}$$

26

– Mean anomaly, eccentric anomaly, true anomaly and argument of latitude:

$$M_k = M_0 + \left(\sqrt{\frac{\mu}{A^3}} + \Delta n \right) t_k \tag{3.6}$$

$$M_k = E_k - e \sin E_k \qquad \text{(solved iteratively)} \tag{3.7}$$

$$\nu_k = \tan^{-1} \left\{ \frac{\sqrt{1 - e^2} \sin E_k / \left(1 - e \cos E_k \right)}{\left(\cos E_k - e \right) / \left(1 - e \cos E_k \right)} \right\} \tag{3.8}$$

$$\Phi_k = \nu_k + \omega \tag{3.9}$$

– Second harmonic orbital perturbations (argument of latitude, radius and inclination):

$$\delta u_k = c_{us} \sin 2\Phi_k + c_{uc} \cos 2\Phi_k \tag{3.10}$$

$$\delta r_k = c_{rs} \sin 2\Phi_k + c_{rc} \cos 2\Phi_k \tag{3.11}$$

$$\delta i_k = c_{is} \sin 2\Phi_k + c_{ic} \cos 2\Phi_k \tag{3.12}$$

– Corrected argument of latitude, corrected radius, corrected inclination and corrected longitude of ascending node:

$$u_k = \Phi_k + \delta u_k \tag{3.13}$$

$$r_k = A(1 - e \cos E_k) + \delta r_k \tag{3.14}$$

$$i_k = i_0 + \delta i_k + \dot{i} t_k \tag{3.15}$$

$$\Omega_k = \Omega_0 + \left(\dot{\Omega} - \omega_\oplus \right) t_k - \omega_\oplus t_{oe} \tag{3.16}$$

– Satellite position in the orbital plane:

$$x_k' = r_k \cos u_k \tag{3.17}$$

$$y_k' = r_k \sin u_k \tag{3.18}$$

– Satellite position in WGS-84 coordinate system:

$$x_k = x_k' \cos \Omega_k - y_k' \cos i_k \sin \Omega_k \tag{3.19}$$

$$y_k = y_k' \sin \Omega_k + y_k' \cos i_k \sin \Omega_k \tag{3.20}$$

$$z_k = y_k' \sin i_k \tag{3.21}$$

The GPS Interface Specification [11] doesn't provide an algorithm to explicitly determine the satellite velocity, however it can be obtained by derivation of the previous equations according to the following algorithm [19]:

– Derivatives of the mean anomaly, eccentric anomaly and argument of latitude:

$$\dot{M}_k = \left(\sqrt{\frac{\mu}{A^3}} + \Delta n \right) \tag{3.22}$$

$$\dot{E}_k = \frac{\dot{M}_k}{1 - e \cos E_k} \tag{3.23}$$

$$\dot{\Phi}_k = \dot{E}_k \sin E_k \frac{1 + e \cos \Phi_0}{\sin \Phi_0 \left(1 - e \cos E_k \right)} \tag{3.24}$$

– Derivatives of the corrected argument of latitude, corrected radius, corrected inclination and corrected longitude of ascending node:

$$\dot{u}_k = \dot{\Phi}_k + 2\dot{\Phi}_k \left(c_{us} \cos 2u_k - c_{uc} \sin 2u_k \right) \tag{3.25}$$

$$\dot{r}_k = A \frac{e \dot{M}_k \sin E_k}{1 - e \cos E_k} + 2\dot{\Phi}_k \left(c_{rs} \cos 2u_k - c_{rc} \sin 2u_k \right) \tag{3.26}$$

$$\dot{i}_k = \dot{i} + 2\dot{\Phi}_k \left(c_{is} \cos 2u_k - c_{ic} \sin 2u_k \right) \tag{3.27}$$

$$\dot{\Omega}_k = \dot{\Omega} - \omega_\oplus \tag{3.28}$$

– Satellite velocity in the orbital plane:

$$\dot{x}'_k = \dot{r}_k - y'_k \dot{u}_k \tag{3.29}$$

$$\dot{y}'_k = \dot{r}_k + x'_k \dot{u}_k \tag{3.30}$$

– Satellite velocity in WGS-84 coordinate system:

$$\dot{x}_k = \left(\dot{x}'_k - y'_k \dot{\Omega}_k \cos i_k\right) \cos \Omega_k - \left(x'_k \dot{\Omega}_k + \dot{y}'_k \cos i_k - y'_k \dot{i}_k \sin i_k\right) \sin \Omega_k \tag{3.31}$$

$$\dot{y}_k = \left(\dot{x}'_k - y'_k \dot{\Omega}_k \cos i_k\right) \sin \Omega_k + \left(x'_k \dot{\Omega}_k + \dot{y}'_k \cos i_k - y'_k \dot{i}_k \sin i_k\right) \cos \Omega_k \tag{3.32}$$

$$\dot{z}_k = \dot{y}'_k \sin i_k + y'_k \dot{i}_k \cos i_k \tag{3.33}$$

From the Almanac parameters

The GPS almanac parameters are a sub-set of the GPS ephemeris parameters, therefore the same algorithms can be applied to determine the satellite position and velocity [11, 19] (absent parameters are considered as zero).

Parameter	Description
WN_a	Reference time in GPS Weeks
t_{oa}	Reference time in seconds of GPS Week
$\sqrt{A}$	Square root of semi-major axis
e	Eccentricity
M_0	Mean anomaly at reference time
ω	Argument of perigee
Δi	Inclination deviation from nominal value
Ω_0	Longitude of ascending node at reference time
$\dot{\Omega}$	Rate of node's right ascension

Table 3.6: GPS Almanac parameters

3.4.2 GLONASS – Orbit determination

From the Ephemeris parameters

The GLONASS ephemeris parameters consists in a set of geocentric Cartesian coordinates and their derivatives at a reference time (t_b). These ephemeris parameters are usually updated every 30 minutes and are referred to the center of this 30 minutes interval.

Parameter	Description
t_b	Reference time in seconds of GLONASS Day
x, y, z	Satellite position at reference time
v_x, v_y, v_z	Satellite velocity at reference time
X'', Y'', Z''	Sun and Moon accelerations at reference time

Table 3.7: GLONASS Ephemeris parameters

Unlike GPS, GLONASS doesn't use close analytical formulae for determine its satellites orbits, being necessary to apply a numerical integration technique.
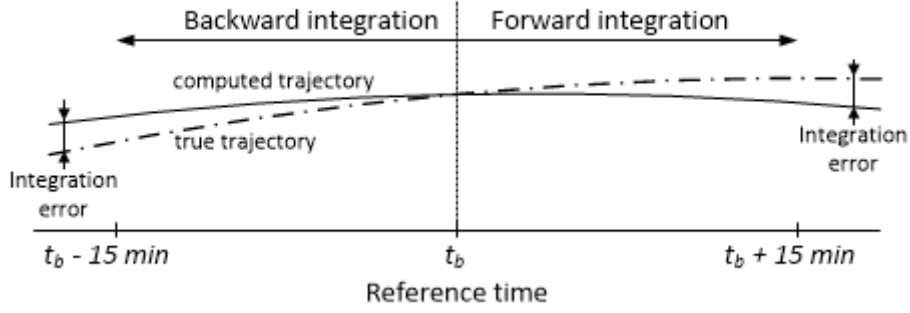
Figure 3.6: Integration process

The Fourth-order Runge–Kutta (RK4) is the integration method recommended by GLONASS Interface Control Document [7], to determine the GLONASS satellites orbits, and this is done by:

– Defining an initial value problem as follows:

$$y_0 = (x, y, z, v_x, v_z, v_z)$$ (3.34)

$$\dot{y} = f(t, y)$$ (3.35)

– The RK4 method for this problem is given by the following equations, [20]:

$$y_{n+1} = y_n + \frac{1}{6}(k_1 + 2k_2 + 2k_3 + k_4)$$ (3.36)

$$t_{n+1} = t_n + h$$ (3.37)

– Where h is the integration step, y_{n+1} is RK4 approximation of $y(t_{n+1})$ and:

$$k_1 = h \cdot f(t_n, y_n)$$ (3.38)

$$k_2 = h \cdot f(t_n + \frac{1}{2}h, y_n + \frac{1}{2}k_1)$$ (3.39)

$$k_3 = h \cdot f(t_n + \frac{1}{2}h, y_n + \frac{1}{2}k_1)$$ (3.40)

$$k_4 = h \cdot f(t_n + h, y_n + k_3)$$ (3.41)

– And $f(t, y)$ is derived from the Newton's Laws of motion in an Earth-Centered Inertial (ECI) referential, taking into account the Coriolis effect due to the Earth's rotation[4], [7, 17]:

$$\frac{dx}{dt} = v_x$$ (3.42)

$$\frac{dy}{dt} = v_y$$ (3.43)

$$\frac{dz}{dt} = v_z$$ (3.44)

$$\frac{v_x}{dt} = -\frac{\mu}{r^3}x - \frac{3}{2}C_{20}\frac{\mu a_e^2}{r^5}x\left(1 - \frac{5z^2}{r^2}\right) + \omega_E^2 x + 2\omega_E v_y + X''$$ (3.45)

$$\frac{v_y}{dt} = -\frac{\mu}{r^3}y - \frac{3}{2}C_{20}\frac{\mu a_e^2}{r^5}y\left(1 - \frac{5z^2}{r^2}\right) + \omega_E^2 y - 2\omega_E v_x + Y''$$ (3.46)

$$\frac{v_z}{dt} = -\frac{\mu}{r^3}z - \frac{3}{2}C_{20}\frac{\mu a_e^2}{r^5}z\left(3 - \frac{5z^2}{r^2}\right) + Z''$$ (3.47)

r represents the orbital radius defined as $r = \sqrt{x^2 + y^2 + z^2}$, and the Sun and Moon accelerations (X'', Y'', Z''), are considered constant during the integration interval $(t_b \pm 15$ minutes$)$.

---

[4]In the English version of the GLONASS – Interface Control Document, contains erros in the equations for $\frac{v_y}{dt}$ and $\frac{v_z}{dt}$.

29

- **Integration Step**

When implementing the RK4 integration method, the accuracy of the computed satellite position and velocity will depend of the size of the integration step (h), which isn't defined by the GLONASS Interface Control Document [7]. It is expected that the accuracy of the position and velocity increases with the reduction of the integration step. On the other hand the reduction of the integration step will increase the computational load of the determination the satellite position and velocity.

To assess the influence of the integration step, over 1200 pairs of adjacent ephemeris were integrated (backward and forward), and their final positions/velocities were compared, the results are summarized in table 3.8 and 3.9.

Step $[s]$	$\overline{|\Delta x|}$ $[m]$	$\overline{|\Delta y|}$ $[m]$	$\overline{|\Delta z|}$ $[m]$	σ_x^2	σ_y^2	σ_z^2
1	0.498	0.498	0.544	0.169	0.184	0.152
10	0.498	0.498	0.544	0.169	0.184	0.152
30	0.498	0.498	0.544	0.169	0.184	0.152
60	0.498	0.498	0.544	0.169	0.184	0.152
90	0.497	0.498	0.544	0.169	0.184	0.152
120	0.496	0.497	0.542	0.169	0.184	0.151
150	0.492	0.495	0.539	0.168	0.184	0.150
225	0.478	0.491	0.518	0.166	0.186	0.145
450	1.674	1.664	0.947	1.232	1.230	0.400
675	6.450	6.325	4.153	18.134	15.481	2.775
900	27.388	26.844	18.154	331.527	270.019	46.996

Table 3.8: Position integration error with different integration steps

Step $[s]$	$\overline{|\Delta v_x|}$ $[m/s]$	$\overline{|\Delta v_y|}$ $[m/s]$	$\overline{|\Delta v_z|}$ $[m/s]$	σ_{vx}^2	σ_{vy}^2	σ_{vz}^2
1	$1.281 \cdot 10^{-3}$	$9.020 \cdot 10^{-4}$	$1.148 \cdot 10^{-3}$	$8.328 \cdot 10^{-7}$	$4.603 \cdot 10^{-7}$	$6.851 \cdot 10^{-7}$
10	$1.281 \cdot 10^{-3}$	$9.020 \cdot 10^{-4}$	$1.148 \cdot 10^{-3}$	$8.328 \cdot 10^{-7}$	$4.603 \cdot 10^{-7}$	$6.851 \cdot 10^{-7}$
30	$1.281 \cdot 10^{-3}$	$9.020 \cdot 10^{-4}$	$1.148 \cdot 10^{-3}$	$8.328 \cdot 10^{-7}$	$4.603 \cdot 10^{-7}$	$6.851 \cdot 10^{-7}$
60	$1.281 \cdot 10^{-3}$	$9.020 \cdot 10^{-4}$	$1.148 \cdot 10^{-3}$	$8.329 \cdot 10^{-7}$	$4.603 \cdot 10^{-7}$	$6.852 \cdot 10^{-7}$
90	$1.281 \cdot 10^{-3}$	$9.021 \cdot 10^{-4}$	$1.148 \cdot 10^{-3}$	$8.329 \cdot 10^{-7}$	$4.603 \cdot 10^{-7}$	$6.854 \cdot 10^{-7}$
120	$1.281 \cdot 10^{-3}$	$9.022 \cdot 10^{-4}$	$1.149 \cdot 10^{-3}$	$8.329 \cdot 10^{-7}$	$4.605 \cdot 10^{-7}$	$6.859 \cdot 10^{-7}$
150	$1.282 \cdot 10^{-3}$	$9.026 \cdot 10^{-4}$	$1.149 \cdot 10^{-3}$	$8.331 \cdot 10^{-7}$	$4.609 \cdot 10^{-7}$	$6.873 \cdot 10^{-7}$
225	$1.285 \cdot 10^{-3}$	$9.058 \cdot 10^{-4}$	$1.154 \cdot 10^{-3}$	$8.345 \cdot 10^{-7}$	$4.631 \cdot 10^{-7}$	$6.964 \cdot 10^{-7}$
450	$1.426 \cdot 10^{-3}$	$1.061 \cdot 10^{-3}$	$1.260 \cdot 10^{-3}$	$9.431 \cdot 10^{-7}$	$5.939 \cdot 10^{-7}$	$9.419 \cdot 10^{-7}$
675	$2.352 \cdot 10^{-3}$	$2.143 \cdot 10^{-3}$	$1.827 \cdot 10^{-3}$	$2.188 \cdot 10^{-6}$	$1.690 \cdot 10^{-6}$	$2.179 \cdot 10^{-6}$
900	$8.029 \cdot 10^{-3}$	$7.854 \cdot 10^{-3}$	$5.229 \cdot 10^{-3}$	$2.034 \cdot 10^{-5}$	$2.041 \cdot 10^{-5}$	$1.749 \cdot 10^{-5}$

Table 3.9: Velocity integration error with different integration steps

The results show that until a step of about 40~50 seconds, the integration errors remain practically constant (practically independent from the integration step size), and that steps higher than 120 seconds should be avoided. Based on this results, to ease the computational load of the GLONASS

satellite orbit determination, a dynamic step scheme can be employed:

$$h = \begin{cases} 50 & \text{while } |t - t_b| > 50 \\ 10 & \text{while } |t - t_b| > 10 \\ 1 & \text{while } |t - t_b| > 1 \\ |t - t_b| & \text{otherwise} \end{cases} \tag{3.48}$$

In addition the intermediary positions and velocities obtained during the integration process to a given epoch t can be cached and used during the integration process for the next epochs to further ease the computational load.

From the Almanac parameters

The GLONASS almanac parameters consists in a set of modified Keplerian orbital parameters, and unlike GPS, the algorithm to determine a GLONASS satellite position and velocity from its almanac parameters is completely different from the algorithm used for its ephemeris parameters.

Parameter	Description
N_A	GLONASS Reference day
λ	Longitude of the ascending node
t_λ	Instant of the first ascending node passage within N_A
Δi	Inclination deviation from the nominal value
ΔT	Orbital period deviation from the nominal value
$\Delta T'$	Rate of change of the orbital period
ϵ	Orbit eccentricity
ω	Argument of perigee

Table 3.10: GLONASS Almanac parameters

The GLONASS satellite position and velocity for a given instant defined by t_i of day N_0 in the GLONASS time-scale is determined using the following algorithm, [7]:

– The satellite inclination and period of revolution:

$$i = 63° + \Delta i \tag{3.49}$$
$$T = 43200 + \Delta T \tag{3.50}$$

– The satellite orbit semi-major axis is determined iteratively:

$$a^{(n+1)} = \sqrt[3]{\left(\frac{T_{osc}^{(n+1)}}{2\pi}\right)^2 \mu_\oplus} \tag{3.51}$$

$$T_{osc}^{(n+1)} = T \left\{ 1 + \frac{3}{2} C_{20} \left(\frac{a_\oplus}{p^{(n)}}\right)^2 \left[\left(2 - \frac{5}{2}\sin^2 i\right) \frac{\left(1 - e^2\right)^{\frac{3}{2}}}{(1 + e\cos\omega)^2} + \frac{(1 + \cos-\omega)^3}{1 - e^2} \right] \right\}^{-1} \tag{3.52}$$

$$p^{(n)} = a^{(n)} \cdot \left(1 - e^2\right) \tag{3.53}$$

With an initial approximation of: $a^0 = \sqrt[3]{\left(\frac{T}{2\pi}\right)^2 \mu_\oplus}$

31

– The time of ascending node passage on k-orbital period ($t_{\lambda k}$) where the instant t_i is located ($|t_i - t_{\lambda k}| < T$) and its respective longitude λ_k is determined by[5]:

$$n = \frac{2\pi}{T} \tag{3.54}$$

$$\Omega' = \frac{3}{2} C_{20} \cdot n \left(\frac{a_\oplus}{a}\right)^2 \cos i \left(1 - \epsilon^2\right)^{-2} \tag{3.55}$$

$$t_* = t_i - t_\lambda + 86400(N_0 - N_A) \tag{3.56}$$

$$W = \left\lfloor \frac{t_*}{T} \right\rfloor \tag{3.57}$$

$$t_{\lambda k} = \left[t_\lambda + T \cdot W + \Delta T' \cdot W^2\right] \mod 86400 \tag{3.58}$$

$$\lambda_k = \lambda + \left(\Omega' - \omega_\oplus\right)\left(T \cdot W + \Delta T' \cdot W^2\right) \tag{3.59}$$

$$\Omega = \lambda_k + S0 + \omega_\oplus(t_{\lambda k} - 10800) \tag{3.60}$$

$S0$ is the mean sidereal time at Greenwich midnight of day N_0, algorithms to compute the sidereal time are presented in appendix A.

– The osculating elements (secular and periodic perturbations caused by the second zonal harmonic C_{20}) from the instant $t_{\lambda k}$ to the instant t_i are determined:

$$\delta a = \delta a^{(2)} - \delta a^{(1)} \tag{3.61} \qquad\qquad \delta\Omega = \delta\Omega^{(2)} - \delta\Omega^{(1)} \tag{3.64}$$

$$\delta h = \delta h^{(2)} - \delta h^{(1)} \tag{3.62} \qquad\qquad \delta i = \delta i^{(2)} - \delta i^{(1)} \tag{3.65}$$

$$\delta l = \delta l^{(2)} - \delta l^{(1)} \tag{3.63} \qquad\qquad \delta\bar{\lambda} = \delta\bar{\lambda}^{(2)} - \delta\bar{\lambda}^{(1)} \tag{3.66}$$

Using the following relationships:

$$\frac{\delta a^{(m)}}{a} = J\left(\frac{a_\oplus}{a}\right)^2 \left[2\left(1 - \frac{3}{2}\sin^2 i\right)\left(l\cos\bar{\lambda} + h\sin\bar{\lambda}\right) + \right.$$
$$\left. \sin^2 i\left(\frac{1}{2}h\sin\bar{\lambda} - \frac{1}{2}l\cos\bar{\lambda} + \cos 2\bar{\lambda} + \frac{7}{2}l\cos 3\bar{\lambda} + \frac{7}{2}\sin 3\bar{\lambda}\right)\right] \tag{3.67}$$

$$\delta h^{(m)} = J\left(\frac{a_\oplus}{a}\right)^2 \left[\left(1 - \frac{3}{2}\sin^2 i\right)\left(l \cdot n \cdot \tau + \sin\bar{\lambda} + \frac{3}{2}l\sin 2\bar{\lambda} - \frac{3}{2}h\cos 2\bar{\lambda}\right) - \right.$$
$$\frac{1}{4}\sin^2 i\left(\sin\bar{\lambda} - \frac{7}{3}\sin 3\bar{\lambda} + 5l\sin 2\bar{\lambda} - \frac{17}{2}l\sin 4\bar{\lambda} + \frac{17}{2}h\cos 4\bar{\lambda} + h\cos 2\bar{\lambda}\right) + \tag{3.68}$$
$$\left. \cos^2 i\left(l \cdot n \cdot \tau - \frac{1}{2}\sin 2\bar{\lambda}\right)\right]$$

$$\delta l^{(m)} = J\left(\frac{a_\oplus}{a}\right)^2 \left[\left(1 - \frac{3}{2}\sin^2 i\right)\left(-h \cdot n \cdot \tau + \cos\bar{\lambda} + \frac{3}{2}l\cos 2\bar{\lambda} + \frac{3}{2}h\sin 2\bar{\lambda}\right) - \right.$$
$$\frac{1}{4}\sin^2 i\left(-\cos\bar{\lambda} - \frac{7}{3}\cos 3\bar{\lambda} - 5h\sin 2\bar{\lambda} - \frac{17}{2}l\cos 4\bar{\lambda} - \frac{17}{2}h\sin 4\bar{\lambda} + l\cos 2\bar{\lambda}\right) + \tag{3.69}$$
$$\left. \cos^2 i\left(-h \cdot n \cdot \tau + \frac{1}{2}h\sin 2\bar{\lambda}\right)\right]$$

$$\delta\Omega^{(m)} = J\left(\frac{a_\oplus}{a}\right)^2 \cos i\left(n \cdot \tau - \frac{7}{2}l\sin\bar{\lambda} + \frac{5}{2}h\cos\bar{\lambda} + \frac{1}{2}\sin 2\bar{\lambda} + \frac{7}{6}l\sin 3\bar{\lambda} - \frac{7}{6}h\cos 3\bar{\lambda}\right) \tag{3.70}$$

$$\delta i^{(m)} = \frac{1}{2}J\left(\frac{a_\oplus}{a}\right)^2 \sin i\cos i\left(-l\cos\bar{\lambda} + h\sin\bar{\lambda} + \cos 2\bar{\lambda} + \frac{7}{3}l\cos 3\bar{\lambda} + \frac{7}{3}h\sin 3\bar{\lambda}\right) \tag{3.71}$$

$$\delta\bar{\lambda}^{(m)} = J\left(\frac{a_\oplus}{a}\right)^2 \left[2\left(1 - \frac{3}{2}\sin^2 i\right)\left(n \cdot \tau + \frac{7}{4}l\sin\bar{\lambda} - \frac{7}{4}h\cos\bar{\lambda}\right) + \right.$$
$$3\sin^2 i\left(-\frac{7}{24}h\cos\bar{\lambda} - \frac{7}{24}l\sin\bar{\lambda} - \frac{49}{72}h\cos 3\bar{\lambda} + \frac{49}{72}l\sin 3\bar{\lambda} + \frac{1}{4}\sin 2\bar{\lambda}\right) + \tag{3.72}$$
$$\left. \cos^2 i\left(n \cdot \tau + \frac{7}{2}l\sin\bar{\lambda} - \frac{5}{2}h\cos\bar{\lambda} - \frac{1}{2}\sin 2\bar{\lambda} - \frac{7}{6}l\sin 3\bar{\lambda} + \frac{7}{6}h\cos 3\bar{\lambda}\right)\right]$$

---

[5]The number of satellite revolutions (W) may need to be corrected by adding or subtracting revolutions, to ensure that the condition $|t_i - t_{\lambda k}| < T$ remains valid

where:

$$E = 2\tan^{-1}\left(\sqrt{\frac{1-\epsilon}{1+\epsilon}}\tan\frac{-\omega}{2}\right) \qquad (3.73)$$

$$J = -\frac{3}{2}C_{20} \qquad (3.76)$$

$$M = E - \epsilon\sin E \qquad (3.74)$$

$$h = \epsilon\sin\omega \qquad (3.77)$$

$$\bar{\lambda} = M + \omega + n\cdot\tau \qquad (3.75)$$

$$l = \epsilon\cos\omega \qquad (3.78)$$

$$\tau = \begin{cases} 0 & \text{if } m = 1 \\ t_i - t_{\lambda k} & \text{if } m = 2 \end{cases} \qquad (3.79)$$

– The orbital elements at instant t_i are determined by:

$$\epsilon_i = \sqrt{(h + \delta h)^2 + (l + \delta l)^2} \qquad (3.80)$$

$$\omega_i = \tan^{-1}\left(\frac{h + \delta h}{l + \delta l}\right) \qquad (3.81)$$

$$a_i = a + \delta a \qquad (3.82)$$

$$i_i = i + \delta i \qquad (3.83)$$

$$\Omega_i = \Omega + \delta\Omega \qquad (3.84)$$

$$M_i = M + \omega + n(t_i - t_{\lambda k}) + \delta\bar{\lambda} - \omega_i \qquad (3.85)$$

$$E_i^{(n)} = M_i + \epsilon_i\sin E_i^{(n-1)} \qquad \text{Computed iteratively with } E_i^0 = M_i \qquad (3.86)$$

$$\nu_i = 2\tan^{-1}\left(\sqrt{\frac{1+\epsilon_i}{1-\epsilon_i}}\tan\frac{E_i^{(n)}}{2}\right) \qquad (3.87)$$

$$u_i = \nu_i + \omega_i \qquad (3.88)$$

– Satellite position in an ECI coordinate system is defined by:

$$r_i = a_i\left(1 - \epsilon_i\cos E_i^{(n)}\right) \qquad (3.89)$$

$$X_i = r_i(\cos u_i\cos\Omega_i - \sin u_i\sin\Omega_i\cos i_i) \qquad (3.90)$$

$$Y_i = r_i(\cos u_i\sin\Omega_i + \sin u_i\sin\Omega_i\cos i_i) \qquad (3.91)$$

$$Z_i = r_i\sin u_i\cos i_i \qquad (3.92)$$

– Satellite velocity in an ECI coordinate system is defined by:

$$v_{r_i} = \sqrt{\frac{\mu_\oplus}{a_i}}\frac{\epsilon_i\sin\nu_i}{\sqrt{1-\epsilon_i^2}} \qquad (3.93)$$

$$v_{u_i} = \sqrt{\frac{\mu_\oplus}{a_i}}\frac{1+\epsilon_i\cos\nu_i}{\sqrt{1-\epsilon_i^2}} \qquad (3.94)$$

$$V_{x_i} = v_{r_i}(\cos u_i\cos\Omega_i - \sin u_i\sin\Omega_i\cos i_i) - v_{u_i}(\sin u_i\cos\Omega_i + \cos u_i\sin\Omega_i\cos i_i) \qquad (3.95)$$

$$V_{y_i} = v_{r_i}(\cos u_i\sin\Omega_i + \sin u_i\cos\Omega_i\cos i_i) - v_{u_i}(\sin u_i\sin\Omega_i - \cos u_i\cos\Omega_i\cos i_i) \qquad (3.96)$$

$$V_{z_i} = v_{r_i}\sin u_i\sin i_i + v_{u_i}\cos u_i\sin i_i \qquad (3.97)$$

– The satellite position and velocity can transformed to PZ-90.02 ECEF coordinate system using the algorithms presented in appendix B.

Chapter 4

Position, Velocity & Time Estimation

4.1 Introduction

In this chapter the tools to solve the satellite navigation problem and obtain one's estimation of position, velocity and time are presented. Firstly the common estimation algorithms are presented, followed by the methods and models used to correct the main source of errors presented in chapter 2 along with precise modelling terms required for precise positioning. Thirdly, algorithms to detect occurrences of possible cycle-slips in carrier-phase measurements are presented along methods to deal with them. Lastly the implementations of Standard Point Positioning and Precise Point Positioning are presented along with the methods and algorithms to estimate one's velocity and time.

4.2 Estimation Algorithms

Solving the satellite navigation problem requires solving a system of equations with at least one equation per visible satellite. Usually the resulting system of equations is overdetermined (there are more equations than unknown variables) and due to observation noise and uncertainties such system doesn't have a solution.

In this section, two common algorithms to solve this problem are briefly described, the Linear Weighted Least Squares (LWLS), which only requires the measurements and their observation models to obtain a solution, and the Extended Kalman Filter (EKF), which is a more powerful approach but in addition to the measurements and their observation models, it also requires knowledge about the physical models that describe the estimation problem (such as receiver dynamics and signal properties) and an estimate of its initial conditions.

Note that the nomenclature for the variables used to describe both algorithms was chosen in order to establish a parallelism between them; consequently the states and observations models presented over the next sections of this chapter can be used directly and without any modification on both algorithms.

4.2.1 Linear Weighted Least Squares

The LWLS is a particular case of the General Least Squares method which is an approach to find a solution of an overdetermined system, by minimizing the sum of the square errors made in the solution of each equation [18].

Considering an overdetermined system of m linear equations in n unknown variables (written in matrix notation):
$$H \cdot \mathbf{x} = Y \tag{4.1}$$
where:

- $\mathbf{x}$ is the state vector that contains the unknown variables to be estimated;
- Y is the observation vector that contains the observations from a system;
- H is the observation model that maps the state space into the observations space.

The objective is to find $\hat{\mathbf{x}}$, which the best fit for $\mathbf{x}$, by solving the quadratic minimization problem:

$$\hat{\mathbf{x}} = \text{argmin}_{\mathbf{x}} S(\mathbf{x}) \tag{4.2}$$

Considering also that the observations are weighted (as they may not be equally reliable), the function $S(\mathbf{x})$ is defined as:

$$S(\mathbf{x}) = \sum_{i=1}^{m} w_i \left| Y_i - \sum_{j=1}^{n} H_{ij}\mathbf{x}_j \right|^2 = \left\| W^{1/2}(Y - H \cdot \mathbf{x}) \right\|^2 \tag{4.3}$$

where:

- w_i is the weight of the ith observation;

- W is a diagonal matrix containing the weights of each observation.

This minimization problem, contrary to the original problem, has only one solution if at least n columns of the design matrix (H) are linearly independent, and it's given by, [18]:

$$\hat{\mathbf{x}} = \left(H^T W H\right)^{-1} H^T W Y \tag{4.4}$$

4.2.2 Extended Kalman Filter

The Kalman filter is an algorithm that operates recursively over a stream of observations containing noise and other uncertainties, minimizing the estimation error and producing statistically optimal estimates of the system state. It addresses the problem of estimate the state of a discrete-time system that is governed by linear stochastic functions, [21]:

$$\mathbf{x} = F_k \mathbf{x}_{k-1} + w_{k-1} \tag{4.5}$$
$$\hat{y} = H_k \mathbf{x} + v_k \tag{4.6}$$

where:

- $\mathbf{x}$ is the state vector that contains the unknown variables to be estimated;

- F_k is the state-transition model that describes how the system evolves from the previous epoch;

- H_k is the observation model that maps the state space into the observations space;

- w_{k-1} and v_k are the process and observation noises, assumed to be zero mean multivariate Gaussian noises with covariance Q_k and R_k respectively [21].

As a recursive algorithm, the Kalman Filter only needs the estimate from the previous epoch and the current observations in order to compute the estimate state for the current epoch, making it suitable for real-time applications.

Conceptually the Kalman filter algorithm can be represented by two distinct stages, the prediction stage and the update stage, as depicted in figure 4.1.
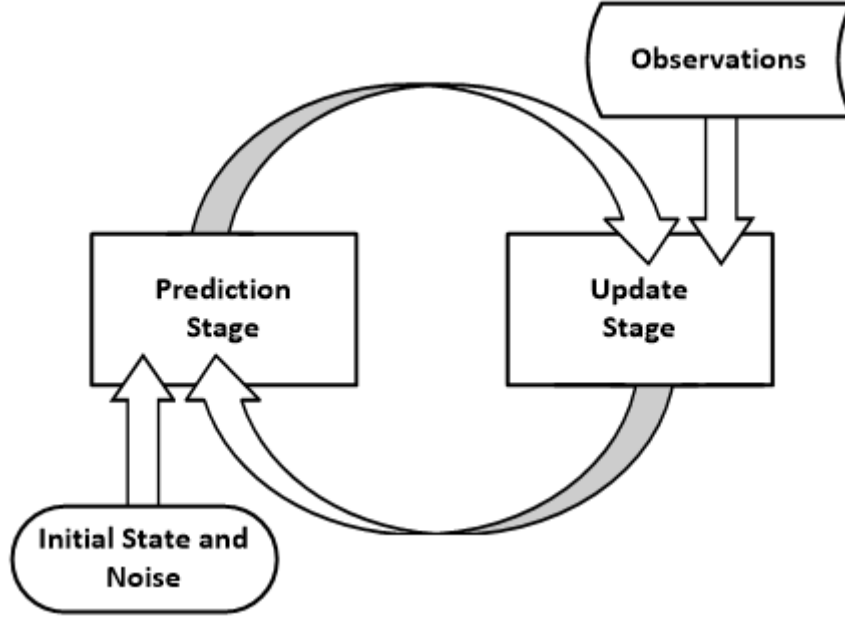
Figure 4.1: Kalman Filter recursive scheme

In the prediction stage at epoch k, the filter uses the previous state estimate $\mathbf{x}_{k-1|k-1}$ to produce an *a priori* estimate of the current state $\mathbf{x}_{k|k-1}$:

$$\mathbf{x}_{k|k-1} = F_k \mathbf{x}_{k-1|k-1} \tag{4.7}$$

$$P_{k|k-1} = F_k P_{k-1|k-1} F_k^T + Q_k \tag{4.8}$$

In the update stage at epoch k, the filter incorporates the current observations y_k in a process referred as innovation z_k [21] (the novelty that y_k brings to system at epoch k), to refine the predicted estimate state:

$$z_k = y_k - \hat{y}_{k|k-1} \tag{4.9}$$

$$S_k = H_k P_{k|k-1} H_k^T + R_k \tag{4.10}$$

$$K_k = P_{k|k-1} H_k^T S_k^{-1} \tag{4.11}$$

$$\mathbf{x}_{k|k} = \mathbf{x}_{k|k-1} + K_k z_k \tag{4.12}$$

$$P_{k|k} = (I - K_k H_k) P_{k|k-1} \tag{4.13}$$

Usually these two stages alternate between them; however an update stages may be skipped if there aren't enough observations, and likewise, several update stages may be performed if multiple independent observations are available.

Although the Kalman Filter, was designed for linear systems, it can be extended to handle non-linear systems, this approach is defined as the EKF. Considering now, that the state-transition model and/or the observation model aren't linear functions, but instead differentiable functions:

$$\mathbf{x} = f(\mathbf{x}_{k-1}) + w_{k-1} \tag{4.14}$$

$$\hat{y} = h(\mathbf{x}) + v_k \tag{4.15}$$

These functions are used to predict the current state and to predict the current observations, however they cannot be used directly to define the state covariances; instead its Jacobian is evaluated at the current epoch k to determine their covariances:

$$F_k = \left.\frac{\partial f}{\partial \mathbf{x}}\right|_{\mathbf{x}_{k-1|k-1}} \quad ; \quad H_k = \left.\frac{\partial h}{\partial \mathbf{x}}\right|_{\mathbf{x}_{k|k-1}} \tag{4.16}$$

37

This process is essentially a linearisation of system dynamics around the last state estimate [21], thus unlike the Kalman Filter, the EKF is not an optimal estimator and incorrect initial state estimate or incorrect model process linearisation, may cause the EKF to diverge quickly.

4.3 GNSS Errors and Modelling

As mentioned in chapter 2, the GNSS measurements are affected by several errors and uncertainties which must be properly modelled in order to solve the satellite navigation problem, in this section the methods to model and correct the main source of errors presented in section 2.5 are described and discussed.

Additionally in order to attain higher precisions (in range of decimetres to millimetres) [22], additional modelling terms, which are usually neglected on most applications, must be taken into account, these precise modelling terms are described and discussed in the end of this section.

4.3.1 Satellite Clock Offset

As mentioned in section 2.5.2, the satellite clock offset is composed by two components, the satellite on-board clock offset component and a relativistic component, thus the satellite clock offset can be expressed as:

$$\delta t_{sat} = \delta \tilde{t}_{sat} + \Delta t_{rel} \tag{4.17}$$

where:

- $\delta \tilde{t}_{sat}$ is the main satellite clock offset which can be determined from the satellite navigation message or from the IGS products;

- Δt_{rel} is the relativistic clock correction.

The relativistic clock correction, relates to the rate of advance of two identical clocks when affected by different gravitational potentials (general relativity) and to their relative motion (special relativity). The general relativity component is constant and is corrected on the satellite by modifying its clock oscillating frequency [11, 7], and the special relativity component is periodic due to the satellite orbital eccentricity and is corrected by:

$$\Delta t_{rel} = -2 \frac{\vec{r}_{sat} \cdot \vec{v}_{sat}}{c^2} \tag{4.18}$$

where:

- $\vec{r}_{sat}$ and $\vec{v}_{sat}$ are the satellite position an velocity.

GPS Satellite Clock Offset

The main component of the GPS satellite clock offset at an epoch t (defined in the GPS time-scale) is determined using a second order polynomial defined as, [11]:

$$\delta \tilde{t}_{sat} = a_0 + a_1(t - t_{oc}) + a_2(t - t_{oc})^2 \tag{4.19}$$

where:

- a_0, a_1 and a_2 are the polynomial coefficients provided by the satellite navigation message, respectively the satellite clock offset, drift and drift rate.

- t_{oc} is the clock correction parameters reference time.

The relativistic clock correction can be corrected using the parameters determined during the process of determining the satellite position as, [11]:

$$\Delta t_{rel} = -2\frac{\sqrt{\mu_\oplus A}}{c^2}e\sin E \tag{4.20}$$

where:

- $\mu_\oplus$ is the WGS-84 Earth's gravitational parameter defined in section 3.2.1;

- A is the semi-major axis of the satellite orbit;

- E is the satellite orbital eccentric anomaly;

- e is the satellite orbit eccentricity.

Additionally for single-frequency measurements, it's also necessary to account for the satellite equipment delay [11]:

$$\delta\tilde{t}_{sat,L1} = \delta\tilde{t}_{sat} + t_{gd} \tag{4.21}$$

$$\delta\tilde{t}_{sat,L2} = \delta\tilde{t}_{sat} + \left(\frac{f_{L1}}{f_{L2}}\right)^2 \cdot t_{gd} \tag{4.22}$$

where:

- t_{gd} is the satellite hardware group delay differential between L1 and L2 carrier frequencies also provided by the satellite navigation message;

- f_{L1} and f_{L2} are the GPS L1 and L2 carrier frequencies.

GLONASS Satellite Clock Offset

The GLONASS satellite clock offset at an epoch t (defined in the GLONASS time-scale), which unlike the GPS, it already contains the relativistic clock correction [7, 10] is determined using using a first order polynomial defined as, [7]:

$$\delta t_{sat} = -\tau_n + \gamma_n(t - t_b) \tag{4.23}$$

where:

- τ_n and γ_n are satellite clock offset and relative deviation from the predicted carrier frequency provided by the satellite navigation message;

- t_b is the clock correction parameters reference time.

Additionally for single-frequency measurements, it's also necessary to account for the satellite equipment delay [7]:

$$\delta t_{sat,L1} = \delta t_{sat} \tag{4.24}$$

$$\delta t_{sat,L2} = \delta t_{sat} - \Delta\tau_n \tag{4.25}$$

where $\Delta\tau_n$ is the satellite hardware group delay differential between the satellite L1 and L2 carrier frequencies, which is also provided by the satellite navigation message.

4.3.2 Sagnac Effect

The Sagnac effect mentioned in section 2.5.1 can be corrected using the following expression [10], which can be applied directly to the raw pseudorange/carrier-phase measurements:

$$\delta\rho = \frac{\omega_\oplus}{c}(X_s \cdot y - Y_s \cdot x) \tag{4.26}$$

where:

- $\omega_\oplus$ is the Earth's rotation rate defined in section 3.2.1 or 3.2.2 depending on the used reference coordinate system;

- X_s and Y_s are the satellite position coordinates at the signal transmission time;

- x and y are the receiver position coordinates at the signal arrival time.

4.3.3 Ionospheric Delay

As mentioned in section 2.5.3, the ionospheric layer of the Earth's atmosphere acts as dispersive medium to GNSS signals and its refraction depends on the inverse square of the signals frequency [11, 7, 23]; therefore dual-frequency measurements can be combined to form the ionosphere-free combination, which removes 99.9% of the first order ionospheric delay and in addition it also removes the differential code bias (DCB)[1], however this combination tends to increase the measurements noise by a factor of three [23]:

$$P_{IF} = \frac{f_{L1}^2 P_{L1} - f_{L2}^2 P_{L2}}{f_{L1}^2 - f_{L2}^2} = \rho + c \cdot (\delta t_{rcv} - \delta t_{sat}) + T_d + \epsilon'_P \tag{4.27}$$

$$\Phi_{IF} = \frac{f_{L1}^2 \Phi_{L1} - f_{L2}^2 \Phi_{L2}}{f_{L1}^2 - f_{L2}^2} = \rho + c \cdot (\delta t_{rcv} - \delta t_{sat}) + T_d + \lambda N + \epsilon'_\Phi \tag{4.28}$$

where:

- ρ represents the geometric range between the receiver and the satellite as defined in equation 2.2;

- δt_{rcv} represents the receiver clock offset from the respective GNSS time-scale;

- δt_{sat} represents the satellite clock offset from the respective GNSS time-scale;

- λ represents the ionosphere-free combination wavelength defined as:

$$\lambda = \frac{f_{L1}^2 \lambda_{L1} - f_{L2}^2 \lambda_{L2}}{f_{L1}^2 - f_{L2}^2} \tag{4.29}$$

- N represents the ionosphere-free combination carrier-phase ambiguity defined as:

$$N = \frac{f_{L1}^2 N_{L1} - f_{L2}^2 N_{L2}}{f_{L1}^2 - f_{L2}^2} \tag{4.30}$$

- T_d represents tropospheric delay;

- ϵ'_P and ϵ'_Φ represents the relevant measurement noise components.

If only single-frequency measurements are available, the ionospheric delay must be corrected through a model, the GPS navigation message provides the parameters for the Klobuchar model, which allows to correct up to 50% of the first order ionospheric delay [11]. These parameters ($\alpha_{0...3}$ and $\beta_{0...3}$) are usually valid for a week after its generation.

---

[1]For GPS signals the L2P signal is encrypted and DCB may not be completely removed, depending on how the receiver generates L2P signal

Considering the estimated geodetic coordinates of the receiver position (φ, λ, h) as defined in appendix B.1 in semi-circles; the satellite azimuth and elevation (az, el) as defined in appendix B.2.1 in semi-circles; for a signal with frequency f at an epoch t (in GPS-time), the ionospheric delay and its expected variance can be determined using the following algorithm [11]:

— Determine the ECEF angle:

$$\Psi = \frac{0.0137}{el + 0.11} - 0.022 \tag{4.31}$$

— Determine the latitude and longitude of the ionospheric pierce point:

$$\varphi_i = \mathrm{clamp}(\varphi + \Psi \cos az, -0.416, +0.416) \tag{4.32}$$

$$\lambda_i = \lambda + \frac{\Psi \sin az}{\cos \phi_i} \tag{4.33}$$

— Determine the local time and the geomagnetic latitude at ionospheric pierce point:

$$t_i = \mathrm{mod}\big(4.32 \cdot 10^4 \lambda_i + t, 86400\big) \tag{4.34}$$

$$\varphi_m = \varphi_i + 0.065 \cos\big(\lambda_i - 1.617\big) \tag{4.35}$$

— Determine the period, amplitude and phase of the ionospheric delay:

$$P_{I_d} = \max\left(\sum_{n=0}^{3} \beta_n \varphi_m^n, 72000 \right) \tag{4.36}$$

$$A_{I_d} = \max\left(\sum_{n=0}^{3} \alpha_n \varphi_m^n, 0 \right) \tag{4.37}$$

$$X_{I_d} = \frac{2\pi(t_i - 50400)}{P_{I_d}} \tag{4.38}$$

— Determine the slant factor:

$$F = 1 + 16(0.53 - el)^3 \tag{4.39}$$

— Determine the ionospheric and it's expected variance:

$$I_d = \left(\frac{f_{GPS,L1}}{f} \right)^2 c \begin{cases} \left[5 \cdot 10^{-9} + A_{I_d} \left(1 - \frac{X_{I_d}^2}{2} + \frac{X_{I_d}^4}{24} \right) \right] F & \text{if } |X_{I_d}| < 1.57 \\ 5 \cdot 10^{-9} F & \text{if } |X_{I_d}| \geqslant 1.57 \end{cases} \tag{4.40}$$

$$\sigma_{I_d} = 0.3 I_d \tag{4.41}$$

Although this model is provided by GPS constellation, it's suggested that it can also be applied to GLONASS measurements [17].

4.3.4 Tropospheric delay

Unlike the ionospheric layer, the tropospheric layer of the Earth's atmosphere act as non-dispersive media to GNSS signals, therefore the tropospheric delay cannot be removed with dual-frequency combinations, and the only way to remove it is either through estimation or through models [9, 8].

Considering the estimated geodetic coordinates of the receiver position (φ, λ, h) as defined in appendix B.1, and the satellite azimuth and elevation (az, el) as defined in appendix B.2.1, the tropospheric delay and is expected variance can be modelled as:

$$T_d = M_h \cdot Z_{hd} + M_w \cdot (Z_{wd} - Z_{hd}) \tag{4.42}$$

$$\sigma_{T_d} = \frac{0.01}{\sin el} \tag{4.43}$$

where:

- Z_{hd} represents the zenith hydrostatic delay, caused by the dry gases of the atmosphere, it accounts for 90% of the tropospheric delay and fortunately varies very slowly and predictably.

- Z_{wd} represents the zenith wet delay, caused by the water vapor and water condensation of the atmosphere, it depends heavily on the weather conditions and contrary to the zenith hydrostatic delay, this delay is very difficult to model.

- M_h and M_w represent the obliquity factors for the hydrostatic and wet components which depend on the geographic location of the station as well on the seasonal atmospheric conditions.

The zenith hydrostatic delay and the zenith wet delay are determined using the Saastamoinen model [24]:

$$Z_{hd} = \left(\frac{0.0022768 \cdot P}{1 - 0.00266 \cos 2\varphi - 0.28 \cdot 10^{-6}h} \right) \tag{4.44}$$

$$Z_{wd} = 0.0022770 \cdot e \left(\frac{1255.0}{T} + 0.05 \right) \tag{4.45}$$

where:

- P, T and e are the atmospheric parameters at the station, if the station isn't equip with atmospheric monitoring equipment these parameters can interpolated from seasonal weather tables [9] or estimated from the standard atmosphere [25]:

$$P = 1013.25 \left(1.0 - 2.2557 \cdot 10^{-5}h \right)^{5.2568} \tag{4.46}$$

$$T = 15.0 - 6.5 \cdot 10^{-3} + 273.16 \tag{4.47}$$

$$e = 6.108 r_h \exp \left(\frac{17.15T - 4684}{T - 38.45} \right) \tag{4.48}$$

and r_h is the relative humidity assumed to be 0.3 if unknown.

The obliquity factors for the hydrostatic delay component and wet delay component are determined using the Niell Mapping functions [24, 26]:

$$M_h = m(a_d, b_d, c_d) + h \cdot 10^3 \left[\frac{1}{\sin el} - m(a_h, b_h, c_h) \right] \tag{4.49}$$

$$M_w = m(a_w, b_w, c_w) \tag{4.50}$$

where:

- $m(a, b, c)$ is the Niell mapping normalised to unity at zenith, defined as [26]:

$$m(a,b,c) = \frac{1 + \dfrac{a}{1 + \dfrac{b}{1 + c}}}{\sin el + \dfrac{a}{\sin el + \dfrac{b}{\sin el + c}}} \tag{4.51}$$

- The hydrostatic parameters a_d, b_d and c_d are given by:

$$\xi(\varphi, t) = \xi_{avg}(\varphi) - \xi_{amp}(\varphi) \cos \left[2\pi \left(\frac{t - 28}{365.25} + \begin{cases} 0 & \text{if } \varphi < 0 \\ 0.5 & \text{if } \varphi > 0 \end{cases} \right) \right] \tag{4.52}$$

Where t is the day of the year (being 0 on January 1st) and the coefficients $\xi_{avg}(\varphi)$ and $\xi_{amp}(\varphi)$ are linearly interpolated from the coefficients presented on the table 4.1.

- The altitude corrections a_h, b_h and c_h are presented on the table 4.1.

– The wet parameters a_w, b_w and c_w are linearly interpolated from the coefficients presented on the table 4.2.

The coefficients required by the Niell Mapping model are summarized in the following tables [26]:

	Latitude (φ)				
	15°	**30°**	**45°**	**60°**	**75°**
ξ	**Average**				
a	$1.2769934 \cdot 10^{-3}$	$1.2683230 \cdot 10^{-3}$	$1.2465397 \cdot 10^{-3}$	$1.2196049 \cdot 10^{-3}$	$1.2045996 \cdot 10^{-3}$
b	$2.9153695 \cdot 10^{-3}$	$2.9152299 \cdot 10^{-3}$	$2.9288445 \cdot 10^{-3}$	$2.9022565 \cdot 10^{-3}$	$2.9024912 \cdot 10^{-3}$
c	$62.610505 \cdot 10^{-3}$	$62.837393 \cdot 10^{-3}$	$63.721774 \cdot 10^{-3}$	$63.824265 \cdot 10^{-3}$	$64.258455 \cdot 10^{-3}$
ξ	**Amplitude**				
a	0.0	$1.2709626 \cdot 10^{-5}$	$2.6523662 \cdot 10^{-5}$	$3.4000452 \cdot 10^{-5}$	$4.1202191 \cdot 10^{-5}$
b	0.0	$2.1414979 \cdot 10^{-5}$	$3.0160779 \cdot 10^{-5}$	$7.2562722 \cdot 10^{-5}$	$11.723375 \cdot 10^{-5}$
c	0.0	$9.0128400 \cdot 10^{-5}$	$4.3497037 \cdot 10^{-5}$	$84.795348 \cdot 10^{-5}$	$170.37206 \cdot 10^{-5}$
ξ	**Altitude Corrections**				
a	$2.53 \cdot 10^{-5}$				
b	$5.49 \cdot 10^{-3}$				
c	$1.14 \cdot 10^{-3}$				

<div align="center">Table 4.1: Coefficients of the hydrostatic mapping function</div>

	Latitude (φ)				
ξ	**15°**	**30°**	**45°**	**60°**	75°
a	$5.8021897 \cdot 10^{-4}$	$5.6794847 \cdot 10^{-4}$	$5.8118019 \cdot 10^{-4}$	$5.9727542 \cdot 10^{-4}$	$6.1641693 \cdot 10^{-4}$
b	$1.4275268 \cdot 10^{-3}$	$1.5138625 \cdot 10^{-3}$	$1.4572752 \cdot 10^{-3}$	$1.5007428 \cdot 10^{-3}$	$1.7599082 \cdot 10^{-3}$
c	$4.3472961 \cdot 10^{-2}$	$4.6729510 \cdot 10^{-2}$	$4.3908931 \cdot 10^{-2}$	$4.4626982 \cdot 10^{-2}$	$5.4736038 \cdot 10^{-2}$

<div align="center">Table 4.2: Coefficients of the wet mapping function</div>

4.3.5 Precise Modelling Terms

Second order relativistic effect

In addition to the Sagnac effect presented in section 4.3.2, a secondary relativistic effect caused by the space-time curvature due to the Earth's gravitational field is also applied to the geometric range between the receiver and the satellite [10]:

$$\Delta \rho_{rel} = \frac{2\mu_\oplus}{c^2} \ln \left(\frac{\|\vec{r}_{sat}\| + \|\vec{r}_{rcv}\| + \|\vec{r}_{sat} - \vec{r}_{rcv}\|}{\|\vec{r}_{sat}\| + \|\vec{r}_{rcv}\| - \|\vec{r}_{sat} - \vec{r}_{rcv}\|} \right) \tag{4.53}$$

where:

– $\vec{r}_{sat}$ is the satellite position at the signal transmission time;

– $\vec{r}_{rcv}$ is the receiver position at the signal arrival time;

– $\mu_\oplus$ is the Earth gravitational parameter.

Antenna biases and orientation

- **Phase center variation**

There is a small variation of the antenna phase center which depends of the mutual orientation of the satellite and receiver antennas as well of the frequency of carrier signals. The ANTEX files [27] provided by the IGS contains the corrections for each satellite antenna phase center and they also contains the corrections for several commercial antennas phase center. The magnitude of this correction is depicted in figure 4.2.
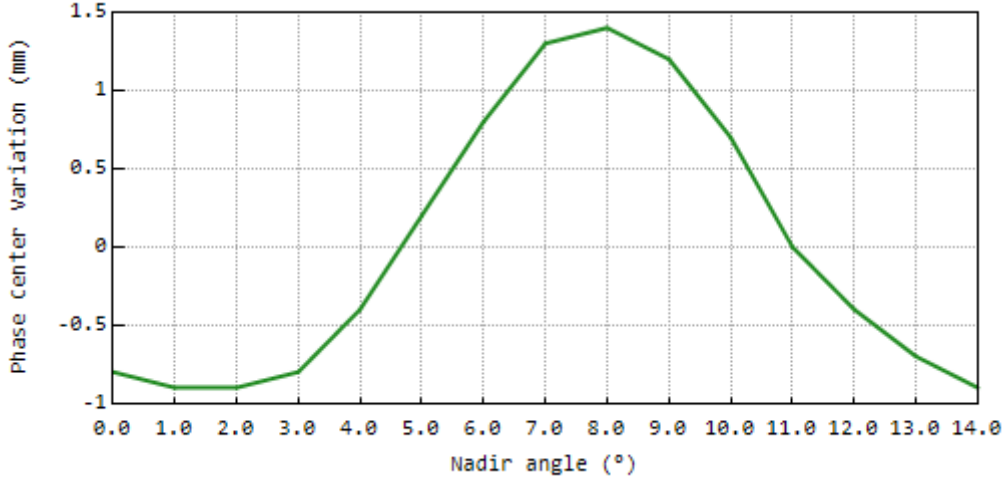

Figure 4.2: Phase center variation for satellite - GPS 01

- **Carrier-phase wind-up effect**

Both GPS and GLONASS transmit Right Circular Polarized (RCP) [7, 11] radio waves meaning that the observed carrier-phase depends on the mutual orientation of both the satellite and receiver antennas. As the satellite orbits the Earth, its antenna undergo through slow rotations as the satellite solar panels are being re-oriented towards the Sun. For a moving receiver this effect is fully absorbed by the clock offset solution however for a stationary receiver this effect must be corrected as it can reach up to one carrier-phase cycle in half an hour. These carrier-phase wind-up correction can be determined by, [22]:

$$\delta\phi = \text{sign}\left(\hat{k}\left(\vec{D}_{sat} \times \vec{D}_{rcv}\right)\right)\cos^{-1}\left(\frac{\vec{D}_{sat}\vec{D}_{rcv}}{\|\vec{D}_{sat}\|\|\vec{D}_{rcv}\|}\right) \tag{4.54}$$

$$\Delta\phi_k = \delta\phi + 2\pi\left\lfloor\frac{\Delta\phi_{k-1} - \delta\phi}{2\pi}\right\rceil \tag{4.55}$$

where:

- $\hat{k}$ is the unit vector from the satellite to the receiver;
- $\vec{D}_{sat}$ and $\vec{D}_{rcv}$ are the effective dipole vectors for the satellite and receiver defined as:

$$\vec{D}_{sat} = \hat{x}_{sat} - \hat{k}\left(\hat{k} \cdot \hat{x}_{sat}\right) - \hat{k} \times \hat{y}_{sat} \tag{4.56}$$

$$\vec{D}_{rcv} = \hat{x}_{rcv} - \hat{k}\left(\hat{k} \cdot \hat{x}_{rcv}\right) + \hat{k} \times \hat{y}_{rcv} \tag{4.57}$$

$(\hat{x}, \hat{y}, \hat{z})_{sat}$ are the unit vectors of the satellite local coordinate system (appendix B.3);
$(\hat{x}, \hat{y}, \hat{z})_{rcv}$ are the unit vectors of the receiver local coordinate system (appendix B.2).

- $\Delta\phi_{k-1}$ is the phase wind-up correction from the previous epoch;

44

– $\Delta\phi_0$ can be initialized at zero, as it unknown value will absorbed in the carrier-phase ambiguity.

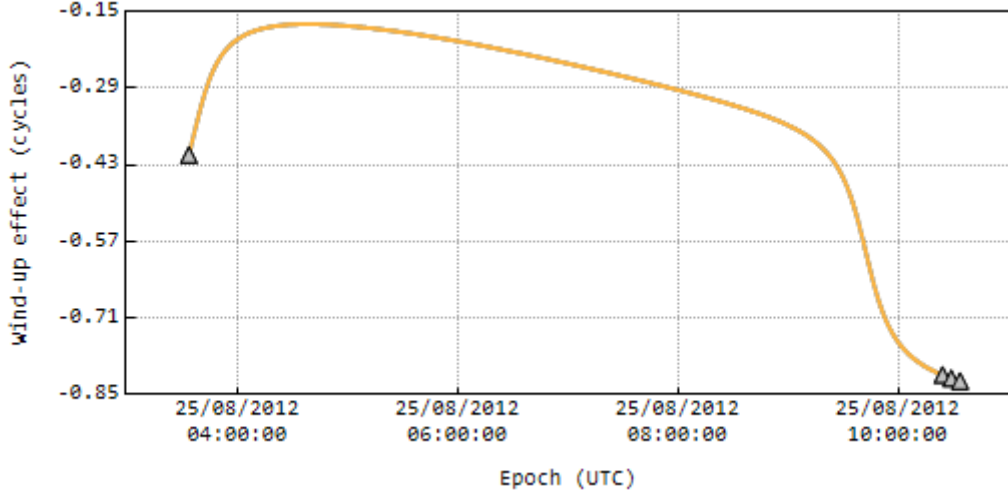The magnitude of this correction is depicted on figure 4.3.

Figure 4.3: Phase wind-up effect for satellite - GPS 27

- **Eclipsed satellites**

As the GNSS satellites orbit the Earth, they undergo into eclipse seasons (where the satellite is fully covered by the Earth's shadow). During these eclipse seasons, the lack of the Sun's radiation pressure and the attempts to keep the satellite solar panels facing Sun, degrades the satellite attitude control thus introducing errors in the satellite orbit [22].
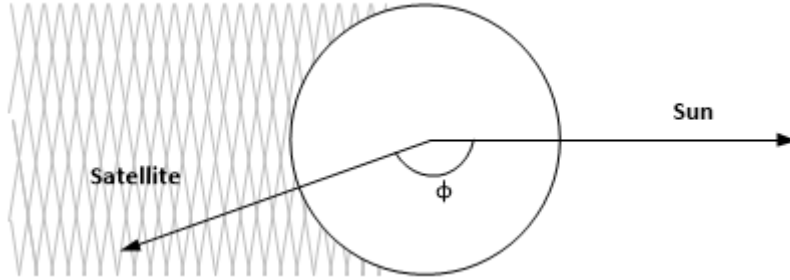
Figure 4.4: Eclipsed Satellite

These eclipsed or recently eclipsed satellites should be removed from the solution as their observables aren't reliable. A simple approach to check if the satellite is eclipsed, is to check if the satellite position ($\vec{r}_{sat}$) satisfies the following conditions:

$$\cos\phi = \frac{\vec{r}_{sat} \cdot \vec{r}_{\odot}}{|\vec{r}_{sat} \cdot \vec{r}_{\odot}|} < 0 \tag{4.58}$$

$$\left\| \vec{r}_{sat} \right\| \sqrt{1 - \cos^2\phi} < a_{\oplus} \tag{4.59}$$

where:

– $\vec{r}_{sat}$ is the satellite position at the signal transmission time;

– $\vec{r}_{rcv}$ is the receiver position at the signal arrival time;

– $\vec{r}_{\odot}$, is the Sun position in an ECEF reference frame (the Sun position can be determined using the algorithm presented in appendix A.4).

Non-rigid earth effects

- **Solid tides**

   Solid tides are the primary deformation caused by elastic response of the Earth's crust due to the gravitational forces produced by external bodies such as the Sun and Moon. The displacement caused by the solid tides can be modelled as [22, 28]:

$$\Delta r = f_2(\vec{r}_\odot, \mu_\odot) + f_2(\vec{r}_\mathbb{C}, \mu_\mathbb{C}) + f_3(\vec{r}_\odot, \mu_\odot) + f_3(\vec{r}_\mathbb{C}, \mu_\mathbb{C}) \tag{4.60}$$

   - $\vec{r}_\odot$ and $\vec{r}_\mathbb{C}$ are the Sun and Moon positions in ECEF reference frame (the Sun and Moon positions can be computed using the algorithm presented in appendix A.4 and A.5);

   - $\mu_\odot$ and $\mu_\mathbb{C}$ are the the Sun and Moon standard gravitational parameters, which are defined as $1.327124 \cdot 10^{20}$ and $4.902801 \cdot 10^{12}$ respectively.

   The functions f_2 and f_3 are the models for 2nd and 3rd degree tide displacements, defined as, [28]:

$$f_2\left(\vec{R}, \mu\right) = \frac{\mu a_\oplus^4}{\mu_\oplus \|\vec{R}\|^3} \left\{ h_2 \hat{r}\left(\frac{3}{2}\left(\hat{R} \cdot \hat{r}\right)^2 - \frac{1}{2}\right) + 3l_2\left(\hat{R} \cdot \hat{r}\right)\left[\hat{R} - \left(\hat{R} \cdot \hat{r}\right)\hat{r}\right] \right\} \tag{4.61}$$

$$\begin{aligned} f_3\left(\vec{R}, \mu\right) = \frac{\mu a_\oplus^5}{\mu_\oplus \|\vec{R}\|^4} \Bigg\{ &h_3 \hat{r}\left(\frac{5}{2}\left(\hat{R} \cdot \hat{r}\right)^3 - \frac{3}{2}\left(\hat{R} \cdot \hat{r}\right)\right) + \\ &l_3\left(\frac{15}{2}\left(\hat{R} \cdot \hat{r}\right)^2 - \frac{3}{2}\right)\left[\hat{R} - \left(\hat{R} \cdot \hat{r}\right)\hat{r}\right] \Bigg\} \end{aligned} \tag{4.62}$$

   - $\hat{R}$ is the unit vector of $\vec{R}$;

   - $\hat{r}$ is the unit vector from Earth's center to the station;

   - h_2, l_2, h_3 and l_3 are the Love and Shida numbers defined as, [28]:

$$h_2 = 0.6078 - 0.0006\left(\frac{3\sin^2\varphi - 1}{2}\right); \qquad h_3 = 0.292 \tag{4.63}$$

$$l_2 = 0.0847 - 0.0002\left(\frac{3\sin^2\varphi - 1}{2}\right); \qquad l_3 = 0.015 \tag{4.64}$$

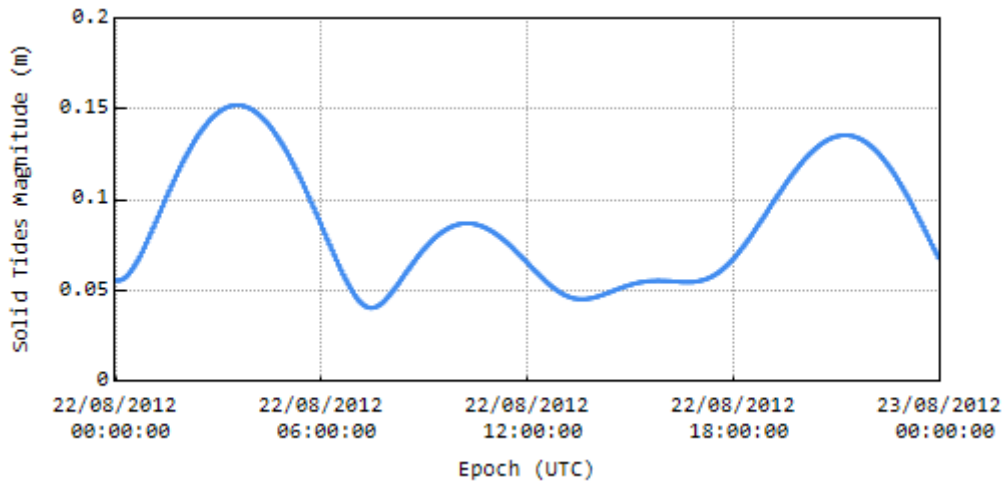The magnitude of this correction is depicted on figure 4.5.

Figure 4.5: Solid Tides Magnitude

- **Ocean loading**

  Ocean loading is a secondary deformation caused by the elastic response of the Earth's crust due to ocean tides; it shall be taken into account for observations periods longer than 24 hours in areas close to the oceans [22].

- **Pole tides**

  Pole tide is a secondary deformation caused by the elastic response of the Earth's crust due to shifts in the Earth's rotation axis; it should be taken into account for observation periods longer than two months [22].

4.4 Carrier-phase Ambiguities and Cycle-Slip detection

The use of carrier-phase measurements is necessary to attain high precision positioning. However, as mentioned in section 2.6.2, carrier-phase measurements are biased by an unknown integer number of wavelengths (carrier-phase ambiguity) which must be estimated. This process is known as ambiguity fixing or ambiguity resolution.

Furthermore the carrier-phase measurements are also subjected to cycle-slips, sudden arbitrary jumps of an unknown integer number of wavelengths on the carrier-phase ambiguity. The occurrence of cycle-slips can significantly degrade the filter's performance, unless they are detected and corrected or filtered out.

In this section a way to estimate the carrier-phase measurements ambiguity suitable for single-receiver real-time precise positioning is presented, along with algorithms to detect occurrences of possible cycle-slips and methods to mitigate their effect.

The performance of the cycle-slip detection algorithms is demonstrated, using one hour of GNSS data from the satellite GPS 08, were at epoch 16:20:00 a jump of one cycle was artificially introduced to the L1 carrier-phase measurement and at epoch 16:40:00 a jump of one cycle was artificially introduced on both the L1 and L2 carrier-phase measurements.

4.4.1 Carrier-phase Ambiguity resolution

Over the last decades, many methods were developed on the subject of carrier-phase ambiguity resolution. Typically these methods usually invoke double-difference linear combinations of carrier-phase ambiguities estimates from pairs of satellites and pairs of receivers, requiring simultaneous measurements from at least two receivers.

Such methods aren't usually suitable for single-receiver real-time precise positioning, due to their computational burden [29] and due to receiver hardware delays and initial phase bias (also referred as un-calibrated phase or fractional cycles biases) [30].

However if the receiver hardware delays are kept stable in time (see section 2.5.5), the carrier-phase ambiguities can be estimated together with the receiver coordinates and clock offsets, as non-integer values instead of integer values absorbing this hardware delays and the initial phase bias into their solution [22].

4.4.2 Cycle-Slip Single-frequency Detectors

In this subsection two detectors are presented which are capable to detect possible occurrences of cycle-slips using only single-frequency measurements.

Phase-Code detector

The Phase-Code detector is a very simple approach to detect a possible occurrence of a cycle-slip, and as its name indicates, is based on the following combination of carrier-phase and pseudorange measurements:

$$d = \Phi - P = \lambda N - 2I_d + \epsilon' \tag{4.65}$$

where:

- λ is the carrier wavelength;

- N is the non-integer carrier-phase ambiguity;

- I_d is the ionospheric delay;

- ϵ' is the combination noise.

This combination removes all non-dispersive delays, but increases the ionospheric delay by a factor of two. Nerveless as the ionospheric delay tends to vary slowly between adjacent epochs, a cycle-slip can be detected by:

$$\left| d - \bar{d} \right| > p \cdot \sigma \tag{4.66}$$

where:

- $\bar{d}$ and σ are the mean value and standard deviation of the last n measurements of d, since the beginning of the signal tracking or since the last cycle-slip detection;

- p is scale factor of the threshold of cycle-slip detection (defines the ability of detecting a cycle-slip).

The drawback of this detection method is that it tends to produce fault detections environments of high ionospheric activity and in situations of low SNR.

Doppler aided detector

The Doppler aided detector is another very simple approach to detect a possible occurrence of a cycle-slip being more reliable than previous detector and it can be also be used to reliably determine the size of cycle-slip jump. However this approach requires an high sampling rate (about one epoch per second) and the Doppler measurements, which unfortunately aren't usually available on low-end receivers.

Considering the change of geometry range from the receiver to satellite in absence of cycle-slips between two adjacent epochs, defined by, [31]:

$$dr_\Phi = \frac{d\Phi}{dt} \approx \Phi_{k-1} - \Phi_k \tag{4.67}$$

$$dr_f = -\lambda \int f \, dt \approx \frac{1}{2} [f_{k-1} - f_k] \lambda \Delta t \tag{4.68}$$

where:

- Φ_{k-1} and Φ_k are the carrier-phase measurements from the previous epoch and the current epoch;

- f_{k-1} and f_k are the Doppler shift measurements from the previous epoch and the current epoch;

- λ is the signal wavelength;

- Δt is the interval between epochs.

As mentioned in section 2.6.3, the Doppler shift measurements aren't affected by the occurrence of cycle-slips, therefore the occurrence of one can be detected by:

$$\delta = dr_\Phi - dr_f \tag{4.69}$$

$$\left|\delta - \bar{\delta}\right| > p \cdot \sigma \tag{4.70}$$

where:

- $\bar{\delta}$ and σ are the mean value and variance of the previous δ measurements, since the beginning of the signal tracking or last cycle-slip detection;

- p is scale factor of the threshold of cycle-slip detection (defines the ability of detecting a cycle-slip).

Results

Figure 4.6, illustrates the detection process of both detectors.
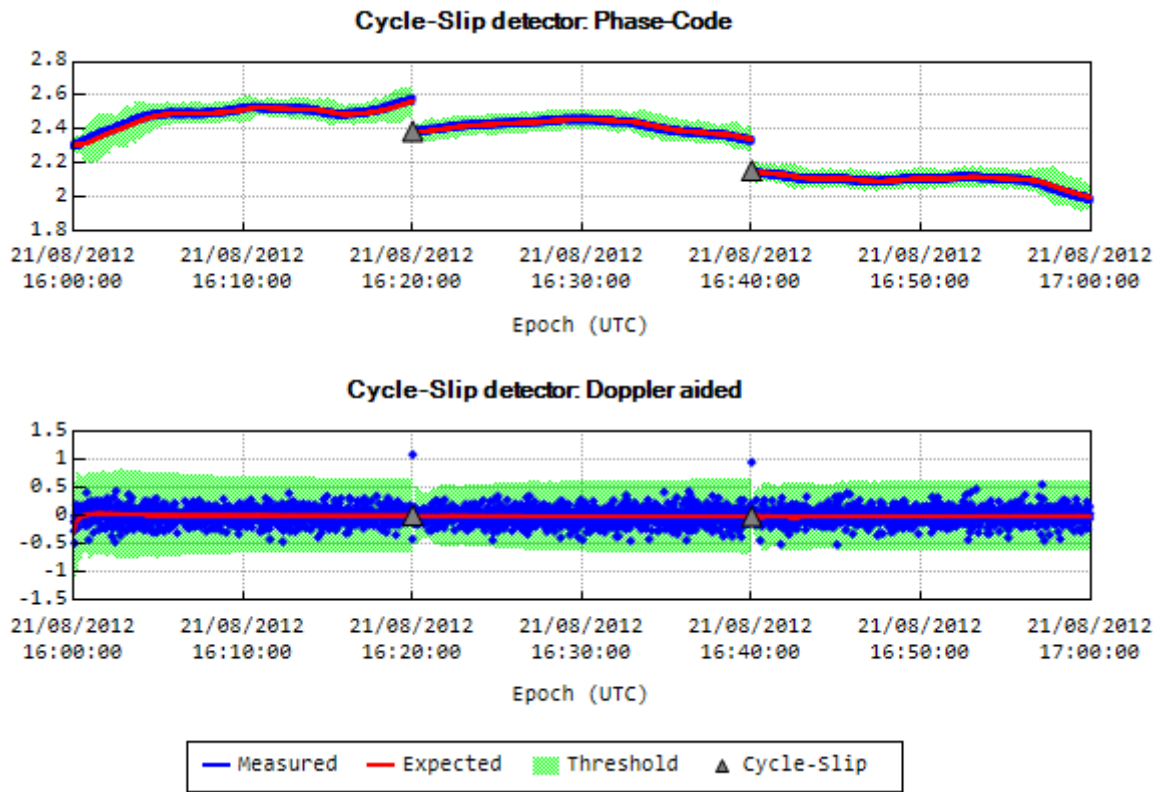
Figure 4.6: Single-frequency cycle-slip detection results (L1 frequency)

4.4.3   Cycle-Slip Dual-frequency Detectors

In this subsection two detectors are presented which are capable to detect possible occurrences of cycle-slips using dual-frequency measurements. These detector tends to produce better results than the single-frequency detectors as the combination of dual-frequency measurements allows the removal of the most undesirable effects that can cause false detections [8, 9].

Geometry-free combination detector

Considering the geometry-free combination of dual-frequency carrier-phase measurements:

$$\Phi_{GF} = \Phi_{L1} - \Phi_{L2} = I'_d + \lambda_1 N_1 - \lambda_2 N_2 + \epsilon'_\Phi \tag{4.71}$$

As long as the carrier-phase ambiguities N_1 and N_2 remain constant, this combination will vary smoothly with the ionospheric delay and any sudden discontinuities could indicate a possible cycle-slip in either Φ_1 or Φ_2. Therefore, the occurrence of a cycle-slip can be detected by, [29]:

$$|\Phi_{GF} - P| > \frac{3}{2}(\lambda_2 - \lambda_1)\left[1 - \frac{1}{2}\exp\left(\frac{\Delta t}{60}\right)\right] \tag{4.72}$$

where:

- P is the expected geometry-free combination, computed using a second degree polynomial fit from the previous n samples of Φ_{GF}, since the beginning of the signal tracking or last cycle-slip detection;

- Δt is the interval between adjacent epochs.

Melbourne-Wübbena combination detector

Considering the narrow-lane combination of the dual-frequency code measurements R_1 and R_2, and the wide-lane combination of the dual-frequency carrier-phase Φ_1 and Φ_2:

$$R_{NL} = \frac{f_{L1}R_{L1} + f_{L2}R_{L2}}{f_{L1} + f_{L2}}; \qquad \Phi_{WL} = \frac{f_{L1}\Phi_{L1} - f_{L2}\Phi_{L2}}{f_{L1} - f_{L2}} \tag{4.73}$$

The Melbourne-Wübbena combination is defined as:

$$L_{MW} = \Phi_{WL} - R_{NL} = \lambda_W(N_1 - N_2) + \epsilon'_{MW} \tag{4.74}$$

And by exploiting the advantages of both the wide-lane carrier-phase combination and narrow-lane code combination, the Melbourne-Wübbena combination benefits from:

- Removal of the ionospheric delay;

- Enlargement of the ambiguity spacing by the wide-lane wavelength ($\lambda_W = \frac{c}{f_{L1}-f_{L2}}$);

- Reduction of the measurement noise by the narrow-lane wavelength ($\lambda_W = \frac{c}{f_{L1}+f_{L2}}$).

The occurrence of a cycle-slip in either Φ_1 or Φ_2, can be detected by, [29]:

$$\left|L_{MW} - \bar{L}\right| > p \cdot \sigma \tag{4.75}$$

where:

- $\bar{L}$ and σ are the mean value and covariance of the previous L_{MW} measurements since the beginning of the signal tracking or last cycle-slip detection;

- p is scale factor of the threshold of cycle-slip detection (defines the ability of detecting a cycle-slip).

However unlike the geometry-free combination detector, this detection method cannot detect simultaneous jumps on both signals of equal magnitude.

Results

The test signals provided by the dual-frequency detectors are more stable and cleaner than the ones from the single-frequency detectors, as can be seen in figure 4.7.
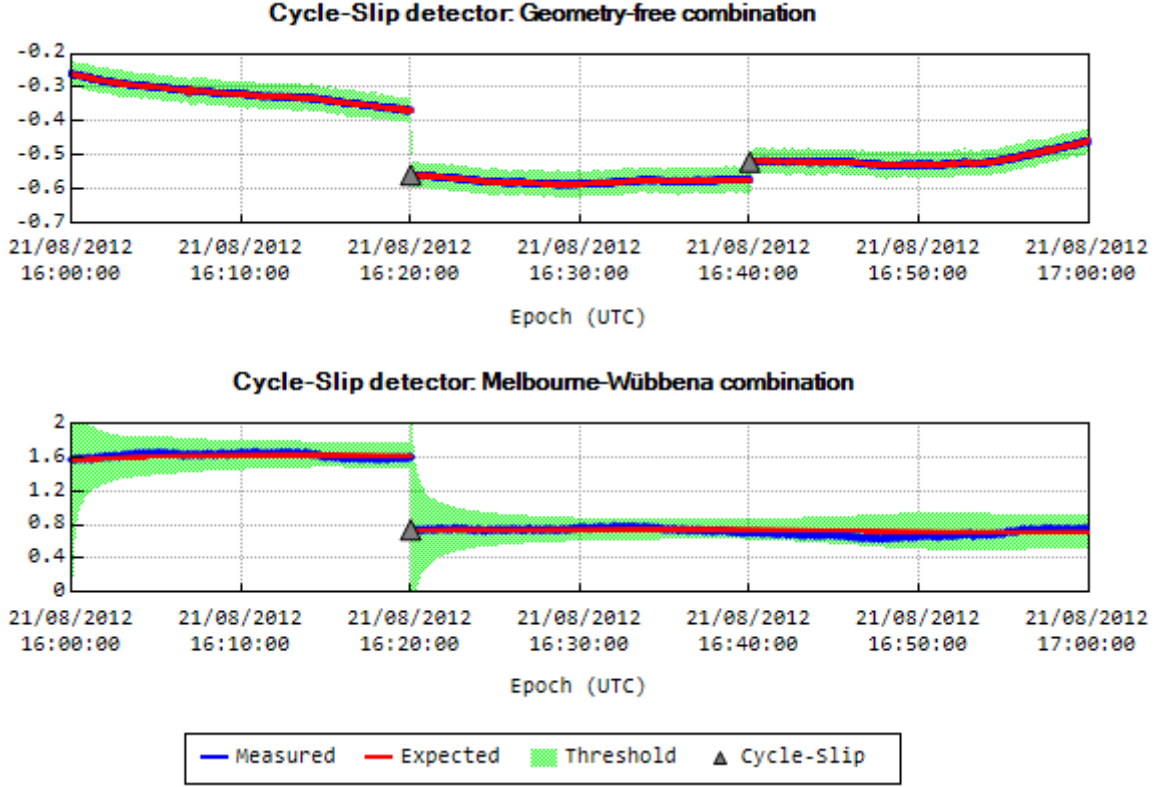

Figure 4.7: Dual-frequency cycle-slip detection results

Is also noticeable that the simultaneous jump of both the L1 and L2 carrier-phase wasn't detected by the Melbourne-Wübbena combination detector, as expected.

4.4.4 Cycle-slip Filter Absorption

When a cycle-slip is detected, the current carrier-phase ambiguity must be updated to reflect the occurrence of the cycle-slip. Although the optimal solution would be to determine the size of the cycle-slip and add it to the estimated carrier-phase ambiguity, a faulty cycle-slip detection or incorrect cycle-slip size determination can impact the filter's performance as much as the cycle-slip occurrence itself [29].

A more suitable approach is to allow the cycle-slip to be gracefully absorbed by the filter. During the prediction stage of the EKF, the following state-transition model and process covariance can be applied to the carrier-phase ambiguity estimation:

$$F_N = \begin{cases} 0 & \text{if cycle-slip} \\ 1 & \text{otherwise} \end{cases} \qquad Q_N = \begin{cases} Q_{cs} & \text{if cycle-slip} \\ 0 & \text{otherwise} \end{cases} \tag{4.76}$$

- Q_{cs} is the covariance of the unknown ambiguity, and it should be defined based on the receiver properties.

To further mitigate the impact of a cycle-slip and speed-up the convergence of ambiguity estimation and therefore reliability of the carrier-phase measurement, at the start of signal tracking or after the

occurrence of a cycle-slip, its ambiguity can be (re-)initialized as:

$$\mathbf{x}_N = \Phi - R. \tag{4.77}$$

4.5 Position Estimation

4.5.1 Standard Point Positioning - Implementation

Standard Point Positioning (SPP) also referred as Single Positioning Service or Code Based Positioning, is an approach to solve the satellite navigation problem, using pseudorange measurements and navigation parameters provided by satellites only.

Assuming that main source of errors that affect the GNSS measurements have been properly modelled and accounted for, the pseudorange observation equation presented in section 2.6.1 for a given epoch can be written as:

$$P_G = \rho + c \cdot \delta t_G + \epsilon_P \qquad \text{(GPS Satellite)} \tag{4.78}$$
$$P_R = \rho + c \cdot \delta t_R + \epsilon_P \qquad \text{(GLONASS Satellite)} \tag{4.79}$$

where:

- ρ is the geometric range between the receiver and the satellite as defined in equation 2.2;

- δt_G is the receiver clock offset with the GPS time-scale;

- δt_R is the receiver clock offset with the GLONASS time-scale;

- ϵ_P represents the relevant measurement noise components.

The system of equations presented above contains five unknowns (the receiver position coordinates and the receiver clock offsets), meaning that at least five visible satellites are required (if all visible satellite belong to the same constellation only four satellites are required). These unknowns define the state to be estimated:

$$\mathbf{x} = \begin{bmatrix} x & y & z & c \cdot \delta t_G & c \cdot \delta t_R \end{bmatrix}^T \tag{4.80}$$

The observation model is obtained by linearising the observation equations using the Taylor expansion series approximation, neglecting the higher order terms [14]. This yields the following submatrices:

$$H_{P_G} = \begin{bmatrix} \dfrac{x - X_s}{\rho} & \dfrac{y - Y_s}{\rho} & \dfrac{z - Z_s}{\rho} & 1 & 0 \end{bmatrix} \tag{4.81}$$

$$H_{P_R} = \begin{bmatrix} \dfrac{x - X_s}{\rho} & \dfrac{y - Y_s}{\rho} & \dfrac{z - Z_s}{\rho} & 0 & 1 \end{bmatrix} \tag{4.82}$$

The state-transition model for the receiver coordinates is defined based on the receiver dynamics, if measurements from inertial measurement units (IMU) are available they can be used as state-transition model [32]. For the receiver clocks offsets can be modelled as white noise process with zero mean [13, 17, 24].

4.5.2 Precise Point Positioning - Implementation

Precise Point Positioning (PPP), not to be confused with Precise Point Service (a GPS service provided by United States Department of Defense to authorized users), is an approach to solve the satellite navigation problem that aims to provide very precise positions estimations up to a few centimetres of error.

Unlike Differential-GNSS positioning methods that combine measures from a receiver with the measures from one or more reference stations at known positions to differentiate the common errors, PPP uses only one dual-frequency receiver and the precise orbits and clocks from IGS.

To achieve this very precise position estimates both the ionosphere-free combinations of pseudorange and carrier-phase measurements are used, the zenith wet delay the most volatile component of the tropospheric delay is estimated together with the receiver position and the precise modelling terms presented in section 4.3.5 must be taken into account.

Following the same reasoning used in section 4.5.1, assuming that main source of errors that affect the GNSS measurements have been properly modelled and accounted for, the pseudorange observation equation presented in section 4.27 for a given epoch can be written as:

$$P_{IF,G} = \rho + c \cdot \delta t_G + M_w \cdot Z_{wd} + \epsilon'_P \qquad \text{(GPS Satellite)} \qquad (4.83)$$

$$P_{IF,R} = \rho + c \cdot \delta t_R + M_w \cdot Z_{wd} + \epsilon'_P \qquad \text{(GLONASS Satellite)} \qquad (4.84)$$

And carrier-phase observation equation presented in section 4.28 for a given epoch can be written as:

$$\Phi_{IF,G} = \rho + c \cdot \delta t_G + M_w \cdot Z_{wd} + \lambda N + \epsilon'_\Phi \qquad \text{(GPS Satellite)} \qquad (4.85)$$

$$\Phi_{IF,R} = \rho + c \cdot \delta t_R + M_w \cdot Z_{wd} + \lambda N + \epsilon'_\Phi \qquad \text{(GLONASS Satellite)} \qquad (4.86)$$

where:

- ρ is the geometric range between the receiver and the satellite as defined in equation 2.2;

- δt_G is the receiver clock offset with the GPS time-scale;

- δt_R is the receiver clock offset with the GLONASS time-scale;

- M_w is the obliquity factor for the zenith wet component and it can be determined from the tropospheric model presented in section 4.3.4;

- Z_{wd} is the zenith wet component of the tropospheric delay;

- λ is the ionosphere-free combination wavelength defined in equation 4.29;

- N is the ionosphere-free combination carrier-phase ambiguity defined in equation 4.30;

- ϵ'_P and ϵ'_Φ represents the relevant measurement noise components.

The system of equations presented above contains six unknowns (the receiver position coordinates, the receiver clock offsets and the zenith wet delay) plus n unknowns one for each visible satellite (the carrier-phase ambiguities), but in this case only six visible satellites are required (if all visible satellite belong to the same constellation only five satellites are required) because each visible satellite contributes with two linearly independent observations. These unknowns define the state to be estimated:

$$\mathbf{x} = \begin{bmatrix} x & y & z & c \cdot \delta t_G & c \cdot \delta t_R & Z_{wd} & \lambda \cdot N \end{bmatrix}^T \qquad (4.87)$$

And the linearisation of the observation equations yields the following sub-matrices:

$$H_{P_{IF,G}} = \begin{bmatrix} \dfrac{x - X_s}{\rho} & \dfrac{y - Y_s}{\rho} & \dfrac{z - Z_s}{\rho} & 1 & 0 & M_w & 0 \end{bmatrix} \qquad (4.88)$$

$$H_{P_{IF,R}} = \begin{bmatrix} \dfrac{x - X_s}{\rho} & \dfrac{y - Y_s}{\rho} & \dfrac{z - Z_s}{\rho} & 0 & 1 & M_w & 0 \end{bmatrix} \qquad (4.89)$$

$$H_{\Phi_{IF,G}} = \begin{bmatrix} \dfrac{x - X_s}{\rho} & \dfrac{y - Y_s}{\rho} & \dfrac{z - Z_s}{\rho} & 1 & 0 & M_w & 1 \end{bmatrix} \qquad (4.90)$$

$$H_{\Phi_{IF,R}} = \begin{bmatrix} \dfrac{x - X_s}{\rho} & \dfrac{y - Y_s}{\rho} & \dfrac{z - Z_s}{\rho} & 0 & 1 & M_w & 1 \end{bmatrix} \qquad (4.91)$$

The state-transition model is same as defined in the previous subsection, additionally the zenith wet delay should be modelled as random-walk process with a variation in the order of a few centimetres per hour [22] and the carrier-phase ambiguities use the state-transition model presented in section 4.4.4.
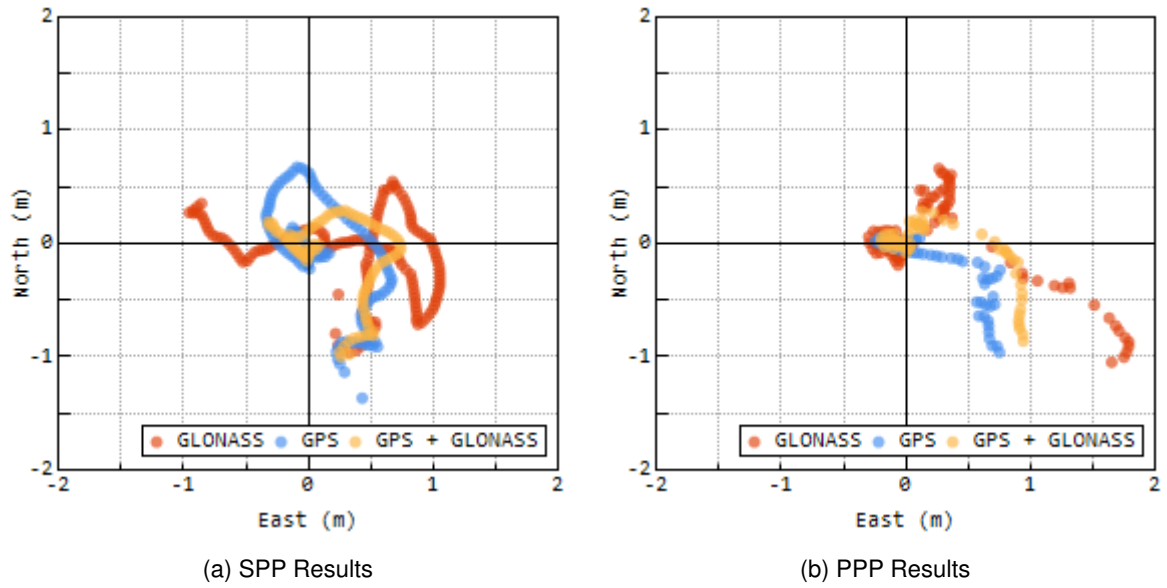

(a) SPP Results

(b) PPP Results

Figure 4.8: Comparsion between SPP and PPP

Precise orbits and clocks

Instead of the orbits and clocks provided by the satellite navigation messages, precise orbits and clocks computed from a global network of reference stations must be used. The IGS provides the following products [33]:

		Product	Accuracy	Latency	Updates	Sampling
GPS	**Ultra-Rapid**	Orbits	5 cm	Real time	—	15 minutes
		Clocks	3 ns			
	Rapid	Orbits	2.5 cm	17–41 hours	17:00 UTC	15 minutes
		Clocks	75 ps			5 minutes
	Final	Orbits	2.5 cm	12–18 days	Thursdays	15 minutes
		Clocks	75 ps			5 minutes
GLONASS	**Ultra-Rapid**	Orbits	—	—	—	—
		Clocks				
	Rapid	Orbits	—	—	—	—
		Clocks				
	Final	Orbits	5 cm	12–18 days	Thursdays	15 minutes
		Clocks	—			

Table 4.3: Available IGS products

To obtain the precise satellite orbit at a given epoch, it's necessary to apply an interpolation technique [34]. For efficiency the Lagrange interpolation method can be used. This interpolation method

is defined as, [20]:

$$P_n = \sum_{i=0}^{n} y_i \prod_{\substack{j=0 \\ i \neq j}}^{n} \frac{x - x_j}{x_i - x_m}$$ (4.92)

And unlike the orbits determined from the navigation messages, these precise orbits are referenced to the satellite center of mass [34], therefore the antenna phase center offset must be determined and applied to the orbit by, [22, 27]:

$$\vec{r}_{sat} = (\vec{r}_{sat})_{MC} + R_{sat} \cdot \vec{\Delta}_{APC}$$ (4.93)

where:

- $\vec{\Delta}_{APC}$ is the absolute antenna phase center offset provided by the IGS ANTEX files [27].

- R_{sat} is the transformation matrix to the satellite local coordinate system presented in appendix B.3.

4.5.3 Observation noise

The characterization of the measurements error is very difficult, ill-defined measurement noise covariance may lead to a filter poor performance or even divergences. A common simplification is to assume that the measurements from different satellites are uncorrelated:

$$R = \begin{bmatrix} \sigma_{Y,1}^2 & 0 & \cdots & 0 \\ 0 & \sigma_{Y,2}^2 & \cdots & 0 \\ \vdots & \vdots & \ddots & \vdots \\ 0 & 0 & \cdots & \sigma_{Y,n}^2 \end{bmatrix}$$ (4.94)

where:

- $\sigma_{Y,i}^2$ is the user equivalent range error, defined as, [35]:

$$\sigma_{Y,i}^2 = \sigma_{eph}^2 + \sigma_{clk}^2 + \sigma_{T_d}^2 + \sigma_{I_d}^2 + \sigma_{\epsilon_i}^2$$ (4.95)

- σ_{eph}^2 is the expected variance of the determination of the satellite orbit;

- σ_{clk}^2 is the expected variance of the determination of the satellite clock offset;

- $\sigma_{I_d}^2$ is the expected variance of the ionospheric delay model;

- $\sigma_{T_d}^2$ is the expected variance of the tropospheric delay model;

- $\sigma_{\epsilon_i}^2$ is the expected variance of the unmodelled relevant observation noise including multipath, it also used to add *"stabilization noise"* to the filter preventing it from diverge [21].

The values for σ_{eph} and σ_{clk} are given in the navigation message of each satellite by the parameter user range accuracy (URA) [11, 7], if the satellite orbits and clock offsets are determined from the IGS products its expected variances are used instead [34], and the values for σ_{I_d} and σ_{T_d} are given by their respective models as presented in section 4.3.3 and section 4.3.4.

The value for σ_{ϵ_i} is defined by, [35]:

$$\sigma_\epsilon = a + \frac{b}{\sin el}$$ (4.96)

where:

- a and b are tunable parameters which should be defined base on the quality of the receiver as well on the conditions of the survey site;

– el is the satellite elevation at the epoch of the observation.

And if the observation is an ionosphere-free combination as defined in section 4.3.3, this value is multiplied by three to account for the increased measurement noise caused by the combination.

Finally when combining pseudorange measurements with carrier-phase measurements it's necessary to ensure that the estimation process gives *more importance* to the carrier-phase measurements, this is accomplished by [22]:

$$\frac{\sigma_P}{\sigma_\Phi} > 100 \tag{4.97}$$

Since this observation noise matrix is a diagonal matrix, it can also be used as weight matrix in the LWLS by using:

$$W = R^{-1} \tag{4.98}$$

4.6 Velocity Estimation

The receiver velocity is an important measurement for many dynamic applications. Usually the velocity measurements are obtained by differencing the position solutions or directly estimated from the Doppler shift measurements.

The first approach yields the average receiver velocity between epochs, and its accuracy is limited by the accuracy of the position estimation process and the time elapsed between adjacent epochs. This velocity is determined from:

$$\vec{v}_{rcv} = \frac{\vec{r}_{rcv,k} - \vec{r}_{rcv,k-1}}{\Delta t} \tag{4.99}$$

where:

– $\vec{r}_{rcv,k}$ and $\vec{r}_{rcv,k-1}$ are the receiver position at epoch k and epoch $k-1$;

– Δt is the time elapsed between the two epochs.

The second approach yields the instantaneous receiver velocity, and its accuracy is limited by the quality of the Doppler shift measurements and the quality of its models. Following the same reasoning used in section 4.5, the estimation state is defined as [13]:

$$\mathbf{x} = \begin{bmatrix} v_x & v_y & v_z & c \cdot \delta \dot{t}_G & c \cdot \delta \dot{t}_R \end{bmatrix}^T \tag{4.100}$$

where:

– v_x, v_y and v_z are the receiver velocity components;

– $\delta \dot{t}_G$ and $\cdot \delta \dot{t}_R$ are the receiver clock drift from the GPS time-scale and the GLONASS time-scale.

And the linearisation process around the current epoch yields the following observation model submatrices [13]:

$$H_G = \begin{bmatrix} \dfrac{x - X_s}{\rho} & \dfrac{y - Y_s}{\rho} & \dfrac{z - Z_s}{\rho} & 1 & 0 \end{bmatrix} \tag{4.101}$$

$$H_R = \begin{bmatrix} \dfrac{x - X_s}{\rho} & \dfrac{y - Y_s}{\rho} & \dfrac{z - Z_s}{\rho} & 0 & 1 \end{bmatrix} \tag{4.102}$$

Note that the resulting design matrix is identical to the design matrix used for the position estimation, this property can be exploited to reduce the computational load of the velocity estimation.

Since the Doppler shift measurement are closely tied to the carrier-phase measurements, the same observation noise model presented in section 4.5 can be used to weight the Doppler shift measurements in the estimation process.

4.7 Time Estimation

After solving the satellite navigation problem, the current time in the UTC time-scale can be determined using the parameters provided by either the GPS satellite navigation message or the GLONASS satellite navigation message. The accuracy provided by those parameters in no worse than 90 nanoseconds [17].

4.7.1 GPS time-scale to the UTC time-scale

Let t_G be the time expressed in the GPS time-scale estimated by the receiver, the respective time in the UTC time-scale is determined by applying one of the following relationships [11]:

1. The time defined by WN_{LSF} and DN is in the future, and $t_G \notin [DN + 3/4; DN + 5/4]$:

$$t_{UTC} = (t_G - \Delta t_{UTC}) \mod 86400 \tag{4.103}$$
$$\Delta t_{UTC} = \Delta t_{LS} + A_0 + A_1(t_G - t_{ot} + 604800(WN - WN_t)) \tag{4.104}$$

2. The time defined by WN_{LSF} and DN is in the future, and $t_G \in [DN + 3/4; DN + 5/4]$:

$$t_{UTC} = W \mod (86400 + \Delta t_{LSF} - \Delta t_{LS}) \tag{4.105}$$
$$W = (t_G - \Delta t_{UTC} - 43200) \mod 86400 + 43200 \tag{4.106}$$

And Δt_{UTC} is the same as defined in equation 4.104.

3. The time defined by WN_{LSF} and DN is in the past:

$$t_{UTC} = (t_G - \Delta t_{UTC}) \mod 86400 \tag{4.107}$$
$$\Delta t_{UTC} = \Delta t_{LSF} + A_0 + A_1(t_G - t_{ot} + 604800(WN - WN_t)) \tag{4.108}$$

Using the following parameters provided the GPS navigation message [11]:

– A_0 and A_1 are polynomial coefficients representing the offset and drift between the two time-scales;

– WN_t and t_{ot} are the reference GPS week and reference GPS time of week of the UTC parameters;

– Δt_{LS} is the current number of leap seconds between the two time-scales;

– WN_{LSF} is the GPS week of the next scheduled change of leap seconds;

– DN is the day of week within WN_{LSF}, in witch the change of leap seconds will occur;

– Δt_{LSF} is the future number of leap seconds.

4.7.2 GLONASS time-scale to the UTC time-scale

Let t_R be the time expressed in the GLONASS time-scale estimated by the receiver, the respective time in the UTC time-scale is determined by [7]:

$$t_{UTC} = t_R + t_c - 3^h\, 00^m\, 00^s \tag{4.109}$$

Where t_c is GLONASS time-scale to UTC time-scale offset provided by the GLONASS navigation message.

Additionally the GLONASS navigation message also allows to determine the current year number unambiguously by [7]:

$$Y = 1996 + 4 \cdot (N_4 - 1) + \left(1 + \begin{cases} 1 & \text{if } 1 \leqslant N_T \leqslant 366 \\ 2 & \text{if } 367 \leqslant N_T \leqslant 731 \\ 3 & \text{if } 732 \leqslant N_T \leqslant 1096 \\ 4 & \text{if } 1097 \leqslant N_T \leqslant 1461 \end{cases}\right) \tag{4.110}$$

where:

– N_4 is the number of four year intervals since 1996 provided by the GLONASS navigation message;

– N_T is the current GLONASS day of year.

Chapter 5

Research Setup

5.1 Introduction

In this chapter the implementation and experimental are briefly described. In starts with an overview of the GNSS receiver and antenna used, then an overview of the developed tools and software and finally a description of the experimental setup used to draw the conclusions of this thesis.

5.2 GNSS Receiver and Antenna

To gather the necessary data to test the algorithms presented in the previous chapters, a ProFlex 500 from Ashthec was used. The ProFlex 500 is an high-end receiver, capable of track multiple GNSS constellations including signals from various Satellite-Based Augmentation Systems (SBAS) (WASS/EGNOS/MSAS). Equipped with 75 frequency channels it's capable of processing signals, on both L1 and L2 carrier frequencies of the GPS (L1 C/A, L1/L2 P-code and L2C) and GLONASS (L1 C/A, L2 C/A and L2P code). The receiver provides real-time PVT estimation and it also provides the observables (pseudorange, carrier-phase and Doppler shift) along with other signal relevant properties and ephemeris parameters of each tracked satellite, the almanacs parameters for each tracked GNSS constellation, ionospheric parameters and GNSS-time to UTC parameters, through a binary message (Asthec legacy messages, ATOM messages) [12].The antenna used was the L1/L2 GPS+GLONASS ProFlex 500 survey antenna (AT1675-7M) equipped with a choke ring to reduce multipath effects.

Figure 5.1: ProFlex 500 – GNSS Receiver

Figure 5.2: AT1675-7M – GNSS Antenna

5.3 Developed Software

A number of GNSS software tools were developed during the work on this thesis. These tools were mainly developed in C# (some routines tied to the data acquisition process were developed in C) and

the main purpose of these tools were to test and evaluate the algorithms presented in the previous chapters. All the results presented throughout this thesis were obtaining using these tools.

5.3.1 Data Acquisition tool

The Data Acquisition Tool was an important aspect of the developed software, not by its complexity but by its implications on the results and conclusions of this work.

The problem arises from the fact that the ProFlex 500 receiver was designed to be a powerful survey tool, and in order to achieve high accuracies and precisions it uses the information from SBAS to correct the GNSS observations which are mostly only available for the GPS constellation [36], along with proprietary algorithms to perform corrections which the scope of action is unknown. Since the main objective of this thesis is to assess the performance of GPS and GLONASS, these corrections could potentially skew the results towards the GPS.

As mentioned earlier the ProFlex 500 receiver allows three data output formats [12], the Legacy Ashtech messages, the ATOM binary messages and wildly used RINEX format, and although they are very good for surveying applications, each one by itself doesn't fully meet the *requirements* defined above:

- The Legacy Ashtech messages, is outdated and doesn't include new parameters introduced to the GLONASS navigation messages which are required to properly assess the performance of both systems. Furthermore the format is rather ambiguous in its implementation and some of the raw measurements cannot be recovered.

- The ATOM binary messages, provides everything required to properly asses the performance of both systems (corrections applied by the receiver, corrections from SBAS), but its format is quite complicated to understand and decode [37].

- The RINEX format, is a very simple format easy to understand and easy to decode, but it also lacks some of the new parameters introduced to the GLONASS navigation messages [38], it lacks the temporal coherency required to tie the navigational messages to the GNSS observations and since it is a by-product of the ATOM binary messages it is impossible to recreate some of the raw measurements due to the corrections applied by the receiver.

To solve this problem, the following process was implemented; firstly the data acquisition process reads the ATOM binary messages from the receiver and stores them on the computer; secondly from the raw ATOM binary messages the Ashtech RINEX conversion tool is used to generate the RINEX observations files and the RINEX navigation files. Thirdly the raw ATOM binary files processed by a custom decoder developed for this thesis which extracts the required parameters (SBAS corrections and Ashtech proprietary corrections) to recreate the raw GNSS measurements along with the true time-stamps of each navigational message and the missing GLONASS parameters (refined health information and user expected accuracy), and combines them with the RINEX files, packing them into a single custom file. This process is illustrated in the following figure:
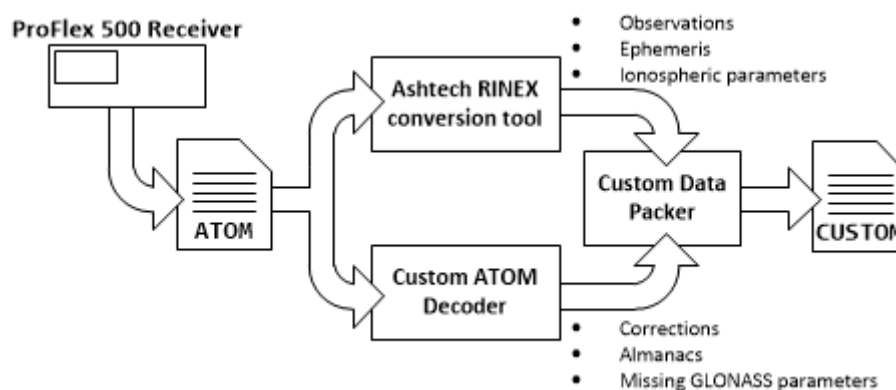

Figure 5.3: Data acquisition process

60

5.3.2 GNSS Suite tool

The GNSS Suite is the main tool developed for this thesis and it encompasses all the other tools; it was designed to allow an intuitive and easy way to analyse the GNSS observations, the GNSS navigation parameters and GNSS solutions obtained from the previously gathered data:
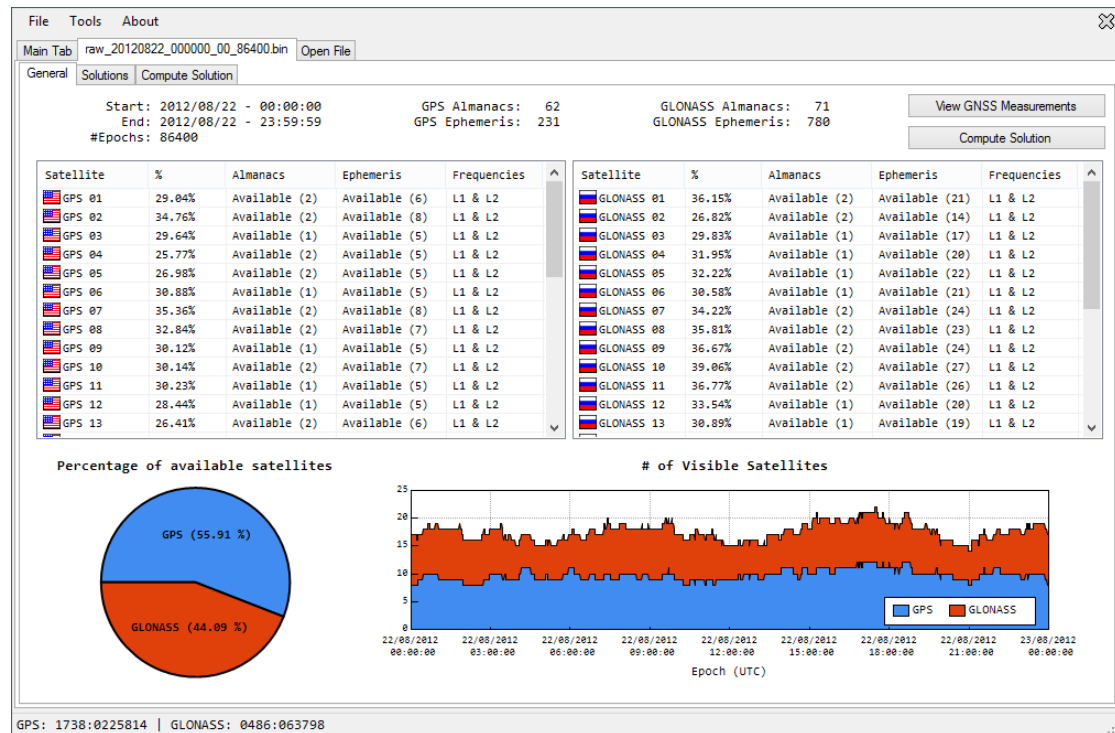

Figure 5.4: Screenshot of the GNSS Suite: General data viewer

GNSS Planning Tool

The GNSS planning tool, as it's expressed by its name, is intended to plan a GNSS survey mission. It uses the most recent GPS almanacs and GLONASS almanacs fetched from its respective web sites, and allows one to plan a GNSS survey mission under various visibility conditions and it also allows to simulate satellites outages to assess their impact on the overall solution.
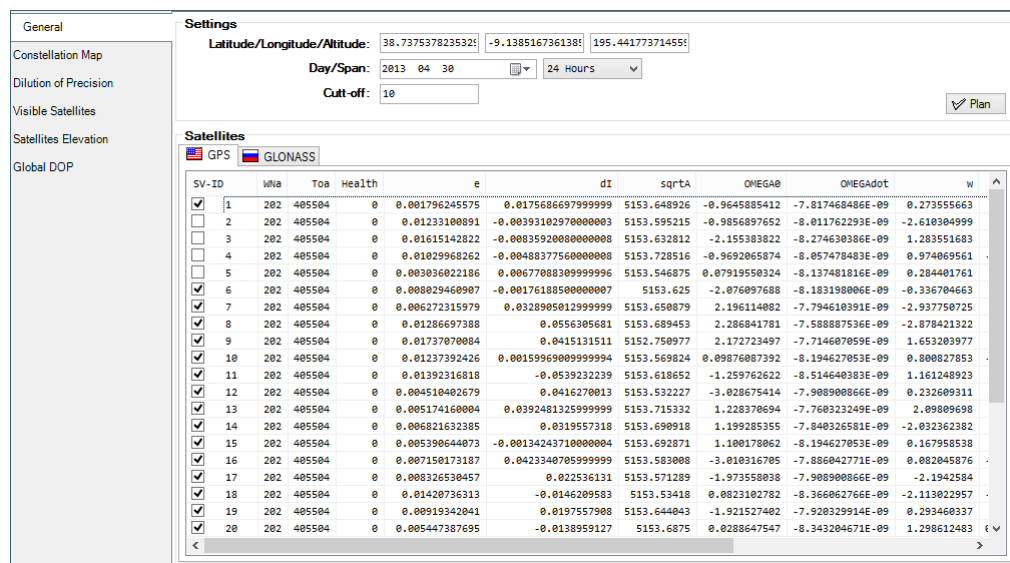
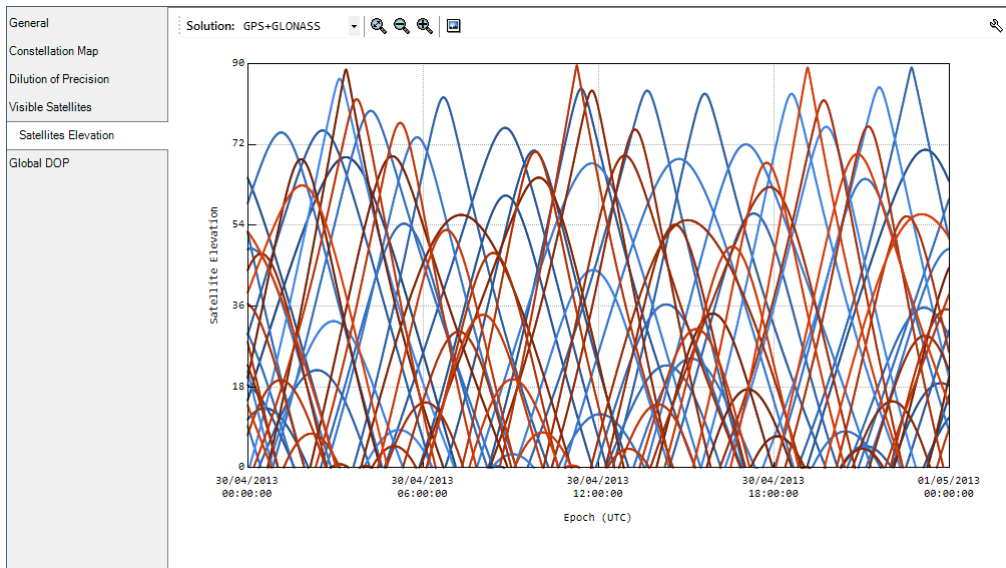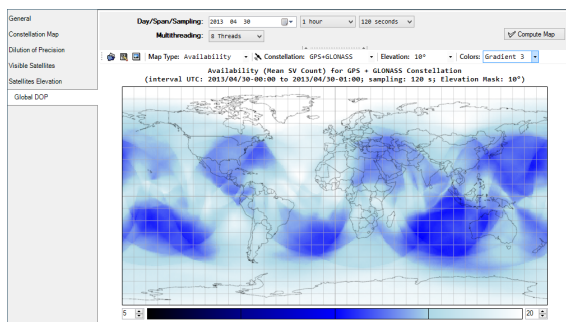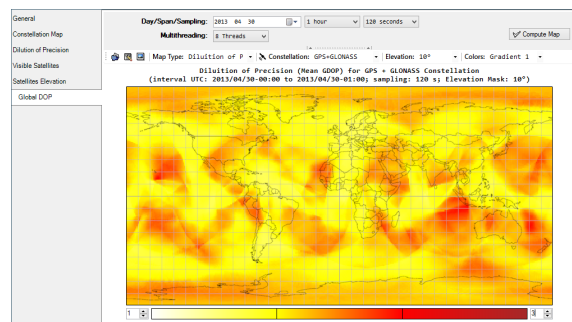Figure 5.5: Screenshot of the GNSS Planning Tool: Configuration

Figure 5.6: Screenshot of the GNSS Planning Tool: Expected satellite elevations

Additionally this tool also allows one to compute instantaneous and integral availability global maps for the GPS constellation, GLONASS constellation and the GPS+GLONASS combined constellation, at different elevation masks and sampling rates.


(a) Availability

(b) Dilution of Precision

Figure 5.7: Screenshots of the GNSS Planning Tool: Global Maps

GNSS Observations Analyser

The GNSS Observations analyzer allows the user to perform an in-depth analysis of each satellite observations and their combinations along with its navigational parameters (ephemeris and almanacs); it also provides tools to export this data to CSV files in order to use them on other applications:
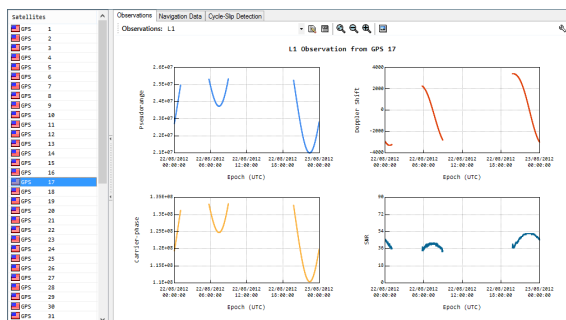
(a) Observation plots
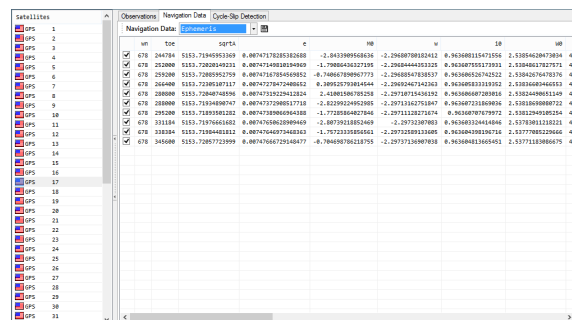
(b) Navigational parameters

Figure 5.8: Screenshots of the GNSS Observations Analyser: General

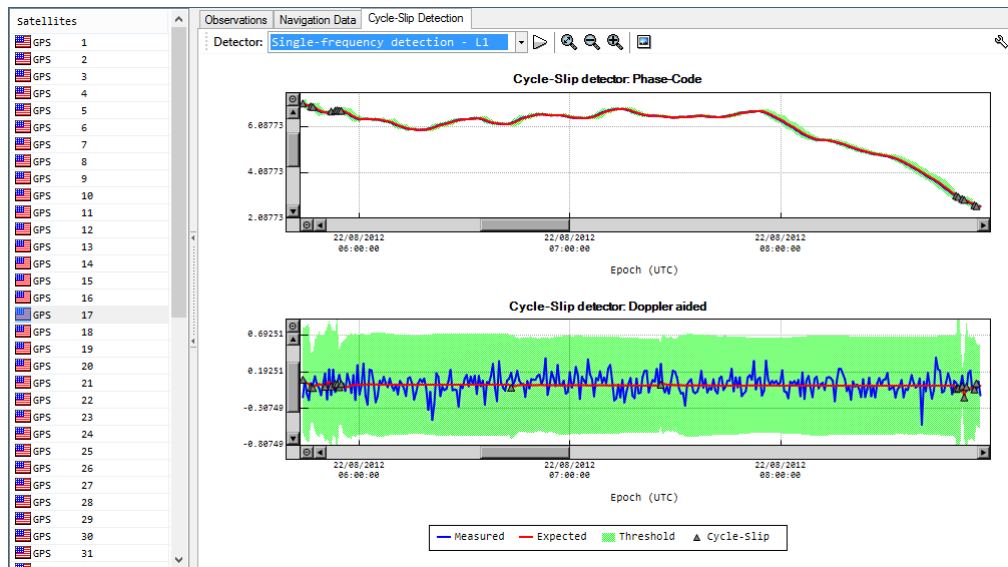Additionally it's also possible to run the cycle-slip detection algorithms described in the previous chapter:

Figure 5.9: Screenshot of the GNSS Observations Analyser: Cycle-Slip detection tool

GNSS Solution Analyser

Main focus was given to the solution analyser, where the user is presented with the three solutions (GPS-Only, GLONASS-Only and GPS+GLONASS) and their statistical obtained from a given set GNSS observations and navigational parameters:
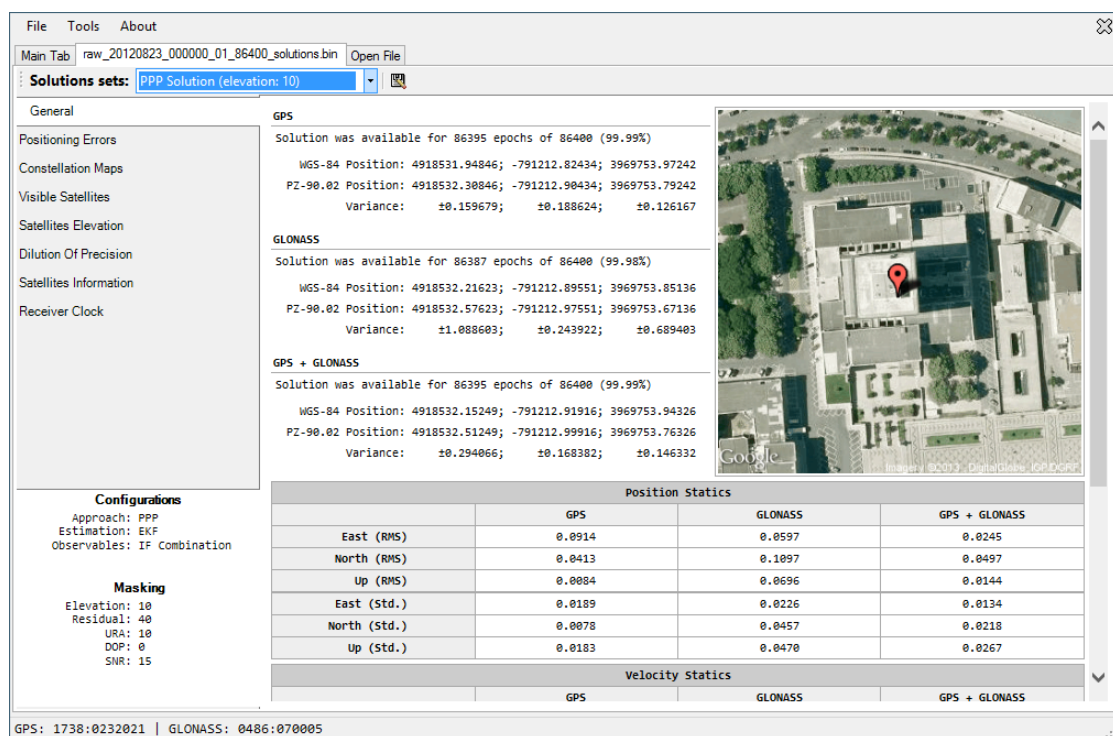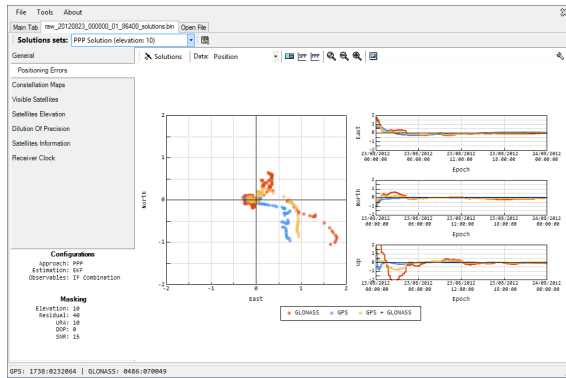

Figure 5.10: Screenshot of the GNSS Solution Analyser

From here the user can view the evolution the positional error, view constellations maps and sky-plots for a given epoch, DOP plots, estimation parameters evolution and access to an in-depth and

epoch-by-epoch information about the used satellites, such as observations residuals, corrections applied, ambiguity resolution state and cycle-slip detection state.
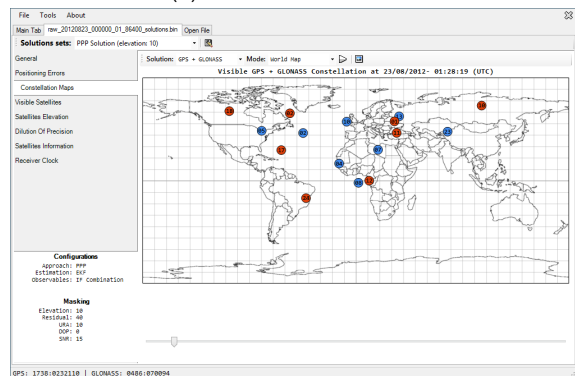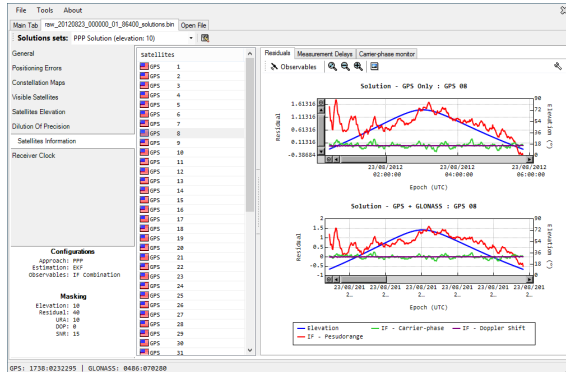

(a) Positioning Errors
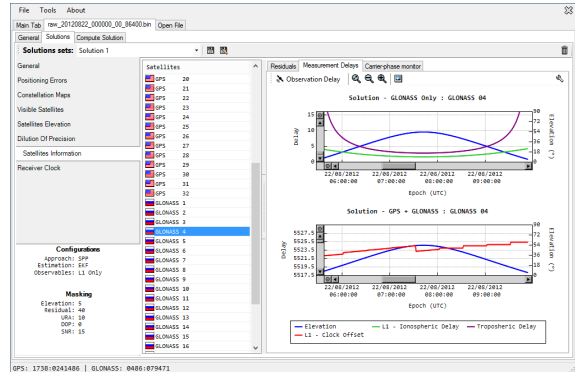

(b) Dilution of Precision
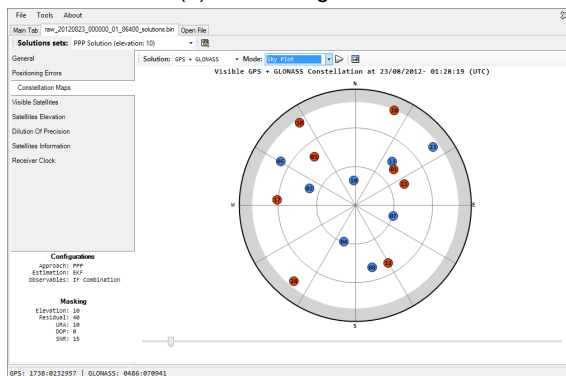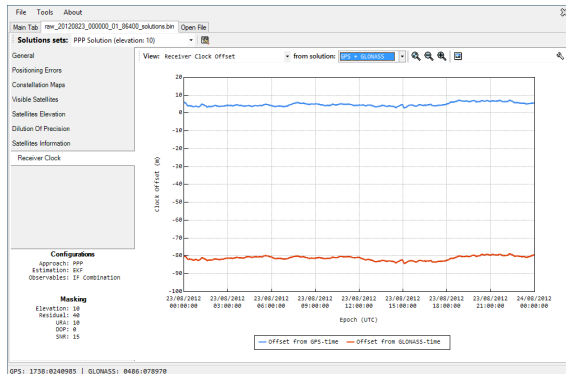

(c) Epoch Sky-plot

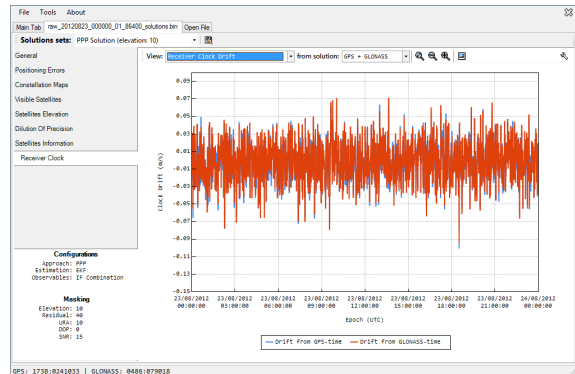(d) Epoch World Map

(e) In-depth satellite information 1

(f) In-depth satellite information 2

(g) Receiver clock offsets

(h) Receiver clock drifts

Figure 5.11: Screenshots of the GNSS Solution Analyser

64

5.4 Experimental Setup

5.4.1 Antenna Location

The receiver antenna was located on the top of North Tower of IT/IST in Lisbon, Portugal. This location grants a privileged view of the sky (being possible to track satellites at atleast 5° of elevation) with negligible multipath effects.

Figure 5.12: Antenna location

Reference position

To establish a reference position required to evaluate the accuracy and precision of the presented algorithms, 12 days of continuous observations (from 22/08/2012 to 03/09/2012) were performed using the full capabilities of the receiver; the mean position estimated by the receiver was:

$$38° \; 44' \, 15.15'' \, N; \qquad 9° \; 08' \, 18.65'' \, W; \qquad 196.02 \, m$$

5.4.2 Experimental trial description

The purpose of this experimental trial is to assess the performance of the algorithms presented throughout this thesis (mainly SPP vs. PPP), and to evaluate the performance of the combined GPS+GLONASS solution against the GPS-Only and GLONASS-Only solutions with real data.

The performance of the combined GPS+GLONASS solution against the GPS-Only and GLONASS-Only solutions, is evaluated by three parameters, the solution accuracy, the solution precision and the solution availability.

The solution accuracy and precision are tested using the performance metrics presented in section 2.8 against the antenna reference position, and the solution availability is tested by considering various elevation cut-off angles for the visible satellites; this simulates several survey site conditions as described in table 5.1.

Elevation	Sky visibility	Description
10°	∼82.635%	Wastelands and ocean surface
20°	∼65.798%	Small cities, locations near trees
30°	∼50.000%	Big cities, locations near mountains or heavy tree foliage
40°	∼35.721%	Mega-cities (composed mainly by skyscrapers), under heavy tree foliage, mine-shafts, canyons

Table 5.1: Trials Visibility conditions

Chapter 6

Experimental results

6.1 Introduction

In this chapter the results from the experimental setup described in previous chapter, are presented along with a discussion from which the conclusions of this thesis are obtained.

6.2 Dataset Analysis

The dataset used to test the implemented algorithms, corresponds to a day of data from the twelve days of data gathered to determine the reference position, its properties are presented bellow:

Start	2012/08/23 00:00:00
End	2012/08/23 23:59:59
Epochs	86400
Almanacs	62 / 24
Ephemeris	219 / 660

Table 6.1: Dataset – Properties
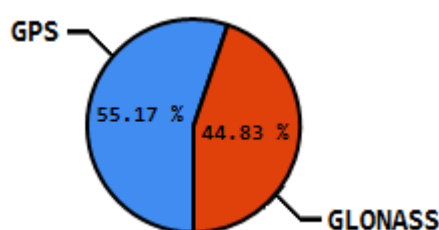
Figure 6.1: Dataset – Constellations availability
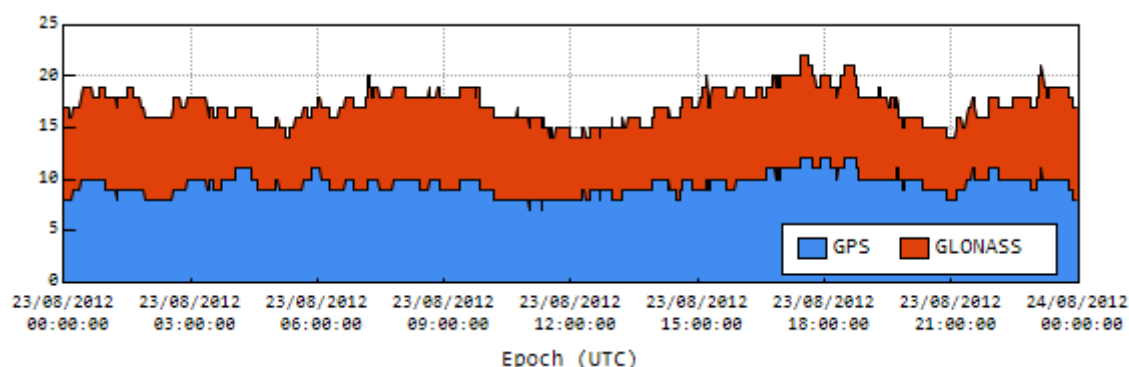
Figure 6.2: Dataset – Number of visible satellites

6.2.1 DOP under the different elevation masks

This dataset analysis serves to quantify the quality of the estimates that may be obtained from the visible satellite geometry for the different elevation angles considered. The results shows that up until $10°$ the DOP values for both systems are always bellow five ensuring a good quality for each system alone, for the combined solution the respective DOP values were always bellow two and a half.

For cut-off elevation angles ranging from $10°$ to $20°$(figures 6.3 and 6.4), the results show that

67

GLONASS alone starts to lose quality significantly, while the GPS alone stills retains DOP values always bellow ten. Again the combined solution presents DOP values bellow five 99.9% of the time;

For cut-off elevation angles ranging from 20° to 30°(figures 6.4 and 6.5), the GLONASS visible satellite geometry gets severally degraded, but it is still possible to obtain rough navigational fixes, however the GPS visible satellite geometry is still capable of provide DOP values bellow ten most of time, and the combination both provides DOP values in the range of five;

For cut-off elevation angles ranging from 30° to 40°(figures 6.5 and 6.6), the GLONASS starts to present severe service outages being unable to satisfy the basic requisites for most GNSS applications, GPS also starts to present services outages but it is still capable of provide service and good DOP values most of the time.
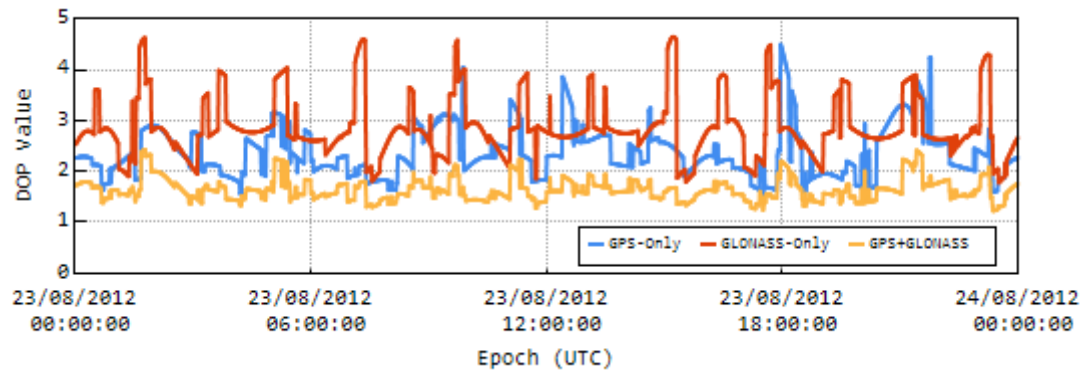
Figure 6.3: Dataset – DOP for a cut-off elevation angle of 10°
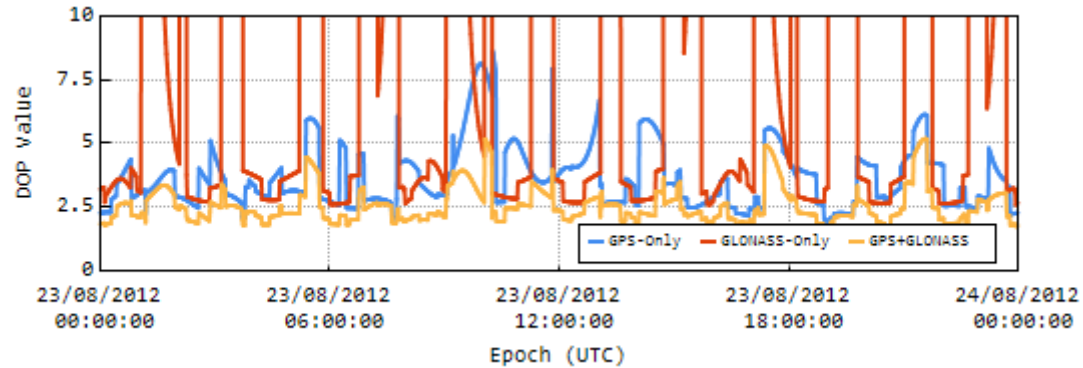
Figure 6.4: Dataset – DOP for a cut-off elevation angle of 20°
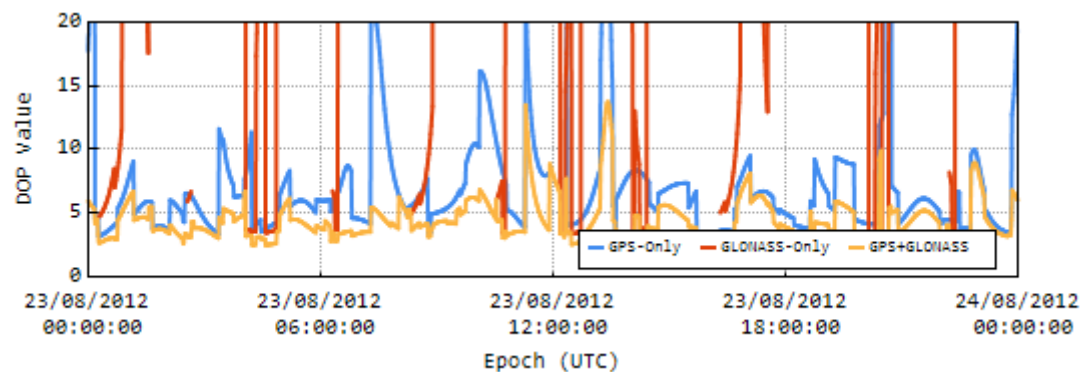
Figure 6.5: Dataset – DOP for a cut-off elevation angle of 30°
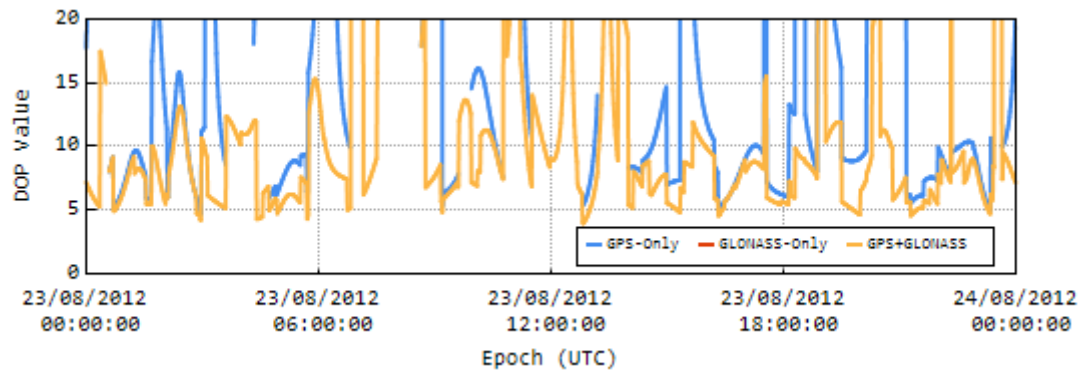
Figure 6.6: Dataset – DOP for a cut-off elevation angle of 40°

To further investigate the causes of the GLONASS poor performance at the test site, using the GNSS almanacs gathered during the experimental trials, the average DOP values for 864000 seconds (one day span) were computed for a world grid world grid with 1° of resolution and a cut-off elevation angle of 5°.

The results shows an expected global DOP improvement of 26% when compared to the GPS-Only DOP values, and an expected DOP improvement of 34% when compared to the GLONASS-Only DOP values. However, from these results it's also noticeable that the GLONASS provides much better results for higher latitudes (mainly over the Russian territory), accounting for its poor performance at the test site. These results are illustrated in figure 6.7.
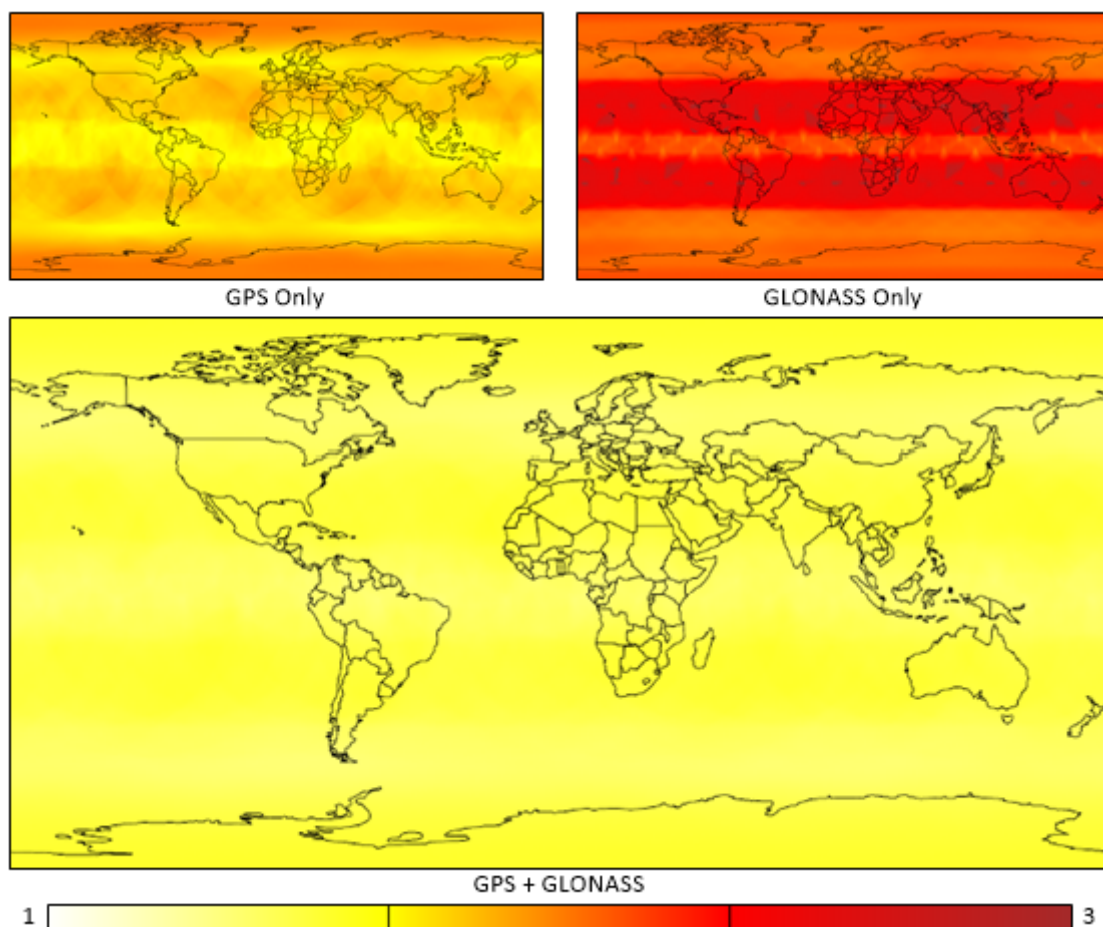
Figure 6.7: Global DOP improvement from combining GPS and GLONASS

69

6.3   Standard Point Positioning – Results

In this section, the results for the satellite navigation problem resolution are presented using the SPP approach. Here only the information broadcast by the satellites and the pseudoranges measurements were used to obtain the receiver position and velocity. Initially the receiver position and velocity is assumed to be unknown, and the first estimate is obtained using the LWLS algorithm, after the first estimation the process continues using the EKF algorithm.

The results show that for the east and north coordinates of the receiver position both systems performed well, being the GPS-Only solutions marginally better than GLONASS-Only solutions. However for the Up coordinate of the receiver position the GLONASS-Only solutions presented an error of almost one order of magnitude higher than the GPS-Only solutions. Generally GPS+GLONASS solutions presented improved results over than GPS-Only and GLONASS-Only solutions, these improvements are specially noticeable in the Up coordinate of the receiver position.

	Solution Availability		
Elevation Cut-Off	GPS-Only	GLONASS-Only	GPS+GLONASS
10°	100.000%	100.000%	100.000%
20°	100.000%	100.000%	100.000%
30°	98.527%	90.856%	100.000%
40°	80.515%	37.657%	99.267%

Table 6.2: SPP – Solutions Availability

Results with a cut-off elevation angle of 10°

Figure 6.8: SPP Results – GPS-Only vs. GLONASS-Only vs. GPS+GLONASS positioning errors

Error $[m]$		GPS-Only	GLONASS-Only	GPS + GLONASS
RMS	East	0.1231	0.9127	0.2937
	North	0.0993	0.2709	0.1610
	Up	0.0185	0.6747	0.1706
Std.	East	0.0175	0.0466	0.0177
	North	0.0311	0.0329	0.0217
	Up	0.0737	0.2156	0.0970

Table 6.3: SPP Results – Position Statistics for the last 43200 epochs

Error $[m/s]$		GPS-Only	GLONASS-Only	GPS + GLONASS
RMS	East	$4.1585 \cdot 10^{-4}$	$8.2694 \cdot 10^{-4}$	$4.8789 \cdot 10^{-4}$
	North	$4.0977 \cdot 10^{-4}$	$4.2381 \cdot 10^{-4}$	$4.2474 \cdot 10^{-4}$
	Up	$7.6531 \cdot 10^{-4}$	$4.4439 \cdot 10^{-4}$	$6.9878 \cdot 10^{-4}$
Std.	East	$6.1489 \cdot 10^{-5}$	$3.9848 \cdot 10^{-5}$	$5.4777 \cdot 10^{-5}$
	North	$9.5781 \cdot 10^{-5}$	$6.5457 \cdot 10^{-5}$	$8.4925 \cdot 10^{-5}$
	Up	$1.3098 \cdot 10^{-4}$	$2.0018 \cdot 10^{-4}$	$1.3773 \cdot 10^{-4}$

Table 6.4: SPP Results – Velocity Statistics for the last 43200 epochs

Results with a cut-off elevation angle of 20°

Figure 6.9: SPP Results – GPS-Only vs. GLONASS-Only vs. GPS+GLONASS positioning errors

Error $[m]$		GPS-Only	GLONASS-Only	GPS + GLONASS
RMS	East	0.1770	0.7999	0.3197
	North	0.1338	0.2879	0.1889
	Up	0.3471	0.6382	0.1469
Std.	East	0.0215	0.0765	0.0280
	North	0.0402	0.0425	0.0340
	Up	0.0585	0.1951	0.0688

Table 6.5: SPP Results – Position Statistics for the last 43200 epochs

Error $[m/s]$		GPS-Only	GLONASS-Only	GPS + GLONASS
RMS	East	$1.6484 \cdot 10^{-5}$	$7.2916 \cdot 10^{-4}$	$1.0675 \cdot 10^{-4}$
	North	0.0010	0.0011	0.0011
	Up	$9.0853 \cdot 10^{-5}$	$8.8047 \cdot 10^{-4}$	$2.4786 \cdot 10^{-4}$
Std.	East	$4.2446 \cdot 10^{-5}$	$2.3932 \cdot 10^{-5}$	$3.5732 \cdot 10^{-5}$
	North	$8.2526 \cdot 10^{-5}$	$3.6973 \cdot 10^{-5}$	$6.7832 \cdot 10^{-5}$
	Up	$1.3077 \cdot 10^{-4}$	$1.6334 \cdot 10^{-4}$	$1.1822 \cdot 10^{-4}$

Table 6.6: SPP Results – Velocity Statistics for the last 43200 epochs
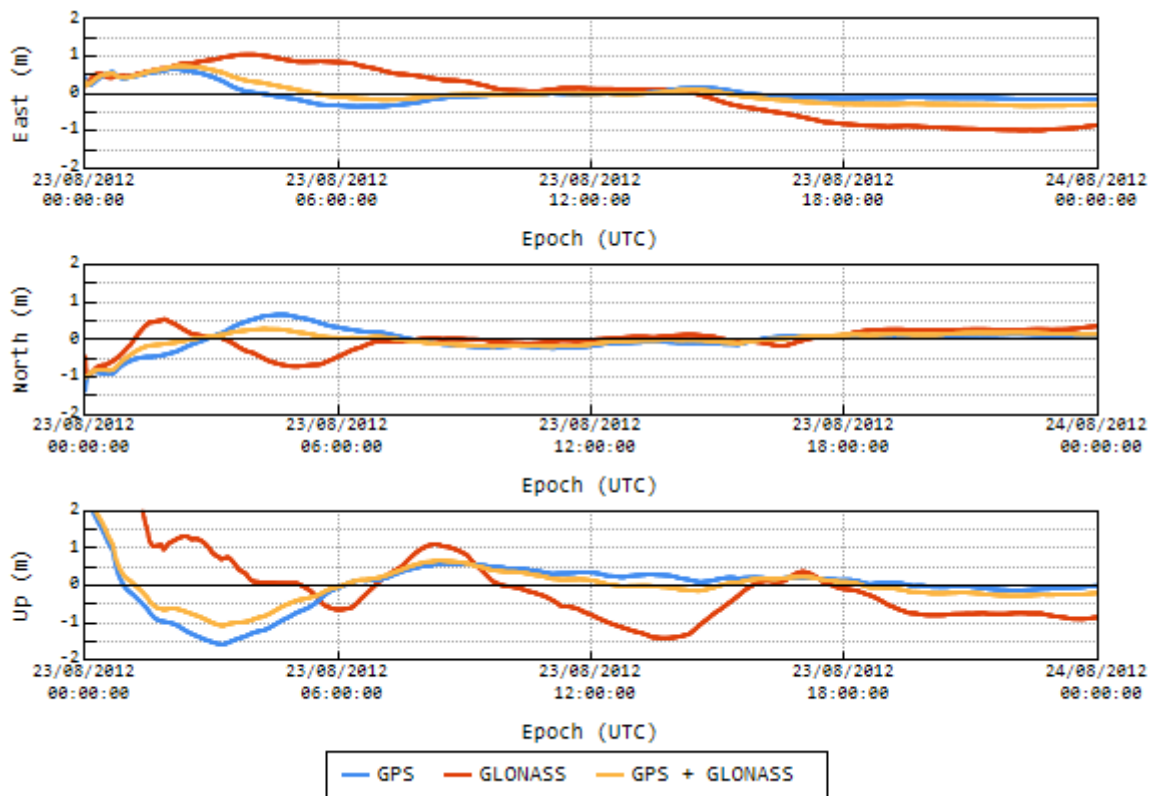
Results with a cut-off elevation angle of 30°

Figure 6.10: SPP Results – GPS-Only vs. GLONASS-Only vs. GPS+GLONASS positioning errors

Error $[m]$		GPS-Only	GLONASS-Only	GPS + GLONASS
RMS	East	0.3114	0.6558	0.3762
	North	0.0422	0.2862	0.1067
	Up	0.3745	1.3791	0.1158
Std.	East	0.0296	0.1456	0.0336
	North	0.0631	0.0245	0.0518
	Up	0.1118	0.1666	0.1052

Table 6.7: SPP Results – Position Statistics for the last 43200 epochs

Error $[m/s]$		GPS-Only	GLONASS-Only	GPS + GLONASS
RMS	East	$8.0008 \cdot 10^{-5}$	$3.0583 \cdot 10^{-4}$	$6.4296 \cdot 10^{-5}$
	North	0.0017	0.0017	0.0017
	Up	0.0013	$8.9134 \cdot 10^{-4}$	0.0013
Std.	East	$3.9222 \cdot 10^{-5}$	$3.4143 \cdot 10^{-5}$	$3.5330 \cdot 10^{-5}$
	North	$8.2584 \cdot 10^{-5}$	$5.5199 \cdot 10^{-5}$	$6.0274 \cdot 10^{-5}$
	Up	$1.8272 \cdot 10^{-4}$	$2.3057 \cdot 10^{-4}$	$1.6207 \cdot 10^{-4}$

Table 6.8: SPP Results – Velocity Statistics for the last 43200 epochs

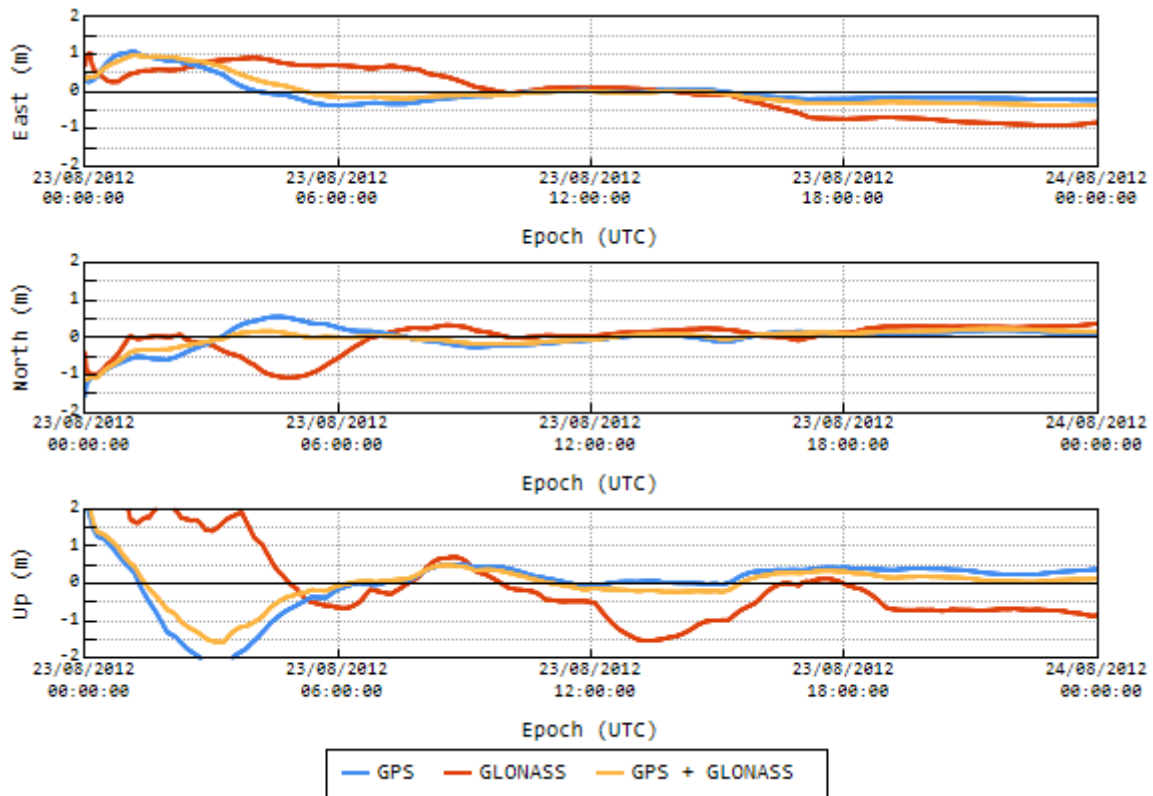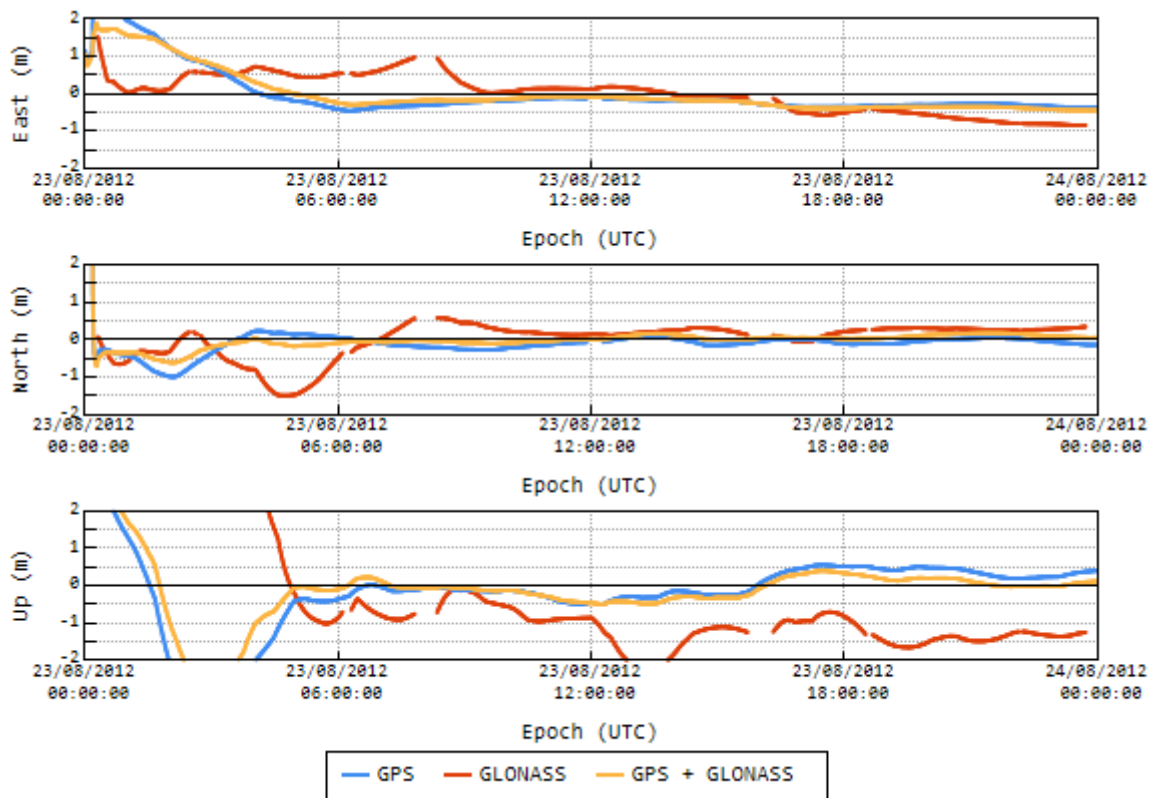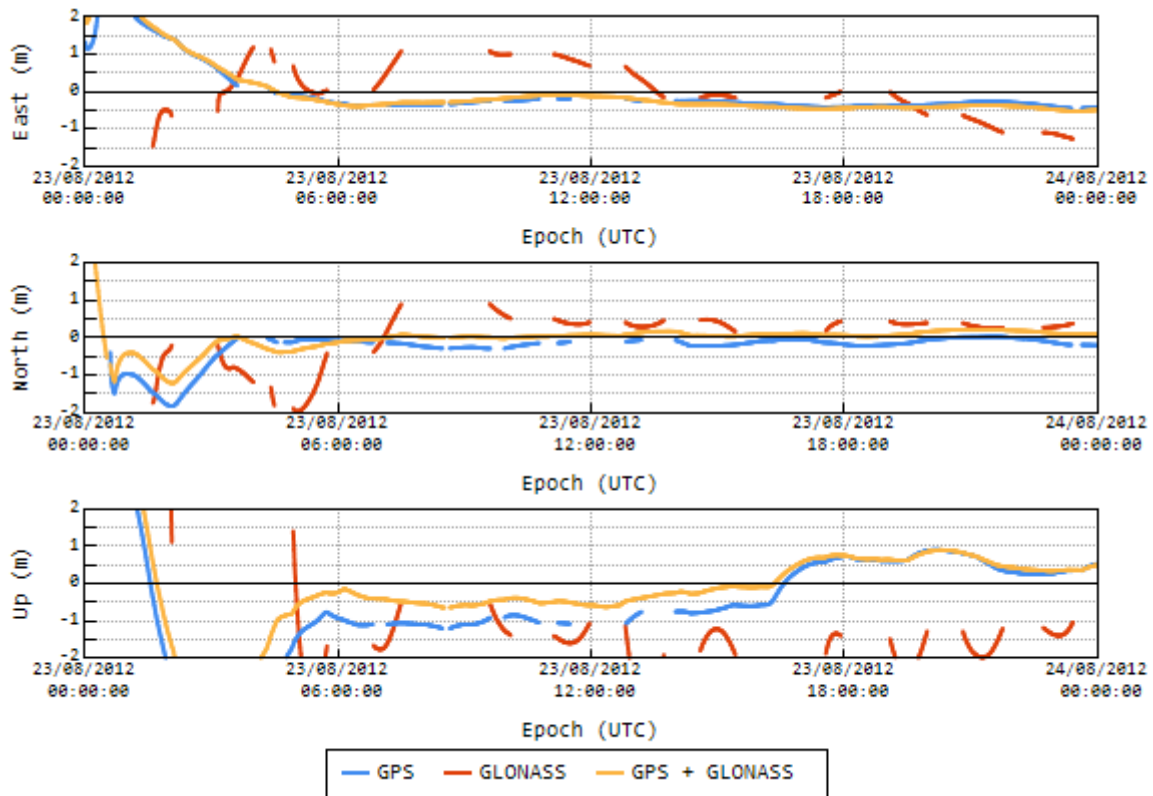## Results with a cut-off elevation angle of 40°

Figure 6.11: SPP Results – GPS-Only vs. GLONASS-Only vs. GPS+GLONASS positioning errors

Error $[m]$		GPS-Only	GLONASS-Only	GPS + GLONASS
RMS	East	0.3476	0.7598	0.4213
	North	0.0917	0.3274	0.1379
	Up	0.5745	1.7028	0.5994
Std.	East	0.0516	0.3613	0.0458
	North	0.0880	0.0514	0.0616
	Up	0.2174	0.3658	0.1848

Table 6.9: SPP Results – Position Statistics for the last 43200 epochs

Error $[m/s]$		GPS-Only	GLONASS-Only	GPS + GLONASS
RMS	East	$1.5468 \cdot 10^{-4}$	$9.0253 \cdot 10^{-4}$	$2.5257 \cdot 10^{-4}$
	North	0.0024	0.0015	0.0023
	Up	0.0018	0.0023	0.0017
Std.	East	$9.0910 \cdot 10^{-5}$	$1.0649 \cdot 10^{-4}$	$8.5046 \cdot 10^{-5}$
	North	$6.4852 \cdot 10^{-5}$	$5.8525 \cdot 10^{-5}$	$4.8014 \cdot 10^{-5}$
	Up	$2.9312 \cdot 10^{-4}$	$9.7187 \cdot 10^{-5}$	$2.3891 \cdot 10^{-4}$

Table 6.10: SPP Results – Velocity Statistics for the last 43200 epochs

6.4 Precise Point Positioning – Results

In this section, the results for the satellite navigation problem resolution are presented using the PPP approach, here the GNSS observations (pseudorange and carrier-phase) were used together with precise satellite orbits and clocks from IGS. Initially the receiver position and velocity is assumed to be unknown, and the first estimate is obtained using the LWLS algorithm, after the first estimation the process continues using the EKF algorithm, additionally a SNR mask of 15 db.Hz and a residual mask of 40 m were used filter out bad observations.

The results show for PPP a massive improvement over SPP, providing results at decimetre to centimetre level after the solution convergence. Like the SPP the GPS-Only solutions marginally outperformed the GLONASS-Only solutions, and due to extra satellite required to estimate the tropospheric delay, the GLONASS-Only solutions for higher cut-off elevation angles presented a greater unavailability. Again in general GPS+GLONASS solutions presented improved results than over GPS-Only and GLONASS-Only solutions.

	Solution Availability		
Elevation Cut-Off	**GPS-Only**	**GLONASS-Only**	**GPS+GLONASS**
10°	100.000%	99.991%	100.000%
20°	99.883%	76.162%	100.000%
30°	87.024%	14.916%	100.000%
40°	32.705%	00.006%	96.457%

Table 6.11: PPP – Solutions Availability

Results with a cut-off elevation angle of 10°

Figure 6.12: PPP Results – GPS-Only vs. GLONASS-Only vs. GPS+GLONASS positioning errors

Error [m]		GPS-Only	GLONASS-Only	GPS + GLONASS
RMS	East	0.0914	0.0597	0.0245
	North	0.0413	0.1097	0.0497
	Up	0.0084	0.0696	0.0144
Std.	East	0.0189	0.0226	0.0134
	North	0.0078	0.0457	0.0218
	Up	0.0183	0.0470	0.0267

Table 6.12: PPP Results – Position Statistics for the last 43200 epochs

Error [m/s]		GPS-Only	GLONASS-Only	GPS + GLONASS
RMS	East	$4.0373 \cdot 10^{-5}$	$4.6279 \cdot 10^{-4}$	$6.6909 \cdot 10^{-5}$
	North	$9.5592 \cdot 10^{-4}$	0.0013	0.0011
	Up	$2.6279 \cdot 10^{-5}$	$2.0018 \cdot 10^{-4}$	$4.0034 \cdot 10^{-6}$
Std.	East	$2.4842 \cdot 10^{-5}$	$1.5809 \cdot 10^{-5}$	$2.0583 \cdot 10^{-5}$
	North	$7.3996 \cdot 10^{-5}$	$4.7827 \cdot 10^{-5}$	$6.1442 \cdot 10^{-5}$
	Up	$9.9362 \cdot 10^{-5}$	$1.9097 \cdot 10^{-4}$	$9.9101 \cdot 10^{-5}$

Table 6.13: PPP Results – Velocity Statistics for the last 43200 epochs

Results with a cut-off elevation angle of 20°

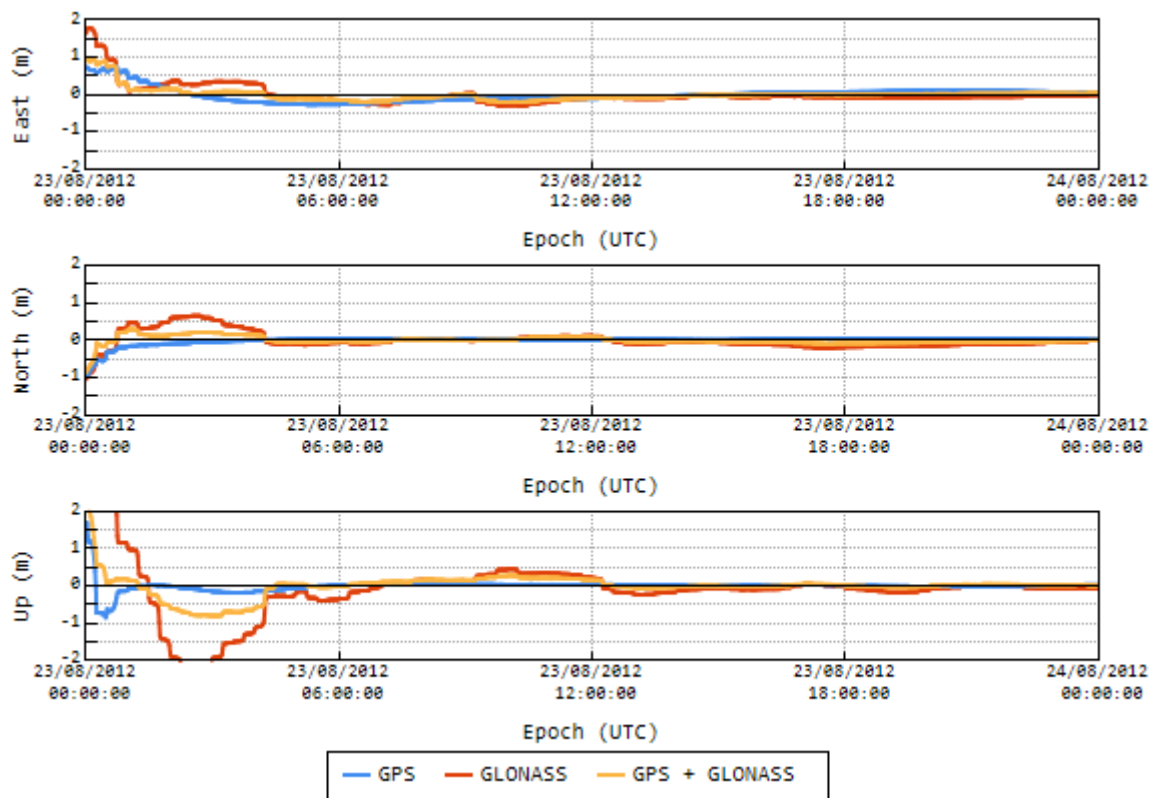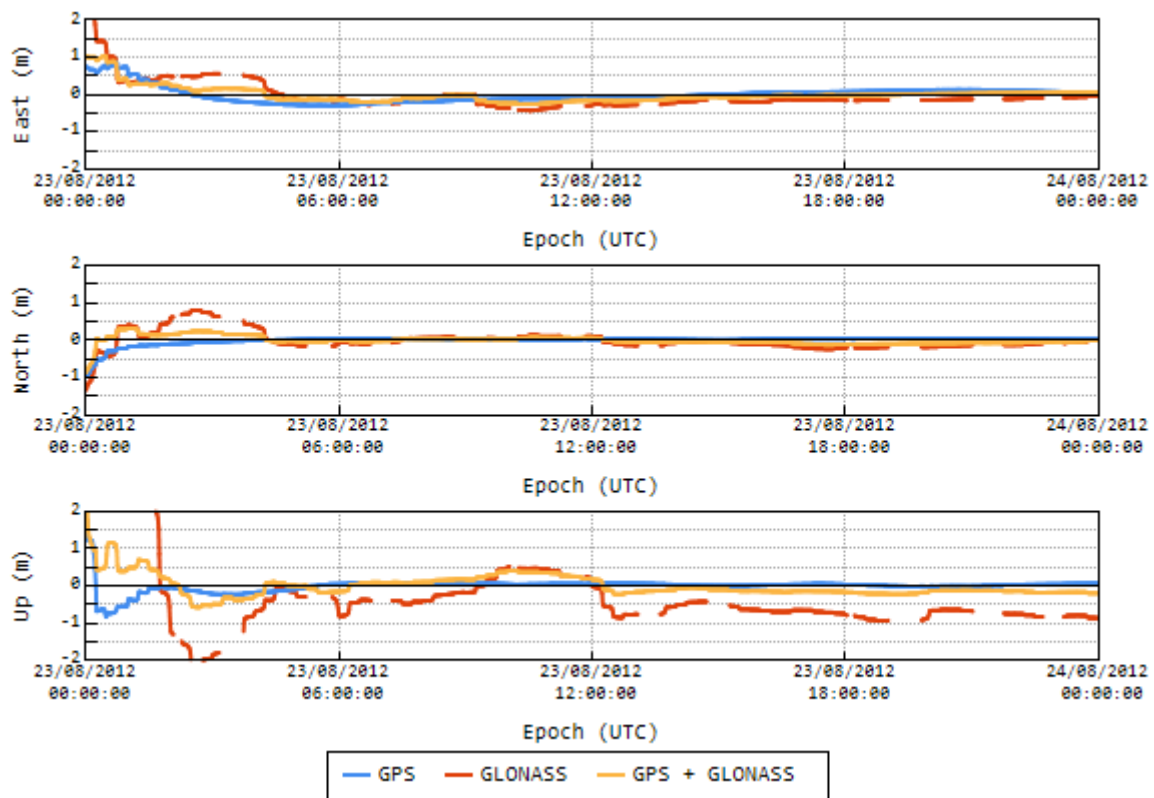Figure 6.13: PPP Results – GPS-Only vs. GLONASS-Only vs. GPS+GLONASS positioning errors

Error $[m]$		GPS-Only	GLONASS-Only	GPS + GLONASS
RMS	East	0.1032	0.1126	0.0274
	North	0.0425	0.1250	0.0670
	Up	0.0234	0.7781	0.1604
Std.	East	0.0230	0.0364	0.0232
	North	0.0087	0.0589	0.0272
	Up	0.0264	0.0936	0.0344

Table 6.14: PPP Results – Position Statistics for the last 43200 epochs

Error $[m/s]$		GPS-Only	GLONASS-Only	GPS + GLONASS
RMS	East	$2.2749 \cdot 10^{-4}$	$4.8911 \cdot 10^{-4}$	$9.2365 \cdot 10^{-5}$
	North	0.0012	0.0016	0.0014
	Up	$6.2226 \cdot 10^{-4}$	$6.1617 \cdot 10^{-4}$	$6.6779 \cdot 10^{-4}$
Std.	East	$2.3697 \cdot 10^{-5}$	$2.0489 \cdot 10^{-5}$	$2.3680 \cdot 10^{-5}$
	North	$6.9730 \cdot 10^{-5}$	$3.5142 \cdot 10^{-5}$	$5.4960 \cdot 10^{-5}$
	Up	$9.5694 \cdot 10^{-5}$	$1.7951 \cdot 10^{-4}$	$8.4962 \cdot 10^{-5}$

Table 6.15: PPP Results – Velocity Statistics for the last 43200 epochs
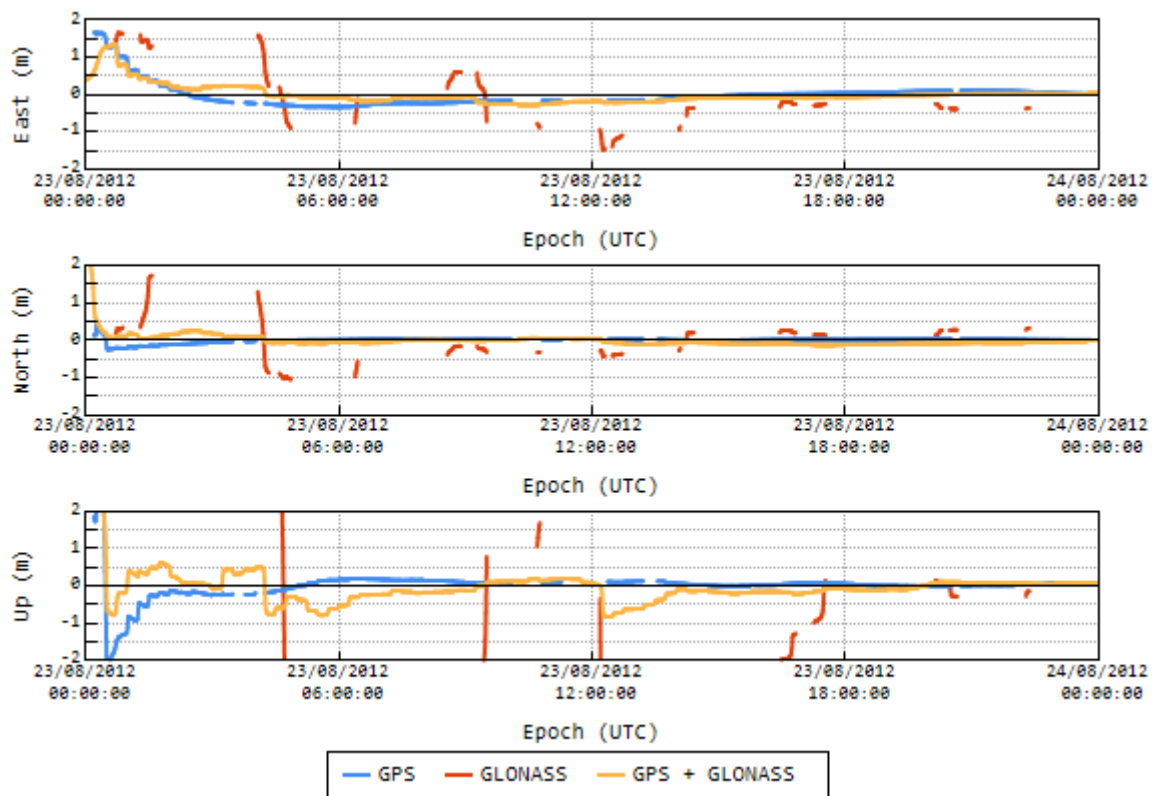
Results with a cut-off elevation angle of 30°

Figure 6.14: PPP Results – GPS-Only vs. GLONASS-Only vs. GPS+GLONASS positioning errors

Error $[m]$		GPS-Only	GLONASS-Only	GPS + GLONASS
RMS	East	0.0755	0.3496	$1.4661 \cdot 10^{-4}$
	North	0.0219	0.2575	0.0726
	Up	0.0280	0.0906	0.0253
Std.	East	0.0271	0.0452	0.0306
	North	0.0083	0.0521	0.0281
	Up	0.0290	0.1703	0.0798

Table 6.16: PPP Results – Position Statistics for the last 43200 epochs

Error $[m/s]$		GPS-Only	GLONASS-Only	GPS + GLONASS
RMS	East	$2.4227 \cdot 10^{-4}$	$3.1972 \cdot 10^{-5}$	$2.3866 \cdot 10^{-4}$
	North	0.0016	0.0023	0.0018
	Up	0.0014	0.0017	0.0014
Std.	East	$4.4171 \cdot 10^{-5}$	$2.7252 \cdot 10^{-5}$	$3.2152 \cdot 10^{-5}$
	North	$7.2197 \cdot 10^{-5}$	$4.8353 \cdot 10^{-5}$	$4.7243 \cdot 10^{-5}$
	Up	$1.3731 \cdot 10^{-4}$	$1.0289 \cdot 10^{-4}$	$1.1220 \cdot 10^{-4}$

Table 6.17: PPP Results – Velocity Statistics for the last 43200 epochs
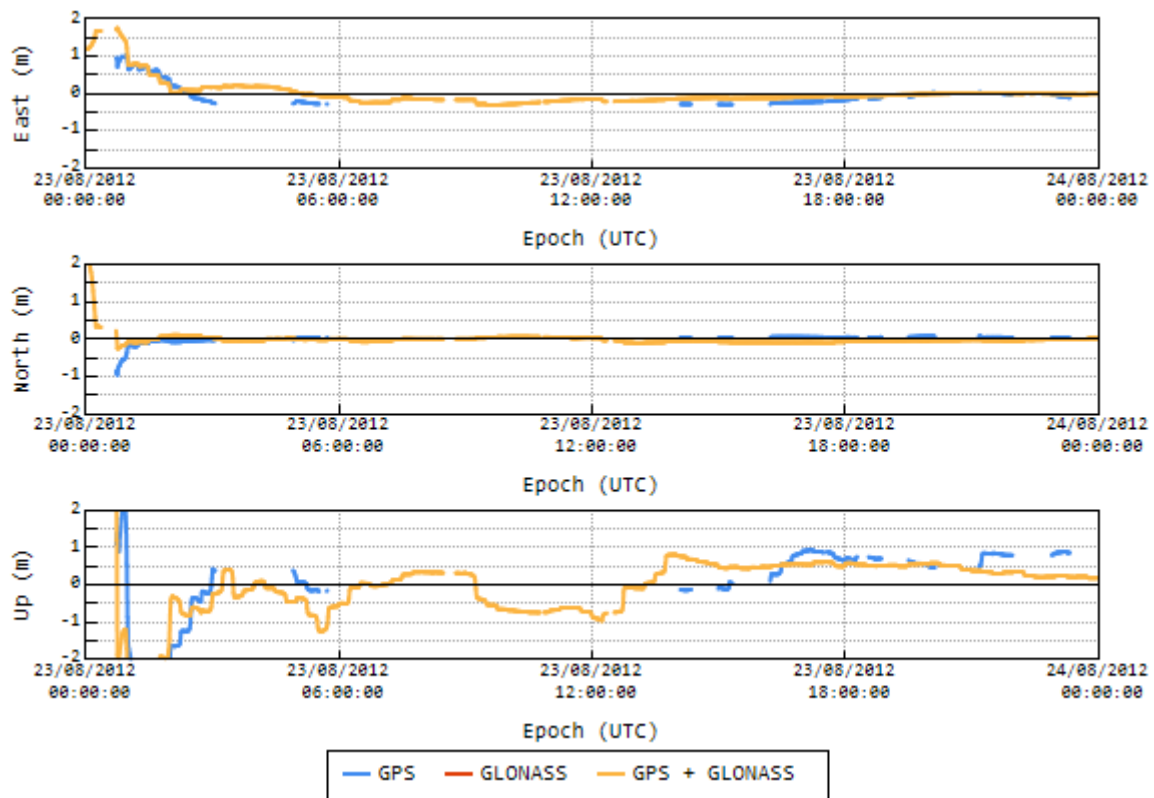
77

Results with a cut-off elevation angle of 40°

Figure 6.15: PPP Results – GPS-Only vs. GLONASS-Only vs. GPS+GLONASS positioning errors

Error $[m]$		GPS-Only	GLONASS-Only	GPS + GLONASS
RMS	East	0.0451	—	0.0116
	North	0.0600	—	0.0276
	Up	0.7311	—	0.4040
Std.	East	0.0614	—	0.0262
	North	0.0126	—	0.0213
	Up	0.1267	—	0.1383

Table 6.18: PPP Results – Position Statistics for the last 43200 epochs

Error $[m/s]$		GPS-Only	GLONASS-Only	GPS + GLONASS
RMS	East	$3.2410 \cdot 10^{-4}$	—	$1.0324 \cdot 10^{-4}$
	North	$9.8986 \cdot 10^{-4}$	—	0.0021
	Up	$5.9453 \cdot 10^{-4}$	—	0.0023
Std.	East	$1.1642 \cdot 10^{-4}$	—	$6.7788 \cdot 10^{-5}$
	North	$1.3866 \cdot 10^{-4}$	—	$4.7298 \cdot 10^{-5}$
	Up	$3.4343 \cdot 10^{-4}$	—	$1.9566 \cdot 10^{-4}$

Table 6.19: PPP Results – Velocity Statistics for the last 43200 epochs

Chapter 7

Conclusions and Future Work

Although the GPS and GLONASS are two very similar systems at the fundamental level, small differences in their implementations dating back to their design phases hinder their combination. These differences and how they affect the combination of the two systems was shown, and its resolution was presented.

Then the discussion moved to methods for determining the position, velocity and time of the receiver, two approaches were presented, the Standard Point Positioning and the Precise Point Positioning, and how they can be extended to cope with multiple GNSS constellations. In addition multiple algorithms to solve many of the GNSS observations problems (such as atmospheric delays and cycleslips), suitable for real-time applications were presented.

Finally using real data, it was shown what improvements to expect from the combination of the two systems. The results show that the combination of GPS with GLONASS brings several improvements over the use of GPS or GLONASS alone, these improvements are especially noticeable for users using GLONASS only. The main advantage was the tremendous increase in service availability especially for users on harsh locations with poor visibility of the sky. All of those improvements are, in fact, the consequence of the increased redundancy provided by the combination of both systems.

As for future work, the developed software tools allow for further research in the field of GPS, GLONASS and Precise Point Positioning. For GPS and GLONASS there is still plenty room for further research especially for kinematic applications which, due to constraints, wasn't performed on this thesis, and further research in the field of DGNSS techniques. For Precise Point Positioning, further research can be done over more precise atmospheric models, additional precise modelling terms specifically for the receiver velocity determination and integer ambiguity resolution.

References

[1] "ESA - GALILEO fact sheet," 2011.

[2] "GPS official webpage (http://gps.gov/) visited on November 2012."

[3] *GLONASS – Status and Progress*, (CGSIC Meeting GA-US), September 2008.

[4] "IGS webpage (http://igscb.jpl.nasa.gov/) visited on November 2012."

[5] "GLONASS official webpage (http://glonass-iac.ru/) visited on November 2012."

[6] *GLONASS – Interface Control Document, Edition 5.0*, 1995.

[7] *GLONASS – Interface Control Document, Edition 5.1*, 2008.

[8] P. Misra and P. Enge, *Global Positioning System: Signals, Measurements, and Performance*. Ganga-Jamuna Press, 2006.

[9] E. D. Kaplan and C. J. Hegarty, *Understanding GPS: Principles and Applications*. Artech House Publishers, 2006.

[10] N. Ashby, "The Sagnac Effect in the Global Positioning System," *Dp of Physics, University of Colorado*, 2004.

[11] *Navstar GPS – Space Segment/Navigation User Segment Interfaces, IS-GPS-200F*, 21th, September 2011.

[12] *Ashtech ProFlex 500 - Reference Manual*, 2011.

[13] Jianjun Zhang, "MSc thesis: Precise Velocity and Acceleration Determination Using a Standalone GPS Receiver in Real Time," 2007.

[14] J. Sanguino, "Lecture Notes – Navigation Systems," 2010.

[15] A. Leick, *GPS - Satellite Surveying.* New Jersey: John Wiley & Sons, Inc, 2004.

[16] *Federal Air Navigation Authority Aeronautical Information Service*, (Russia), 12th, February 2009.

[17] U. Roßbach, "PhD thesis: Positioning and Navigation Using the Russian Satellite System GLONASS," 2000.

[18] B. K. Strang G., *Linear Algebra, Geodesy, and GPS.* Wellesley-Cambridge Press, 1997.

[19] B. W. Remondi, *Computing Satellite Velocity using the Broadcast Ephemeris.* GPS Solutions Volume 8, Number 2 (in press), 2004.

[20] H. Pina, *Métodos Numéricos.* McGraw Hill Portugal, 1995.

[21] M. I. Ribeiro, "Kalman and Extended Kalman Filters Concept, Derivation and Properties," *Institute for Systems and Robotics Instituto Superior Técnico*, 2004.

[22] J. Kouba, "A guide to using International GNSS Service (IGS) products," *Geodetic Survey Division - Natural Resources Canada*, 2009.

[23] J. Bossler, J. Jensen, R. McMaster, and C. Rizos, *Manual of geospatial science and technology*. Taylor & Francis, 2001.

[24] B. Witchayangkoon, "Elements of GPS Precise Point Positioning," 2000.

[25] V. de Bredorode, *Fundamentos de aerodinâmica incompressível.* IDMEC - Instituto de Engenharia Mecânica.

[26] Niell, A., "Global mapping functions for the atmosphere delay at radio wavelengths," *Journal of Geophysical Research*, 1996.

[27] M. Rothacher, R. Schmid, "ANTEX: The Antenna Exchange Format, Version 1.4," 2010.

[28] "IERS Conventions Center," 2003.

[29] G. Blewitt, "An automatic editing algorithm for GPS data," *Geophysical Research Letters*, 1990.

[30] Geng, J., et al., "Ambiguity resolution in precise point positioning with hourly data," *GPS Solutions*, 2009.

[31] J. Z. M. Z. Zhoufeng Ren, Liyan Li and Y. Shen, "A Real-time Cycle-slip Detection and Repair Method for Single," *International Conference on Networking and Information Technology*, 2011.

[32] R. Ventura, "Lecture Notes – Autonomous Systems," 2011.

[33] IGS, "IGS Products," 2009.

[34] P. R. Spofford and B. W. Remondi, "The National Geodetic Survey Standard GPS Format SP3," 1991.

[35] *RTCA-MOPS: Minimum Operational Performance Standards for Global Positioning System / Wide Area Augmentation System Airborne Equipment*, 2006.

[36] A. Fonseca, "Lecture Notes – Integrated Avionic Systems," 2011.

[37] *ATOM - Reference Manual*, 2011.

[38] *RINEX – The Receiver Independent Exchange Format*, 2009.

Appendix A

Astronomical Algorithms

A.1 Julian Time

The Julian Time refers to a continuous time-scale since the beginning of the Julian Period (November 24th, 4714 BCE – Gregorian date), and is primarily used by astronomers; it can be determined by the following algorithm:

– Compute the Julian Day:

$$a = \frac{14 - month}{12} \tag{A.1}$$

$$y = year + 4800 - a \tag{A.2}$$

$$m = month + 12a - 3 \tag{A.3}$$

$$JD = \begin{cases} day + \dfrac{153m + 2}{5} + 365y + \dfrac{y}{4} - \dfrac{y}{100} + \dfrac{y}{400} - 32045 & \text{Gregorian date} \\ day + \dfrac{153m + 2}{5} + 365y + \dfrac{y}{4} - 32083 & \text{Julian date} \end{cases} \tag{A.4}$$

  – The fractional parts resulting from each division must be dropped.

  – Years BCE must negated and incremented towards zero.

– Compute the the fraction of the day and add it to the Julian Day:

$$JT = JD + \frac{hour - 12}{24} + \frac{minute}{1440} + \frac{second}{86400} \tag{A.5}$$

A.2 Greenwich Mean Sidereal Time – GMST

The Greenwich mean sidereal time is defined by the hour angle between the meridian of Greenwich and mean equinox of the date at 00:00 UT1, and in can be determined by (this approximation is valid from 1950 to 2050) [1]:

– Compute t, the number of seconds within the current day.

– Compute t_0, the number of Julian centuries since JD2000 (2000/01/01 – 12:00) to the current day at 00:00.

– Compute GMST at 00:00:

$$GMST_0 = 24110.54841 + 8640184.812866 t_0 + 0.093104 t_0^2 - 6.2 \cdot 10^{-6} t_0^3 \tag{A.6}$$

– Add the remainder of the day and convert to radians:

$$GMST = \frac{2\pi}{43200} \mathrm{mod}\,(GMST_0 + 1.002737909350795t, 86400) \tag{A.7}$$

A.3 Greenwich Apparent Sidereal Time – GAST

The Greenwich apparent sidereal time is defined by the hour angle between the meridian of Greenwich and apparent equinox of the date at 00:00 UT1, and it can be determined from the Greenwich mean sidereal time by applying the equations of equinoxes, or nutation of the mean pole of the Earth (this approximation is valid from 1950 to 2050) [1]:

– Compute t, the number of Julian centuries since JD2000 (2000/01/01 − 12:00) to the current day at 00:00.

– Compute the mean obliquity of the ecliptic (in degrees):

$$\epsilon_m = 23.439291 - 0.0130111t - 1.64 \cdot 10^{-7} t^2 + 5.04 \cdot 10^{-7} t^3 \tag{A.8}$$

– Compute the Earth's nutation in obliquity and longitude (in degrees):

$$\lambda = 280.4665 + 36000.7698t \tag{A.9}$$
$$d\lambda = 218.3165 + 481267.8813t \tag{A.10}$$
$$\Omega = 125.04452 - 1934.136261t \tag{A.11}$$

– Compute the Earth's rotation parameters (in arc-seconds):

$$d\Psi = -17.20 \sin \Omega - 1.32 \sin 2\lambda - 0.23 \sin 2d\lambda + 0.21 \sin 2\Omega \tag{A.12}$$
$$d\epsilon = 9.20 \cos \Omega + 0.57 \cos 2\lambda + 0.10 \cos 2d\lambda - 0.09 \cos 2\Omega \tag{A.13}$$

– Add the corrections to GMST:

$$GAST = GSMT + d\Psi \cos \left(\epsilon_m + d\epsilon \right) \tag{A.14}$$

A.4 Sun Position

This algorithm allows the user to compute the Sun's position in ECI coordinate system without requiring external data sources (this approximation is valid from 1950 to 2050) [1]:

– Compute t, the number of Julian centuries since JD2000 (2000/01/01 − 12:00)

– Compute the obliquity of the ecliptic, the mean anomaly and ecliptic longitude (in degrees):

$$\epsilon = 23.439291 - 0.0130042t \tag{A.15}$$
$$M = 357.5277233 + 35999.05034t \tag{A.16}$$
$$\lambda = 280.460 + 36000.770t + 1.914666471 \sin M + 0.019994643 \sin 2M \tag{A.17}$$

– Compute the distance between the Sun and Earth, and the ECI vector of the Sun's position:

$$r_\odot = 149597870691(1.000140612 - 0.016708617 \cos M - 0.000139589 \cos 2M) \tag{A.18}$$

$$\vec{r}_\odot = \begin{bmatrix} r \cos \lambda \\ r \cos \epsilon \sin \lambda \\ r \sin \epsilon \sin \lambda \end{bmatrix} \tag{A.19}$$

A.5   Moon Position

This algorithm allows the user to compute the Moon's position in ECI coordinate system without requiring external data sources (this approximation is valid from 1950 to 2050) [1]:

- Compute t, the number of Julian centuries since JD2000 (2000/01/01 – 12:00)
- Compute the perturbing factors from the Earth's nutation (in arc-seconds):

$$f_0 = 3600 \cdot 134.96340251 + 1717915923.2178t + 31.8792t^2 + 0.051635t^3 - 0.00024470t^4 \quad (A.20)$$

$$f_1 = 3600 \cdot 357.52910918 + 129596581.0481t - 0.5532t^2 + 0.000136t^3 - 0.00001149t^4 \quad (A.21)$$

$$f_2 = 3600 \cdot 93.27209062 + 1739527262.8478t - 12.7512t^2 - 0.001037t^3 + 0.00000417t^4 \quad (A.22)$$

$$f_3 = 3600 \cdot 297.85019547 + 1602961601.2090t - 6.3706t^2 + 0.006593t^3 - 0.00003169t^4 \quad (A.23)$$

- Compute the obliquity of the ecliptic, ecliptic longitude and perturbation factor (in degrees):

$$\epsilon = 23.439291 - 0.0130042t \quad (A.24)$$

$$\lambda = 218.32 + 481267.883t + 6.29\sin f_0 - 1.27\sin (f_0 - 2f_3) + \\ 0.66\sin 2f_3 + 0.21\sin 2f_0 - 0.19\sin f_1 - 0.11\sin 2f_2 \quad (A.25)$$

$$p = 5.13\sin f_2 + 0.28\sin (f_0 + f_2) - 0.28\sin (f_2 - f_0) - 0.17\sin (f_2 - 2f_3) \quad (A.26)$$

- Compute the distance between the Moon and Earth, and the ECI vector of the Moon's position:

$$r_\leftmoon = \frac{a_\oplus}{\sin (0.9508 + 0.0518\cos f_0 + 0.0095\cos (f_0 - 2f_3) + 0.0078\cos 2f_3 + 0.0028\cos 2f_0)} \quad (A.27)$$

$$\vec{r}_\leftmoon = \begin{bmatrix} r\cos p\cos\lambda \\ r(\cos\epsilon\cos p\sin\lambda - \sin\epsilon\sin p) \\ r(\sin\epsilon\cos p\sin\lambda + \cos\epsilon\sin p) \end{bmatrix} \quad (A.28)$$

References

[1] U.S. Nautical Almanac Office and United States Naval Observatory (USNO), *The Astronomical Almanac For The Year 2004*. United States Government Printing, 2004.

Appendix B

Reference Frame Transformations

B.1   Geodetic coordinates

Considering a point $P = (x, y, z)$ defined in an ECEF reference frame, its geodetic coordinates (latitude φ, longitude λ, altitude h) are defined as, [1]:

$$\varphi = \tan^{-1}\left(\frac{z + e_0^2 \sin^3 \theta}{r - e_1^2 \cos^3 \theta}\right) \tag{B.1}$$

$$\lambda = \tan^{-1}\left(\frac{y}{x}\right) \tag{B.2}$$

$$h = \frac{r}{\cos \varphi} - N \tag{B.3}$$

Where b, r, e_0^2, e_1^2, θ and N are defined as:

$$b_\oplus = a_\oplus(1 - f_\oplus); \qquad r = \sqrt{x^2 + y^2} \tag{B.4}$$

$$e_0^2 = 1 - \left(\frac{b_\oplus}{a_\oplus}\right)^2; \qquad e_1^2 = \left(\frac{a_\oplus}{b_\oplus}\right)^2 - 1 \tag{B.5}$$

$$N = \frac{a_\oplus}{\sqrt{1 - f_\oplus(2 - f_\oplus)\sin^2 \varphi}}; \qquad \theta = \tan^{-1}\left(\frac{a_\oplus \cdot z}{b_\oplus \cdot r}\right) \tag{B.6}$$
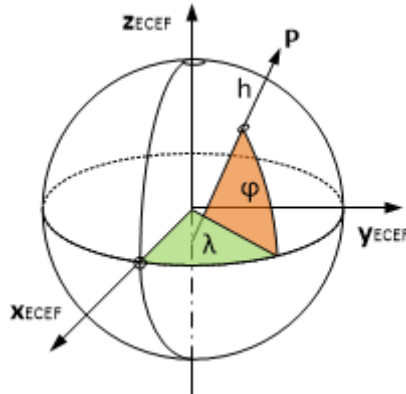

Figure B.1: Earth's geodetic coordinates
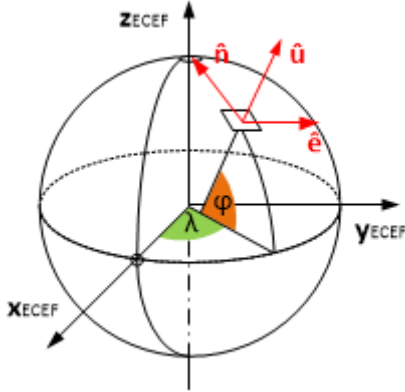
B.2 Local receiver coordinate system

Figure B.2: Receiver local coordinates

Considering the geodetic coordinates of the receiver position, its local coordinate system (east $\hat{e}$, north $\hat{n}$, up $\hat{u}$) is defined as, [1]:

$$\hat{e} = (-\sin\lambda,\ \cos\lambda,\ 0) \tag{B.7}$$

$$\hat{n} = (-\cos\lambda\sin\varphi,\ -\sin\lambda\sin\varphi,\ \cos\varphi) \tag{B.8}$$

$$\hat{u} = (\cos\lambda\cos\varphi,\ \sin\lambda\cos\varphi,\ \sin\varphi) \tag{B.9}$$
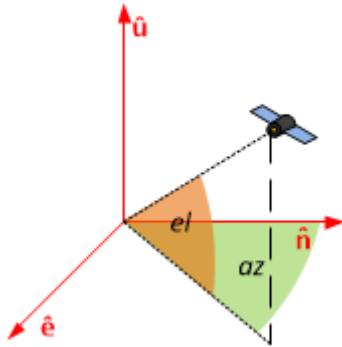
B.2.1 Satellite azimuth and elevation

Figure B.3: Satellite azimuth and elevation

Considering the local receiver coordinates determined from $\vec{r}_{rcv}$ and the satellite position $\vec{r}_{sat}$, the satellite (azimuth az, elevation el) are defined as, [1]:

$$az = \tan^{-1}\left(\frac{\hat{k}\cdot\hat{e}}{\hat{\rho}\cdot\hat{k}}\right) \tag{B.10}$$

$$el = \sin^{-1}\left(\hat{k}\cdot\hat{u}\right) \tag{B.11}$$

And $\hat{k}$ is the vector unit of the line of sight:

$$\hat{k} = \frac{\vec{r}_{sat} - \vec{r}_{rcv}}{\left\|\vec{r}_{sat} - \vec{r}_{rcv}\right\|} \tag{B.12}$$

B.3 Local satellite coordinate system
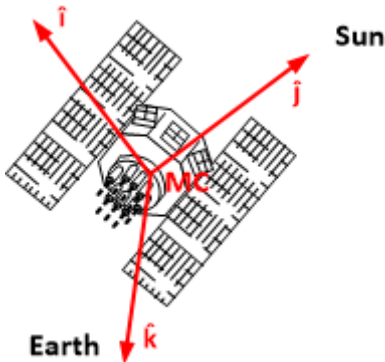
Figure B.4: Satellite local coordinates

Considering the satellite mass center position $(\vec{r}_{sat})_{MC}$ and the Sun position $\vec{r}_{\odot}$, at given epoch and both defined in an ECEF coordinate system, the local satellite coordinate system is defined as, [2]:

$$\hat{k} = -\frac{(\vec{r}_{sat})_{MC}}{\left\|(\vec{r}_{sat})_{MC}\right\|} \tag{B.13}$$

$$\hat{j} = \hat{k}\times\left(\frac{\vec{r}_{\odot} - (\vec{r}_{sat})_{MC}}{\left\|\vec{r}_{\odot} - (\vec{r}_{sat})_{MC}\right\|}\right) \tag{B.14}$$

$$\hat{i} = \hat{j}\times\hat{k} \tag{B.15}$$

B.4   Transformation from ECEF to ECI

The transformation of a position (x, y, z) and a velocity (v_x, v_y, v_z) in ECEF coordinate system to an ECI coordinate system at an instant t in UTC, [3]:

– Compute θ, the Greenwich Apparent Sidereal Time at t:

– Position transformation from ECEF to ECI:

$$X = x\cos\theta - y\sin\theta \tag{B.16}$$
$$Y = x\sin\theta + y\cos\theta \tag{B.17}$$
$$Z = z \tag{B.18}$$

– Velocity transformation from ECEF to ECI:

$$V_X = v_x\cos\theta - v_y\sin\theta - \omega_\oplus y \tag{B.19}$$
$$V_Y = v_x\sin\theta + v_y\cos\theta + \omega_\oplus x \tag{B.20}$$
$$V_Z = v_z \tag{B.21}$$

B.5   Transformation from ECI to ECEF

The transformation of a position (X, Y, Z) and a velocity (V_X, V_Y, V_Z) in ECI coordinate system to an ECEF coordinate system at an instant t in UTC, [3]:

– Compute θ, the Greenwich Apparent Sidereal Time at t:

– Position transformation from ECI to ECEF:

$$x = X\cos\theta + Y\sin\theta \tag{B.22}$$
$$y = Y\cos\theta - X\sin\theta \tag{B.23}$$
$$z = Z \tag{B.24}$$

– Velocity transformation from ECI to ECEF:

$$v_x = V_X\cos\theta + V_Y\sin\theta + \omega_\oplus y \tag{B.25}$$
$$v_y = V_Y\cos\theta - V_X\sin\theta - \omega_\oplus x \tag{B.26}$$
$$v_z = V_Z \tag{B.27}$$

References

[1] J. Sanguino, "Lecture Notes – Navigation Systems," 2010.

[2] J. Kouba, "A guide to using International GNSS Service (IGS) products," *Geodetic Survey Division - Natural Resources Canada*, 2009.

[3] *GLONASS – Interface Control Document, Edition 5.1*, 2008.

Appendix C

Algorithm Application Examples

C.1   GPS Satellite Position & Velocity determination

From the Ephemeris Parameters

Parameter	Value	Parameter	Value
t_{oe}	244800	$\dot{i}$	-4.04659712844163$\cdot 10^{-10}$
$\sqrt{A}$	5153.64949226379	$\dot{\Omega}$	-7.98783272529542$\cdot 10^{-9}$
e	0.00108232197817415	c_{uc}	-4.50760126113892$\cdot 10^{-7}$
M_0	1.12407839668574	c_{us}	1.18259340524673$\cdot 10^{-5}$
ω	0.329807442032348	c_{rc}	148.03125
i_0	0.960473905650565	c_{rs}	-11.34375
Ω_0	-2.73713625728315	c_{ic}	1.26659870147705$\cdot 10^{-7}$
δn	4.50054460860485$\cdot 10^{-9}$	c_{is}	-7.45058059692383$\cdot 10^{-9}$

Table C.1: Ephemeris parameters for GPS Satellite 01

Applying the algorithm to determine the GPS satellite position and velocity for the epoch (WN=678, TOW=252000), results in:

$$\vec{r} = \begin{bmatrix} 20619090.618179 & 10674277.0066471 & 12931468.2741426 \end{bmatrix}^T \quad [m]$$

$$\vec{v} = \begin{bmatrix} 876.082851 & 1406.945595 & -2551.20940 \end{bmatrix}^T \quad [m/s]$$

From the Almanac Parameters

Parameter	Value	Parameter	Value
WN_a	166	ω	0.341262413897905
t_{oa}	405504	Δi	0.0179523689082241
$\sqrt{A}$	5153.58837890625	Ω_0	-2.73842684946435
e	0.00109052658081055	$\dot{\Omega}$	-7.86318467606098$\cdot 10^{-9}$
M_0	-0.579622280645967		

Table C.2: Almanac parameters for GPS Satellite 01

Applying the algorithm to determine the GPS satellite position and velocity for the epoch (WN=678, TOW=252000), results in:

$$\vec{r} = \begin{bmatrix} 20619167.560418 & 10674341.0647708 & 12929587.333059 \end{bmatrix}^T \quad [m]$$

$$\vec{v} = \begin{bmatrix} 875.905738 & 1406.797305 & -2551.231394 \end{bmatrix}^T \quad [m/s]$$

C.2   GLONASS Satellite Position & Velocity determination

From the Ephemeris Parameters

Parameter	Value	Parameter	Value
t_b	8100	v_y	17.4980163574219
x	6647012.6953125	v_z	3564.07260894775
y	-24615855.4687	X''	$-2.79396772384644 \cdot 10^{-6}$
z	424747.55859375	Y''	$-9.31322574615479 \cdot 10^{-7}$
v_x	-157.556533813477	Z''	$-9.31322574615479 \cdot 10^{-7}$

Table C.3: Ephemeris parameters for GLONASS Satellite 01

Applying the algorithm to determine the GLONASS satellite position and velocity for the epoch (N_T=235, t=8500) and the respective transformation to WGS-84, results in:

$$\vec{r} = \begin{bmatrix} 6575027.7471787 & -24569987.4052463 & 1848646.15289283 \end{bmatrix}^T \quad [m]$$

$$\vec{v} = \begin{bmatrix} -200.38258 & 212.198348 & 3553.13717 \end{bmatrix}^T \quad [m/s]$$

From the Almanac Parameters

Parameter	Value	Parameter	Value
N_A	233	ΔT	-2656.015625
λ	-2.04553641613947	$\Delta T'$	0.025390625
t_λ	18605.25	ϵ	0.000487327575683594
Δi	0.0235549940514783	ω	-0.796040155113405

Table C.4: Almanac parameters for GLONASS Satellite 01

Applying the algorithm to determine the GLONASS satellite position and velocity for the epoch (N_T=235, t=8500) and the respective transformation to WGS-84, results in:

$$\vec{r} = \begin{bmatrix} 6576815.704820446 & -24569623.823795 & 1848745.0894068 \end{bmatrix}^T \quad [m]$$

$$\vec{v} = \begin{bmatrix} -200.23685 & 212.245024 & 3553.022939 \end{bmatrix}^T \quad [m/s]$$